

# **Design and Development of a Directional Ultra Wideband Slot Antenna**

**THESIS**

Submitted in the partial fulfillment of the requirements for the degree of

**DOCTOR OF PHILOSOPHY**

by

**Ritish Kumar**  
2016PHXF0007P

Under the supervision of

**Prof. Praveen Kumar A. V.**



**BITS Pilani**  
Pilani | Dubai | Goa | Hyderabad

**BIRLA INSTITUTE OF TECHNOLOGY & SCIENCE**

**PILANI – 333031 (RAJASTHAN) INDIA**

**2022**



**BIRLA INSTITUTE OF TECHNOLOGY & SCIENCE**

**PILANI- 333031 (RAJASTHAN) INDIA**

## **CERTIFICATE**

This is to certify that the thesis entitled “**Design and Development of a Directional Ultra Wideband Slot Antenna**” submitted by **Mr. Ritish Kumar**, ID. No. **2016PHXF0007P** for award of Ph.D. of the Institute embodies original work done by him under my supervision.

Signature in full of the Supervisor \_\_\_\_\_

Name : **Prof. Praveen Kumar A. V.**

Designation : **Associate Professor**

**Department of Electrical and Electronics Engineering**

**BITS Pilani, Pilani campus,**

**Pilani, Rajasthan, 333031, India**

Date : \_\_\_\_\_

*Dedicated*  
*to*  
*My Loving Parents*

## ACKNOWLEDGEMENT

I gratefully acknowledge Prof. Praveen Kumar A.V., Associate Professor, Department of Electrical and Electronics Engineering, BITS Pilani, Pilani campus, Rajasthan for introducing me to the world of Microwave Engineering and Antenna Design. I sincerely appreciate his impeccable knowledge in the subject of Antenna design, and the way he guided and trained me to fulfil my thesis objectives. His timely advice helped in shaping my professional and personal lives. Indeed, my gratitude to him is beyond words. Also, I would like to thank Mr. Mahesh Chandra Saini, technical staff of the Communication Lab for supporting in the fabrication and the measurement of various antennas that I designed for this thesis.

I sincerely express my profound gratitude to Prof. Souvik Bhattacharya, Vice-Chancellor, BITS Pilani for providing me the opportunity to carry out my Doctoral studies at BITS, Pilani. I convey my sincere thankfulness to Prof. Sudhir kumar Barai, Director, BITS Pilani, Pilani campus. I thank Prof. Chandra Shekhar, Emeritus Prof. of EEE Department for his constant encouragement and support. I also express my gratitude to Prof. M.B. Srinivas, Dean, Academic – Graduate Studies & Research Division (AGSRD) and Prof. Jitendra Panwar, Associate Dean, Academic – Graduate Studies & Research Division, for providing me valuable support throughout the doctoral programme.

I would also like to thank my doctoral advisory committee (DAC) members, Prof. V.K.Chaubey, and Prof. Navneet Gupta, for their guidance throughout my PhD programme. I would like to thank Prof. H.D. Mathur, Head of EEE Department for motivating me throughout my degree programme.

I also want to thank staff members of EEE Department, Mr. Ravinder Kumar Yadav, Mr. Tulsi Ram Sharma, Mr. Ashok Saini, Mr. Manoj Kumar, Mr. Amitabh Jangir, Mr. Yogesh, Mr. Sanjay Bharbava, Mr. Ramavatar and Mr. Surendra for their help in the laboratory and other official works. I would like to thank the Central Workshop, BITS Pilani, for providing fabrication facility and rendering necessary technical assistance. The Department of Science and Technology (DST), India is also acknowledged for facilitating the vector network analyzer and antenna simulation tools (ANSYS HFSS and CST Microwave Studio) in EEE department, BITS Pilani through the Fund for Improvement of S&T Infrastructure in Universities and Higher Educational Institutions (DST-FIST, Grant Ref: SR/FST/ETI-

346/2013). I sincerely thank to University Grants Commission, India for providing the UGC-NET-JRF/SRF fellowship.

I cannot conclude this section without mentioning the support from my faculty member Prof. Rahul Singhal, Prof. Abhijit Asati, Dr. Sainath Bitragunta, Dr. Syed Mohammad Zafaruddin, Dr. Nitin Chaturvedi, Dr. Vinay Chamola and senior colleagues Dr. Abhishek Joshi and Dr. Anuj Kumar Ojha. I would also like to thanks to my fellow colleagues, Mr. Ziyaur Rahman, Mr. Pranay Bharadwaj, Mr. Premsai Regalla, Mr. Harshvardhan S, Mr. Devesh Samaiya, Mr. Krishna Veer Singh, Mr. Rahul Sharma, Mr Puneet Khatri, Mr. Anukaran Khanna, Mr. Akhilesh Kumar Mishra, Mr. Abheek Gupta, Ms. Ankita Dixit, and Ms. Shambhavi Shukla. There are many other people whose names do not appear here but whose love, support and contributions in various forms have motivated me and helped me to complete this work. Finally, I am thankful to my Parents, Brother, and Sisters, without whose love, patience and support it would have been impossible to complete this work.

**Ritish Kumar**

## ABSTRACT

This thesis focuses on the design and analysis of a compact directional antenna for ultra wideband (UWB) applications in the ECC UWB of 6–8.5 GHz. In 2007, the Electronic Communications Committee (ECC) in Europe allocated frequency range of 6–8.5 GHz for unlicensed UWB communication. The ECC-UWB regulations are adopted by most of the Asian countries such as India, the United Arab Emirates (UAE), Australia, Malaysia, and New Zealand etc. Major difference between the frequency bands of the FCC-UWB of the US (3.1–10.6 GHz) and the ECC-UWB is that in the latter additional restrictions are imposed for interference mitigation with the result of reduced bandwidth. The antenna technology adopted in this thesis for UWB range is the microstrip slot antenna technology. Microstrip slot antennas have received significant attention in recent years for use in UWB applications due to their merits of wide frequency bandwidth, low profile, lightweight, ease of manufacture, and integration with other devices or RF circuitries / systems. Compared to the microstrip patch antennas, slot antennas provide wider bandwidth, bidirectional radiation pattern, and lower cross-polarization.

In this thesis, the investigations on the UWB slot antenna starts with the performance analysis of a basic rectangular slot antenna excited by a microstrip line. Through proper optimization of the feed offset parameters, two similar radiating modes of the slot are merged for the desired wideband operation from 5.92–8.56 GHz. Resulting radiation pattern of the basic offset fed slot is bidirectional with peak boresight gain of about 3 dBi. To enhance this bidirectional gain, a non-resonant technique is proposed next. A pair of conducting side sheets are loaded in the symmetrically vertical plane of the slot on the ground plane edges to converge the oblique radiation from the slot towards the broadside direction, resulting in increased gain throughout the entire impedance band. In addition, these side sheets also preserve the impedance band and bidirectional nature of radiation pattern. Resulting side sheets loaded slot antenna exhibits an impedance band from 5.97–8.53 GHz (35.31 %) with a maximum boresight gain of 5.52 dBi. The average in-band gain improvement is 3.99 dB while the peak gain improvement is 5.92 dB, relative to the basic offset fed slot antenna without side sheets. To achieve directional radiation from the slot, a conducting reflector-superstrate sheet pair is loaded with the basic offset fed slot antenna. The reflector-superstrate loaded slot antenna exhibits the peak boresight gain of 10.33 dBi with a gain variation of 3 dB within the desired 6–8.5 GHz band. To further

improve the gain and gain variation or gain flatness, previous approach of loading side sheets is used but only in one side of the slot, which results a peak boresight gain of 12.04 dBi with 2.5 dB gain variation within the same 6–8.5 GHz band. Conclusively, a directional, high gain slot antenna with flat gain profile within the 6–8.5 GHz band is achieved. Next, the time domain performance of this final antenna in the 6–8.5 GHz band is numerically analysed. It is found that the final antenna offers nearly flat magnitude and linear phase of transfer function of Tx-Rx system leading to constant group delay and a fidelity factor of 97.67 % compared to the basic slot antenna i.e., 90.95 %.

The key attraction of the proposed UWB antenna design is that the whole structure is based on simple, plane conducting sheets which is very easy to machine and integrate for a given design. In addition, these also provide loose tolerances compared to sheets with specific printed patterns such as frequency selective surfaces, artificial magnetic conductor, metamaterials, and electronic band gap etc.

In the above works, antenna simulations and analysis are carried out with commercial EM simulation tools ANSYS HFSS, and CST Microwave Studio. Antenna fabrication and measurement are conducted respectively in the central workshop, BITS Pilani and Communication lab, EEE Department, BITS Pilani. Easily available and cost-effective FR-4 substrate ( $\epsilon_r = 4.4$ ,  $\tan\delta = 0.02$ , thickness = 1.6 mm) is used for fabricating the slot antenna while copper sheet for the parasitic elements i.e., reflector, superstrate, and side sheets. The proposed antennas are characterized in a compact anechoic chamber by using Keysight vector network analyzer (N9928A), Keysight signal generator (N5173B), and Agilent power meter (E4418B). These facilities are supported through the DST-FIST scheme (Grant Ref: SR/FST/ETI-346/2013).

**Keywords:** Microstrip slot antenna, Offset microstrip feed, Conducting sheets, Superstrate, Reflector, Side sheets, bidirectional radiation pattern, Directional radiation pattern, High gain, Wideband, 3 dB gain-band.

# TABLE OF CONTENTS

<b>CERTIFICATE</b> .....	i
<b>ACKNOWLEDGEMENT</b> .....	iii
<b>ABSTRACT</b> .....	v
<b>TABLE OF CONTENTS</b> .....	vii
<b>LIST OF FIGURES</b> .....	ix
<b>LIST OF TABLES</b> .....	xii
<b>LIST OF ABBREVIATION</b> .....	xiii
<b>Chapter 1</b> .....	1
<b>Introduction</b> .....	1
1.1 Ultra-Wideband (UWB) Technology .....	1
1.1.1 Background .....	1
1.1.2 Advantages .....	2
1.1.3 Regulation (FCC/ECC/India) .....	3
1.1.4 Applications .....	7
1.2 UWB Communication System and Antennas .....	8
1.2.1 UWB Antenna Requirements .....	9
1.2.2 UWB Antenna Technologies .....	10
1.3 Motivation and Objectives .....	12
1.4 Methodology .....	12
1.4.1 Antenna Modelling and Simulation .....	12
1.4.2 Antenna Fabrication and Characterization .....	14
1.5 Thesis outline .....	16
1.6 Conclusion .....	17
<b>Chapter 2</b> .....	18
<b>Literature Review</b> .....	18
2.1 Wideband and UWB slot antenna .....	18
2.2 Directional/high gain slot antenna .....	21
2.3 Wideband-flat gain slot antennas .....	24
2.4 Time domain analysis of UWB antenna .....	26
2.5 Conclusion .....	27
<b>Chapter 3</b> .....	28
<b>Wide Band Bidirectional Slot Antenna Design</b> .....	28
3.1 Radiation characteristics of slot antennas .....	28



3.1.1	<i>Resonant frequency</i> .....	29
3.1.2	<i>Radiation pattern</i> .....	30
3.2	Slot antenna design using ANSYS HFSS .....	33
3.2.1	<i>Center fed Slot Antenna</i> .....	34
3.2.2	<i>Off-center fed Slot Antenna for Wideband Operation</i> .....	41
3.2.3	<i>Conducting Sheet Loading for Gain Enhancement</i> .....	46
3.3	Prototype fabrication, measurements, and discussion.....	52
3.4	Conclusion.....	57
<b>Chapter 4</b>	.....	<b>59</b>
<b>Wide Gain-Band Directional Slot Antenna Design</b>	.....	<b>59</b>
4.1	Conducting sheet loading in the horizontal and vertical planes of the slot.....	59
4.1.1	<i>Reflector sheet loading</i> .....	60
4.1.2	<i>Superstrate sheet loading</i> .....	63
4.1.3	<i>Side sheet loading</i> .....	65
4.2	Prototype fabrication, measurements, and discussion.....	71
4.3	Conclusion.....	75
<b>Chapter 5</b>	.....	<b>76</b>
<b>Time Domain Analysis of UWB Slot Antenna</b>	.....	<b>76</b>
5.1	Defining the UWB source pulse.....	76
5.2	Transfer function.....	78
5.3	Pulse distortion analysis .....	81
5.3.1	<i>Group delay</i> .....	81
5.3.2	<i>Fidelity factor</i> .....	81
5.4	Time domain performance evaluation of antenna.....	82
5.5	Conclusion.....	97
<b>Conclusion and Future Scope</b>	.....	<b>98</b>
6.1	Concluding remarks .....	98
6.2	Future scope of the study .....	100
<b>References</b>	.....	<b>101</b>
<b>List of Publications</b>	.....	<b>111</b>
<b>Brief Biography of the Candidate</b>	.....	<b>112</b>
<b>Brief Biography of the Supervisor</b>	.....	<b>113</b>

## LIST OF FIGURES

<b>Fig.1. 1</b> Ultra-wideband communications spread transmitting energy across a wide spectrum of frequency [6].....	3
<b>Fig.1.2</b> FCC’s indoor and outdoor emission masks.....	4
<b>Fig.1.3</b> European peak emission mask, (a) complete spectrum (b) main frequency spectrum only [2,9].....	6
<b>Fig.1.4</b> Block diagram of a typical (a) UWB transmitter (b) UWB receiver [11].....	8
<b>Fig.1.5</b> UWB antennas (a) Vivaldi antenna [18] (b) Mono-conical and bi-conical antenna [14] (c) Log-periodic antenna [15] and (d) Spiral and conical spiral antenna [17].....	10
<b>Fig.1.6</b> Planar monopole antennas for UWB applications (a) Rectangular (b) Circular and elliptical (c and d) other shapes [24].....	11
<b>Fig.1.7</b> Various types of UWB antennas (a) Printed antenna [24], (b) Slot antenna [25], (c) Metamaterial loaded antenna [26], and (d) Dielectric Resonator Antenna (DRA) [27].....	11
<b>Fig.1.8</b> Antenna fabrication facility at the parent institution.....	14
<b>Fig.1.9</b> Antenna characterization facility at the parent institution.....	15
<b>Fig.3. 1</b> Structure of a conventional microstrip slot antenna with substrate and finite ground size. ....	28
<b>Fig.3.2</b> Rectangular aperture placed on the infinite ground plane.....	29
<b>Fig.3.3</b> Radiation fields of a half-wavelength (a) slot on an infinite sheet and (b) flat dipole in free space [31].....	31
<b>Fig.3.4</b> Theoretical 2D radiation patterns of the rectangular aperture (in fig.3.1) .....	32
<b>Fig.3.5</b> Geometry of the center-fed slot antenna in the Side view (XZ-plane) and Top view (XY-plane). ....	35
<b>Fig.3.6</b> Reflection coefficient of the microstrip slot antenna for $L_{slot} = 13$ mm and $W_{slot}/L_{slot} = 0.25$ . ....	36
<b>Fig.3. 7</b> Simulated E-field distribution within the slot at 6.16 GHz.....	37
<b>Fig.3.8</b> Simulated radiation pattern of conventional rectangular slot antenna with (a) 2D and (b) 3D at 6.16 GHz.....	37
<b>Fig.3.9</b> Reflection coefficients for the center-fed slot antenna ( $L_{slot} = 13$ mm) for various slot width ( $W_{slot}$ ). ....	38
<b>Fig.3.10</b> Reflection coefficients for the center-fed slot antenna for the varying slot length...	41
<b>Fig.3.11</b> Geometry of the offset-fed slot antenna with $W_{slot} / L_{slot} = 0.72$ , $L_{slot} = 13$ mm.....	42
<b>Fig.3.12</b> Effect of offset parameter $d/L_{slot}$ on the reflection coefficient of rectangular slot antenna .....	42
<b>Fig.3.13</b> Reflection coefficient and boresight gain Vs frequency of optimized offset-fed slot antenna ( $W_{slot} / L_{slot} = 0.72$ , $L_f = 25.2$ mm, $d/L_{slot} = 0.35$ and $d = 4.55$ mm).....	43
<b>Fig.3.14</b> Simulated electric-field distributions for a basic slot at 6.45 GHz, 7.52 GHz, and 9.52 GHz. ....	44
<b>Fig.3.15</b> Radiation patterns at (a) 6.45 GHz, (b) 7.52 GHz, and (c) 9.52 GHz for the optimized basic slot.....	44
<b>Fig.3.16</b> Reflection coefficients for the offset fed slot antenna for the varying slot length $L_{slot}$ .....	45
<b>Fig.3.17</b> Geometry of proposed antenna in (a) top view, (b&c) side views, and (d) 3D view. ....	46

<b>Fig.3.18</b> Typical rays and corresponding E and H-fields radiated by the slot in vertical plane (XZ-plane) (Due to symmetry, the same applies in the backward direction which is not shown). .....	47
<b>Fig.3.19</b> Electric field distribution (HFSS) in the XZ plane of the (a) basic slot antenna (b) proposed antenna (side sheets loaded slot antenna). .....	48
<b>Fig.3.20</b> Ray trace models for three representative rays reflected from the conducting side sheet with the point of reflection Q lying (a) above the sheet centre (b) at the sheet centre (c) below the sheet centre (Due to symmetry, the same applies in the backward direction which is not shown). .....	49
<b>Fig.3.21</b> Real Poynting vector distribution (HFSS) in the XZ and YZ-planes of the (a) basic slot antenna (b) proposed antenna (slot with side sheets). .....	52
<b>Fig.3.22</b> Photograph of the fabricated antenna ( $L=W=50$ mm, $L_{\text{slot}}=13$ mm, $W_{\text{slot}}=9.36$ mm, $L_{\text{strip}}=25.2$ mm, $d=4.55$ mm, $L_{\text{sheet}}=90$ mm, $W_{\text{sheet}}=20$ mm). .....	53
<b>Fig.3.23</b> Simulated and measured reflection coefficients of the basic slot antenna and the proposed antenna (slot with side sheets). .....	53
<b>Fig.3.24</b> Simulated Vs measured radiation patterns of the basic slot antenna and the proposed antenna (slot with side sheets) at the center frequency of 7.25 GHz, in the principal planes (XZ and YZ-planes). .....	54
<b>Fig.3.25</b> Simulated vs measured gains versus frequency for the basic slot antenna and the proposed antenna (slot with side sheets). .....	55
<b>Fig.3.26</b> Simulated and measured gain improvement within the operating band of the proposed antenna (slot with side sheets), relative to the basic slot antenna. ....	55
<b>Fig.4.1</b> Geometry of the reflector loaded slot antenna (a) Side view (XZ-plane) (b) Top view (XY-plane). ....	60
<b>Fig.4.2</b> Reflection coefficient and boresight gain vs frequency of reflector loaded basic slot antenna for the varying reflector sheet size. ....	61
<b>Fig.4.3</b> Radiation patterns at (a) 6.45 GHz, (b) 7.52 GHz, and (c) 9.52 GHz for the optimized reflector loaded basic slot. ....	62
<b>Fig.4.4</b> Simulated electric-field distributions for reflector-loaded basic slot at 6.45 GHz, 7.52 GHz, and 9.52 GHz. .....	62
<b>Fig.4.5</b> Geometry of the superstrate and reflector loaded basic slot antenna (a) Side view (XZ-plane) (b) Top view (XY-plane). ....	64
<b>Fig.4.6</b> Reflection coefficient and boresight gain vs frequency of superstrate and reflector loaded basic slot antenna for varying superstrate size. ....	65
<b>Fig.4.7</b> Simulated electric-field distributions for superstrate and reflector loaded basic slot at 6.45 GHz, 7.52 GHz, and 9.52 GHz. ....	65
<b>Fig.4.8</b> Geometry of the proposed antenna (a) 3-D view (b) Side view (XZ-plane) (c) Top view (XY-plane). ....	66
<b>Fig.4.9</b> Reflection coefficient and boresight gain vs frequency of basic slot antenna loaded with side sheet, superstrate, and reflector, for the varying side sheet size. .....	67
<b>Fig.4.10</b> Comparison of (a) reflection coefficients and (b) boresight gains of antennas under various sheet loaded cases. ....	68
<b>Fig.4.11</b> Comparison of radiation patterns of all the antenna designs at (a) 6.50 GHz, (b) 8.50 GHz, and (c) 9.50 GHz. ....	69
<b>Fig.4.12</b> Radiation efficiency of the final antenna. ....	70
<b>Fig.4.13</b> Photograph of fabricated final antenna ..... .....	71

<b>Fig.4.14</b> Reflection coefficient and boresight gain vs frequency for the final antenna. ....	72
<b>Fig.4.15</b> Measured vs simulated radiation pattern of the final antenna at (a) 6.50 GHz, (b) 8.50 GHz, and (c) 9.50 GHz. ....	73
<b>Fig.5.1</b> Gaussian sinusoidal source pulse fitting the ECC mask in (a) time and .....	78
<b>Fig.5.2</b> A simple UWB communication system .....	78
<b>Fig.5.3</b> (a) Transmitting and receiving antenna (Tx-Rx) system and (b) top view of antennas for face-to-face and side-by-side orientation [116]. ....	82
<b>Fig.5.4</b> Geometry of the basic slot antenna of chapter 3. ....	82
<b>Fig.5.5</b> Geometry of the final antenna of chapter 4 (a) 3-D view (b) Side view (XZ-plane) (c) Top view (XY-plane). ....	83
<b>Fig.5.6</b> CST model for time domain analysis of (a) basic slot antenna and (b) final antenna. ....	85
<b>Fig.5.7</b> Simulated magnitude and phase of system transfer function for basic slot antenna (a,b) face to face orientation (c,d) side by side orientations. ....	87
<b>Fig.5.8</b> Simulated magnitude and phase of Tx-Rx system transfer function for final antenna placed at far field distance in (a,b) face to face and (c,d) side by side orientations. ....	89
<b>Fig.5.9</b> Magnitude and phase of the transfer function of channel, transmitting antenna, receiving antenna, and Tx-Rx system for basic slot antenna placed at far field distance in (a,b) face to face (c,d) side by side orientations. ....	91
<b>Fig.5.10</b> Magnitude and phase of the transfer function of channel, transmitting antenna, receiving antenna, and Tx-Rx system for final antenna placed at far field distance in (a,b) face to face (c,d) side by side orientations. ....	93
<b>Fig.5.11</b> Group delay of basic slot antenna placed at far field distance in (a) face to face and (b) side by side orientation. ....	94
<b>Fig.5.12</b> Group delay of final antenna placed at far field distance in (a) face to face and (b) side by side orientation. ....	95
<b>Fig.5.13</b> Input and received pulses when basic slot antenna placed at far field distance in (a) face to face and (b) side by side orientations. ....	96
<b>Fig.5.14</b> Input and received pulses of the final antenna placed at far field distance in (a) face to face and (b) side by side orientations. ....	96

## LIST OF TABLES

<b>Table 3.1</b> Calculated effective permittivity $\epsilon_{re}$ at $f_r = 6$ GHz using equations (3.23) .....	36
<b>Table 3.2</b> Performance characteristics of the of the center-fed slot antenna ( $L_{slot} = 13$ mm) for various aspect ratios ( $W_{slot}/L_{slot}$ ).....	39
<b>Table 3.3</b> Calculated vs simulated effective permittivity for the center-fed slot antenna ( $L_{slot} = 13$ mm) for various aspect ratios ( $W_{slot}/L_{slot}$ ).....	40
<b>Table 3.4</b> Comparison between the simulated and theoretical resonant frequencies as a function of slot length for constant slot width ( $W_{slot}=9.36$ mm). .....	41
<b>Table 3.5</b> Performance characteristics of the slot antenna ( $W_{slot}/L_{slot} = 0.72$ , $L_{slot} = 13$ mm) with various offset parameter ( $d/L_{slot}$ ).....	43
<b>Table 3.6</b> Effect of slot length variation ( $L_{slot}$ ) of the offset-fed slot antenna with $W_{slot}=9.36$ mm .....	45
<b>Table 3.7</b> Conducting sheet optimization for in-band gain improvement of the proposed antenna (side sheets loaded slot antenna) relative to the basic slot antenna (common parameters: $L_{slot} \times W_{slot} = 13$ mm $\times$ 9.36 mm, $L_{strip} = 25.2$ mm, $d = 4.55$ mm, and $W = 50$ mm).....	48
<b>Table 3.8</b> Path difference (in unit of $\lambda_0$ ) at C–C’ plane for the three different rays of Figure 3.20 in the band ( $W_{sheet} \times L_{sheet} = 20$ mm $\times$ 90 mm, $L = 50$ mm, and $R_{OP} = W_{sheet}/2$ ). .....	51
<b>Table 3.9</b> Comparison of the proposed antenna with previously reported superstrate loaded antennas.....	56
<b>Table 3.10</b> Performance comparison of existing bidirectional antennas with the proposed antenna .....	57
<b>Table 4.1</b> Performance comparison of various antennas discussed .....	70
<b>Table 4.2</b> Simulated and measured performance characteristics of the final antenna .....	73
<b>Table 4.3</b> Performance comparison of the proposed antenna with existing broadband-high gain antennas.....	74
<b>Table 5.1</b> Performance characteristics of the slot antennas under comparison.....	83
<b>Table 5.2</b> Performance characteristics of slot antenna placed at far field distance in face-to-face orientation.....	96
<b>Table 5.3</b> Performance characteristics of slot antenna placed at far field distance in side-by-side orientation.....	97
<b>Table 6.1</b> Measured performance characteristics of the antennas discussed in chapters .....	99

## **LIST OF ABBREVIATION**

UWB	Ultra Wideband
FCC	Federal Communications Commission
ECC	Electronic Communications Committee
PSD	Power Spectral Density
IC	Integrated Circuit
VNA	Vector Network Analyzer
Tx	Transmitting Antenna
Rx	Receiving Antenna
FF	Fidelity Factor
EM	Electromagnetic
EMC	Electromagnetic Compatibility
EMI	Electromagnetic Interference
AUT	Antenna Under Test
PEC	Perfect Electric Conductor
LPR	Liquid Photoresist
HFSS	High Frequency Structure Simulator
FEM	Finite Element Method
FIT	Finite Integration Technique
MWS	Microwave Studio
Cx-polar	Cross-polar

# Chapter 1

## Introduction

Although the ultra-wideband (UWB) technology has been in existence since the early 1960s, significant research and development in this field started only in the recent past [1-9]. The availability of high-speed semiconductor switching device technology is the primary reason for the above delay. Another reason is that only in 2002, these systems were authorized for unlicensed use in the frequency spectrum of 3.1–10.6 GHz by the Federal Communications Commission (FCC) [1-5]. Thus started the unlicensed use of UWB wireless transmissions at very low power spectral density [1]. As new wireless application bands are emerging, existing spectrum becomes increasingly crowded, hence the demand for wideband communication with low power density has been driving the UWB technology [2–5]. In 2007, the Electronic Communications Committee (ECC) in Europe also allocated a UWB frequency band of 6–8.5 GHz with the same power spectral density level as the FCC (i.e.  $-41.3$  dBm/MHz). Additional frequency bands of 3.1–4.8 GHz and 8.5–9 GHz incorporated with interference mitigation techniques have also been recommended by ECC for UWB use [4-5,9]. This chapter gives an overview of the UWB technology and explores its essentials, including the advantages, applications and antenna requirements, leading to the identification of gaps in research and formation of objectives of this thesis.

### 1.1 Ultra-Wideband (UWB) Technology

#### 1.1.1 Background

Historically, UWB systems were used in impulse radio which transmitted data in the form of energy pulses at extremely high data rates instead of employing narrow-band frequency carrier. The pulses were often very short in duration, typically a few nanoseconds that leads to an ultra-wideband frequency spectrum from near dc to a few GHz. Guglielmo Marconi invented or researched impulse radio in the 1900s, when spark gap transmitters produced pulsed signals with extremely wide bandwidths [2]. But at that time, there was no means to effectively retrieve the wideband energy emitted by the spark gap transmitter in the presence of other interfering signals. Therefore, wideband radio communication was abandoned in favour of narrowband transmitters that were easier to control and coordinate. Several research works on how to reduce interference and improve performance on impulse radio systems occurred between 1942 and 1945 [3]. However,

many of them were put on hold due to concerns about the US government's potential military use. Later in 1960s, impulse radio technologies were adopted for radar and military uses. The Industrial Scientific and Medical (ISM) bands (902-928 MHz, 2400-2483.5 MHz, and 5725-5850 MHz) were assigned to unlicensed wideband communication use by the FCC in the mid-1980s. WLAN and Wi-Fi have exploded in popularity as a result of this breakthrough spectrum distribution. It also encouraged the communication industry to investigate the benefits and consequences of wider bandwidth communication.

The FCC updated the Part 15 rules governing unlicensed radio devices in February 2002 to accommodate the operation of UWB devices. The FCC also authorised UWB applications a 7.5 GHz bandwidth, ranging from 3.1 GHz to 10.6 GHz and UWB systems can use any signal that covers at least 500 MHz of spectrum [1]. Hence at present, UWB technology implies any device that enables at least 500 MHz spectrum and meets all other UWB requirements such as high data rate, stable gain, linear phase, constant group delay, and high efficiency etc. [4-5]. Commercial UWB communications first started in the United States in 2002. In 2007, the European Commission's Electronic Communications Committee (ECC) designated a frequency range of 6–8.5 GHz to UWB use without any restriction, with the same emission level as the FCC, i.e.  $-41.3$  dBm/MHz. Interference mitigation techniques, such as a low duty cycle (LDC) operation and a detect and avoid (DAA) operation, are needed to protect existing services in the frequency bands 3.1–4.8 GHz and 8.5–9 GHz which are also part of ECC-UWB. The ECC regulations are adopted by most of the Asian countries such as India, the United Arab Emirates (UAE), Australia, Malaysia, and New Zealand etc. Moreover, some Asian countries have still been working to build comprehensive legislation for UWB [2].

### ***1.1.2. Advantages***

UWB offers several benefits that make it a more attractive wireless broadband option than other existing technologies. Its unique characteristics are listed below:

- **High speed and low interference:** The well-known Shannon-Hartley theorem [2] states that channel capacity is directly proportional to its bandwidth. Because UWB provides an extremely broad bandwidth, it can achieve huge capacity as high as hundreds of Mbps or even several Gbps with short range distance from 1 to 10 meters. As the power requirement for such short range is less and this power is distributed over a large frequency spectrum (Figure 1.1), UWB technology ensures reduced interference effects [5].



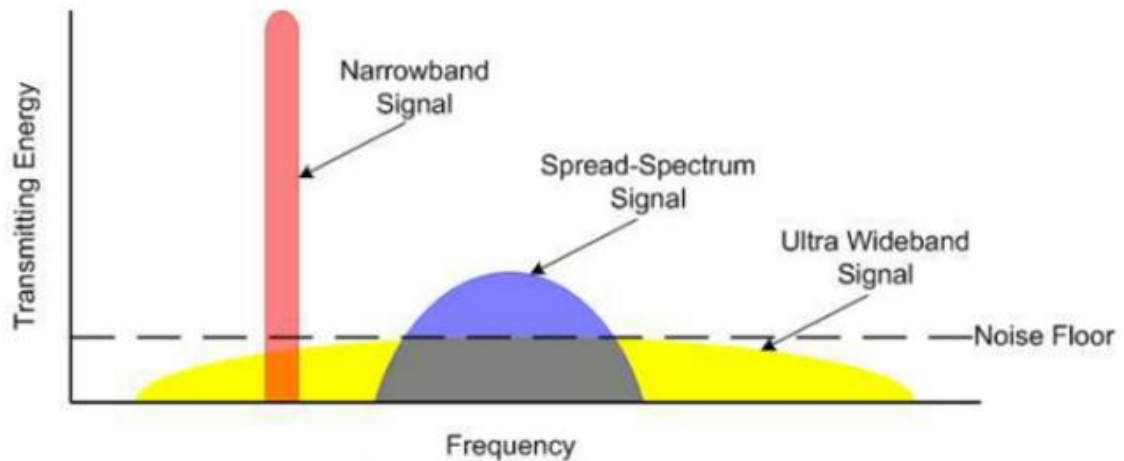


**Fig.1. 1** Ultra-wideband communications spread transmitting energy across a wide spectrum of frequency [6]

- **Low multipath effects:** UWB system has relatively good immunity from multipath fading due to the short duration waveforms. Multi-path fading occurs when a strong enough reflected wave cancels the direct path signal. Due to the very short duration of the UWB pulse, no cancellation will occur because the direct path signal has passed before the reflected path signal arrives. Therefore, UWB implementation of high-speed, mobile wireless services are highly desired.
- **Stability and security:** The signal power spectral density delivered by UWB communication systems is extremely low (i.e.,  $-41.3$  dBm/MHz). As a result, UWB has a low probability of being detected or intercepted. UWB thus offers a highly stable and secure communication solution to applications especially those in the defence sector [5,7].
- **Low-cost technology:** Because of the base-band nature of the signal transmission, UWB technology doesn't require standard modulation-demodulation accessories such as amplifiers, mixers, local oscillators, and filters [8]. It thus offers built-in integration capability for low-cost, low-power integrated circuit (IC) technologies.

### 1.1.3. Regulation (FCC/ECC/India)

Commercial interests have been constantly attempting to persuade regulatory bodies to legalise UWB in order to expand as enormous market as feasible. Everything that initiated by the FCC in the US are being adopted all around the world, but with certain local restrictions and constraints. The European Telecommunications Standards Institute (ETSI) is the institution in charge of establishing the legal foundation for radio communications in Europe. Regulation attempts in Europe are a little more challenging because of the diversity of European Union's member states. Every country is a separate entity that must implement

the suggested rules on its own territory. In various Asian countries, UWB regulations and expansion are rapidly progressing.

### 1.1.3.1. The FCC's regulation in Unites States

The most significant event in the history of UWB in the United States occurred in 2002, when the FCC approved the 3.1-10.6 GHz frequency spectrum. The frequency range was made available for unlicensed reuse of licenced spectrum, allowing unlicensed usage of the 3.1-10.6 GHz band with a maximum average transmit power of -41.3 dBm/MHz. The FCC governs emission mask, which defines the maximum permissible radiated power for UWB devices, in order to effectively minimise unwanted interference. UWB devices are categorized as imaging devices, automobile radar systems, indoor devices, and hand-held devices in the FCC's first report and regulation. The last two categories will be explored because they are of major focus toward commercial UWB applications.

Indoor system devices are designed exclusively for use indoors and require a defined indoor environment to function. Indoor communication uses UWB transmitters to send data at high speeds across short distances. It is forbidden to use an external antenna to intentionally transmit a signal outside of a structure. As illustrated in Figure 1.2, the UWB bandwidth must be restricted from 3.1GHz to 10.6 GHz, and the radiated power spectral density (PSD) must be consistent with the emission mask [2].

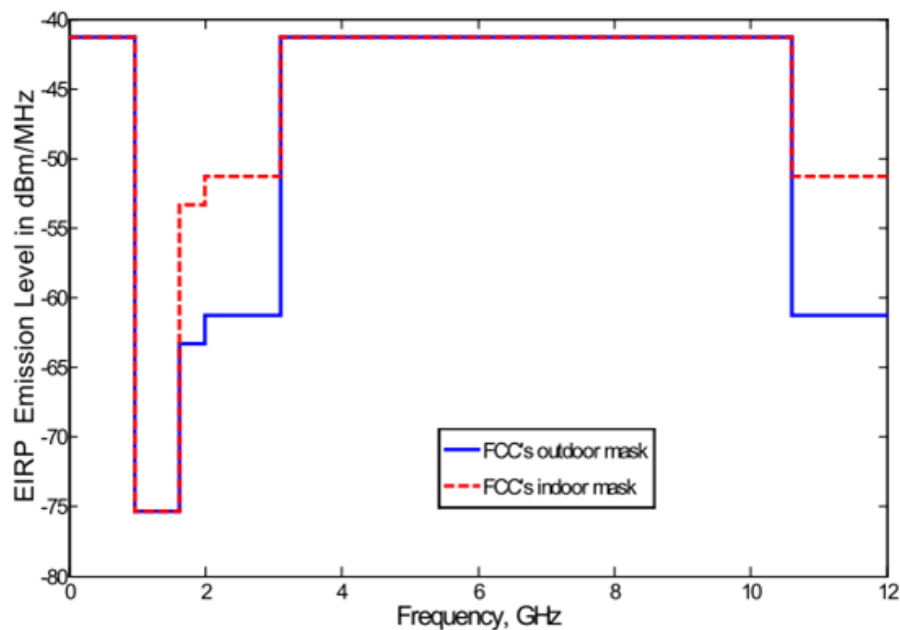


**Fig.1.2** FCC's indoor and outdoor emission masks

Handheld UWB devices do not use a fixed infrastructure. They should only transmit when transmitting data to a receiver with which they are connected. Antennas must be installed on the device and are not permitted on outdoor infrastructures. Handheld UWB devices may be used both indoors and outdoors. Within the UWB spectrum of 3.1 GHz to 10.6 GHz, the outdoor emission mask is the same as the indoor mask at -41.3 dBm/MHz, but beyond this spectrum, it is 10 dB lower to provide other wireless services more protection as demonstrated in Figure 1.2.

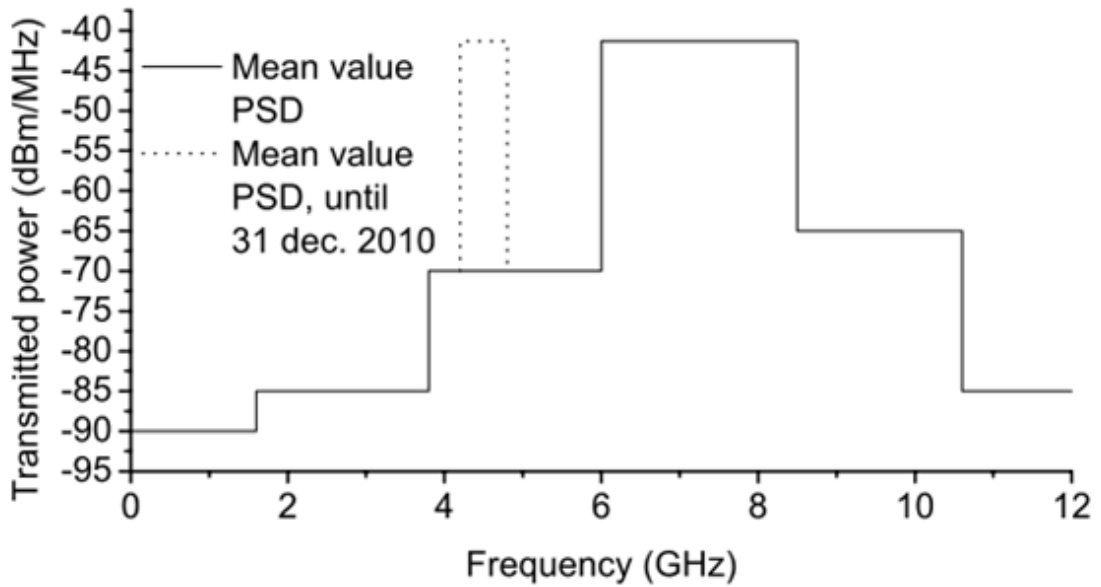
The chances for interference, like with other radio transmitters, is dependent on a variety of factors, including when and where the device is utilised, the transmission power level, the number of devices in operation, the pulse repetition frequency, the transmitted/received signal's direction, and so forth.

#### *1.1.3.2. The ECC's regulation in Europe*

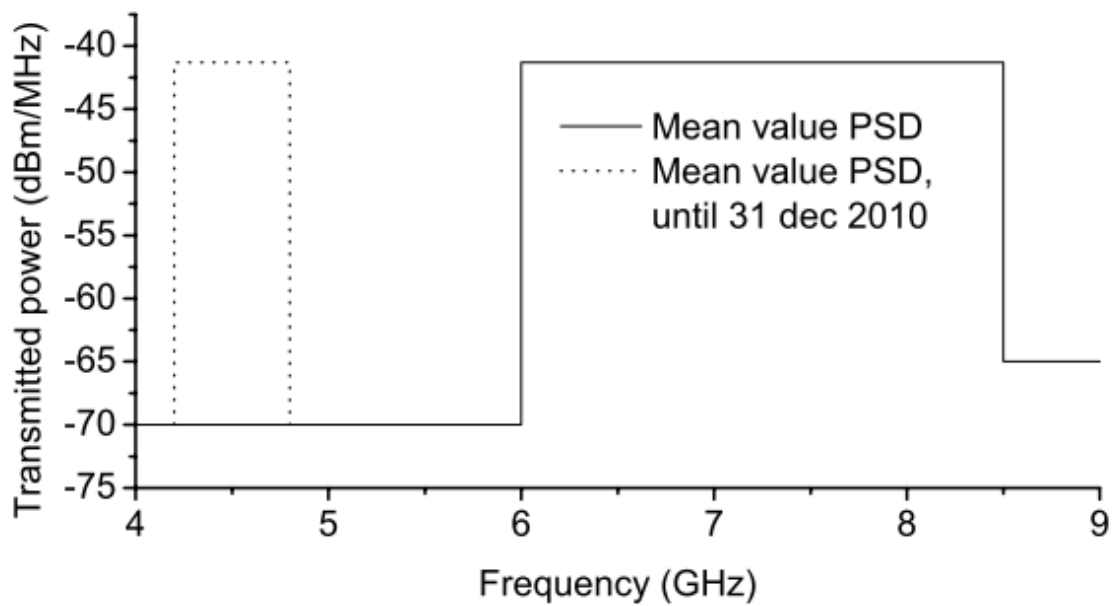
Regulatory authorities outside the United States are also undertaking studies to produce a conclusion on UWB regulations, by adopting the FCC's restrictions with necessary changes. The Electronic Communications Committee (ECC) of the Conference of European Posts and Telecommunications (CEPT) issued a preliminary study on the necessity for radio communication networks to be protected against UWB applications in Europe [2,9]. The CEPT began in 1959 as a platform for collaboration between European postal and telecommunications authorities but has focused only on regulatory problems since 1992. The ECC is a committee comprised of the radio and telecommunications regulatory bodies from the 48 CEPT member countries i.e., the CEPT has 48 members and thus stretches outside the European Union (EU). The ECC provides regulatory rulings and guidelines in this domain. The European Telecommunications Standards Institute (ETSI), which is formally accountable for standardisation of Information and Communication Technologies (ICT) in Europe, is another important participant in the ECC inside the EU. Specification recommendation documents for UWB have been issued by ETSI. The European Commission (EC), on the other hand, has given CEPT and the ECC the task of harmonising UWB rules across Europe.

Presently, ETSI, ECC, and EC have all proposed and allowed the operation of UWB devices in the 6.0–8.5 GHz frequency band, subject to the technical restrictions imposed by the FCC in the United States and without the use of interference mitigation methods. The European UWB mean power spectral emission mask is shown in Figure 1.3. Figure 1.3(a) illustrates the entire frequency range, while Figure 1.3(b) presents the frequency

band restrictions in greater detail. When it comes to applications, the European UWB requirements are not quite as detailed as the FCC UWB requirements. UWB transmitters, on the other hand, are currently forbidden from being utilised within an aircraft or ship, as well as in a fixed outdoor site.



(a)



(b)

**Fig.1.3** European peak emission mask, (a) complete spectrum (b) main frequency spectrum only [2,9].

When the ECC and FCC emission levels are compared, it is clear that the European regulations to UWB emission is more restricted than the FCC, with the exception of the 6-8.5 GHz band, where the emission threshold is the same as the FCC. Some countries, including India, the United Arab Emirates, Australia, Malaysia, and New Zealand, use the same UWB frequency band, which is 6–8.5 GHz.

#### ***1.1.4. Applications***

As described in the section, UWB possesses certain unique characteristics i.e., extremely large bandwidth, low power, high data rate communication, robustness against fading, immunity to multipath, multiple access capability, low-cost of transceivers, and precise positioning, which motivates several potential applications [2,5].

Firstly, UWB has the ability to deliver extremely high data rates while consuming very little power and operating over a very short range, making it a good fit for wireless personal area network (WPAN) applications. The accessibility of using devices such as personal computers and laptops will be enhanced by peripheral connectivity via cableless interfaces to applications such as storage, input/output devices, and wireless USB. High-speed data exchanges between computers and user gadgets such as digital cameras, printers, portable projectors, televisions, and automobiles, will offer new home and personal entertainment experiences. In otherwards, one of the most important aspects in providing seamless connectivity to next-generation mobile users is integrating UWB with existing wireless access technologies.

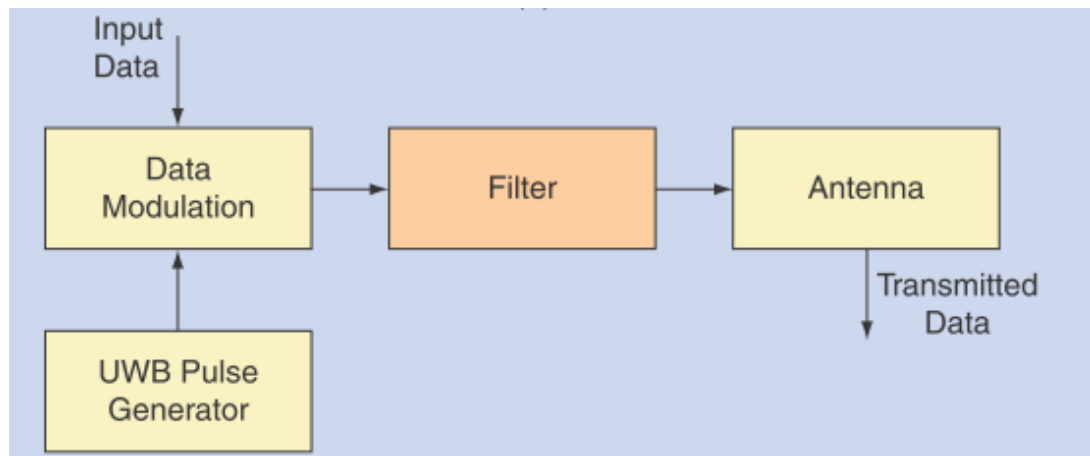
Second distinguishing feature of UWB is its ability to track and position itself. Because of its high data rate in short range, UWB is a great choice for indoor positioning that is considerably more accurate than Global Positioning System (GPS). Furthermore, modern tracking mechanisms allow for the accurate estimation of the detection of moving objects in an interior environment with an accuracy of several centimetres [2,10]. They may also be used to locate people or things in several scenarios, such as fatalities in a destroyed building following an earthquake, missing children in a marketplace, injured visitors in a remote region, fire fighters in a burning structure, etc.

Thirdly, UWB systems can collect, distribute, or exchange a large amount of sensory data in real time. Due to the lack of cables, UWB sensor networks can significantly reduce the cost of construction and repair. This benefit is especially appealing in medical applications because, when intensive medical observation is necessary, a UWB sensor network saves the patient from being tethered by wires and connections.

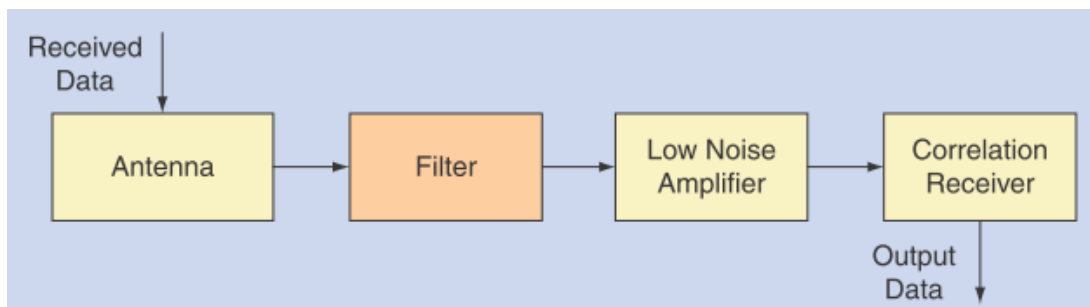
Lastly, UWB can help both radar and imaging applications. It has been utilised in military applications to detect hostile objects hidden in the battleground behind walls and around corners. Commercial applications include rescue services, where a UWB radar might identify a person's movement beneath rubble, and biomedical imaging, where X-ray systems would be less preferred. Besides, UWB automobile radar can also identify the position and movement of objects in the vicinity of a vehicle.

## 1.2 UWB Communication System and Antennas

The block diagrams of general UWB transmitter and receiver communication systems are shown in figure 1.4. With the growing popularity of UWB systems, there has been advancements in UWB antenna design also. One of the challenges in implementing a UWB system is developing an appropriate antenna. This is because the antenna is a crucial component of the UWB system and has an impact on its overall performance.



(a)



(b)

**Fig.1.4** Block diagram of a typical (a) UWB transmitter (b) UWB receiver [11]

A UWB antennas differ from those used in conventional communication systems in that it has an extremely broad frequency bandwidth. An acceptable UWB antenna, according to the FCC's definition, must have an absolute minimum bandwidth of at least 500 MHz or a fractional bandwidth of at least 0.2 with respect to centre frequency. Typically, the UWB range is 3.1–10.6 GHz imposed by FCC [1-2,4-5] and 6–8.5 GHz by ECC/Indian regulations [2,4,9,12].

### **1.2.1 UWB Antenna Requirements**

As any conventional wideband antennas, UWB antennas are also desired to exhibit consistent radiation performance over the entire band. Depending on the type of UWB system to which the antenna is integrated, either directional or omnidirectional radiation characteristics can be preferred. For example, in transportable and hand-held devices, nearly omnidirectional radiation pattern is preferred because it allows for greater flexibility in the receiver and transmitter locations. For directional systems, such as ground penetrating radar, and level probing radar directional radiation characteristics are essential [13]. As the transmit power spectral density is very low ( $-41.3$  dBm/MHz), UWB receiving antennas are expected to have high gain with decent gain flatness over the entire band. Time domain performance of UWB antennas is also very critical as these systems operate with short time domain pulses. The data will not undergo serious distortion only if the antenna exhibits low dispersion. For this, UWB antennas should have linear phase response hence constant group delay over the band. The data thus become insensitive to the antenna [4-5]. Thus, the requirements of UWB antennas are as follows:

#### **Electrical requirements**

- High gain with good gain flatness over the band as the transmit power spectral density is very low.
- Linear phase response to give the constant group delay in Tx-Rx system in order to reduce the pulse dispersion effects.

#### **Mechanical requirements**

- Planar antenna technology to allow easy fabrication
- Compact size and low profile to allow easy integration

### 1.2.2 UWB Antenna Technologies

As illustrated in Figure 1.5, classical antenna technologies that can achieve broad bandwidth includes the biconical antenna, log-periodic antenna, and spiral antenna. Biconical antennas [14] have bulky construction and huge physical dimensions, limiting their uses. Additionally, log-periodic [15] and spiral antennas [16-17] are two types of UWB antennas that can function in the 3.1–10.6 GHz frequency spectrum but are not suggested for indoor wireless communication applications or mobile/portable devices. This is due to their enormous physical dimensions, as well as their frequency dispersive features and significant ringing effect [15].

There have been new contenders for UWB wireless communications capable of overcoming all the above challenges. The planar or printed monopole antenna [18]-[23] is one such candidate. Planar monopole antennas [21, 23] have been proposed for UWB applications in various shapes such as polygonal (rectangular, trapezoidal... etc), circular, elliptical...etc, some of which are illustrated in Figure 1.6. Therefore, printed planar monopole antennas are considered attractive options for UWB communications applications due to their large frequency bandwidth, simple structure, and ease of fabrication etc [24]. Apart from these, slot antenna [25], metamaterial based [26] and dielectric resonator based [27] UWB antennas are also reported as shown in Figure 1.7.

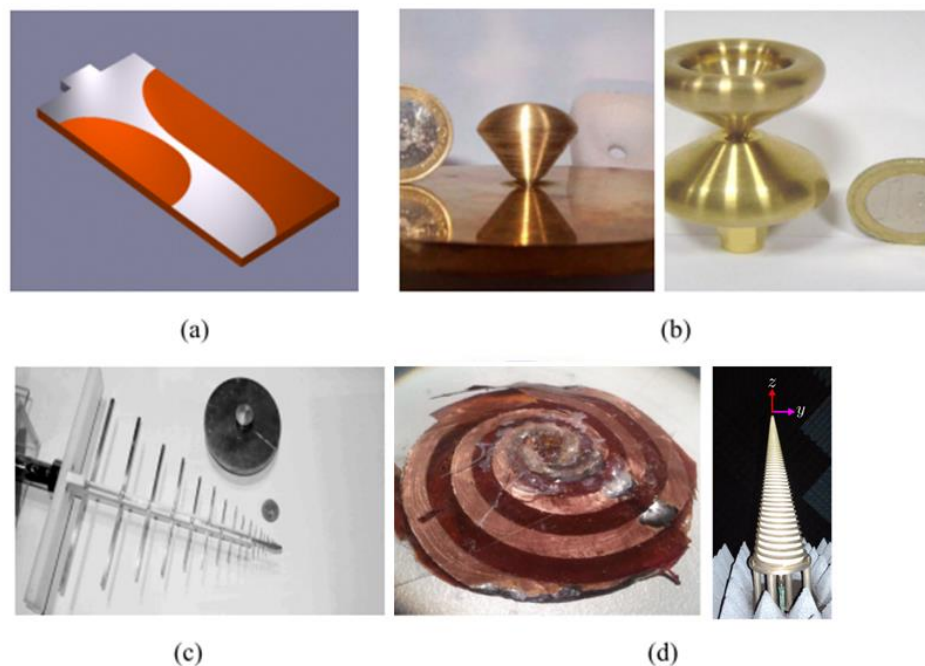


**Fig.1.5** UWB antennas (a) Vivaldi antenna [18] (b) Mono-conical and bi-conical antenna [14] (c) Log-periodic antenna [15] and (d) Spiral and conical spiral antenna [17].



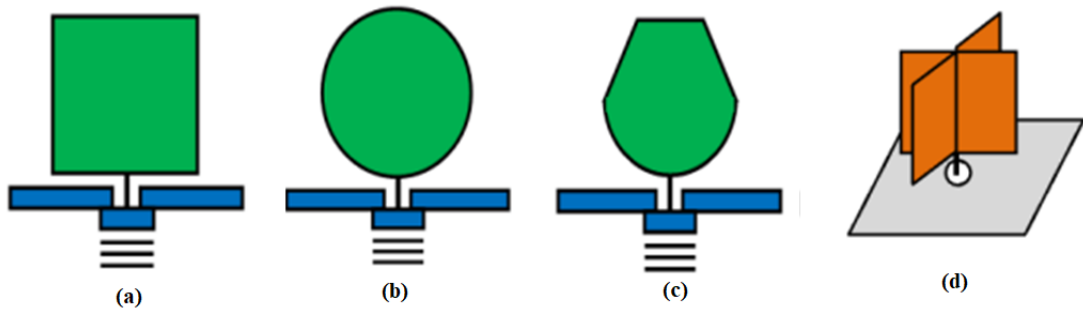


**Fig.1.6** Planar monopole antennas for UWB applications (a) Rectangular (b) Circular and elliptical (c and d) other shapes [24].

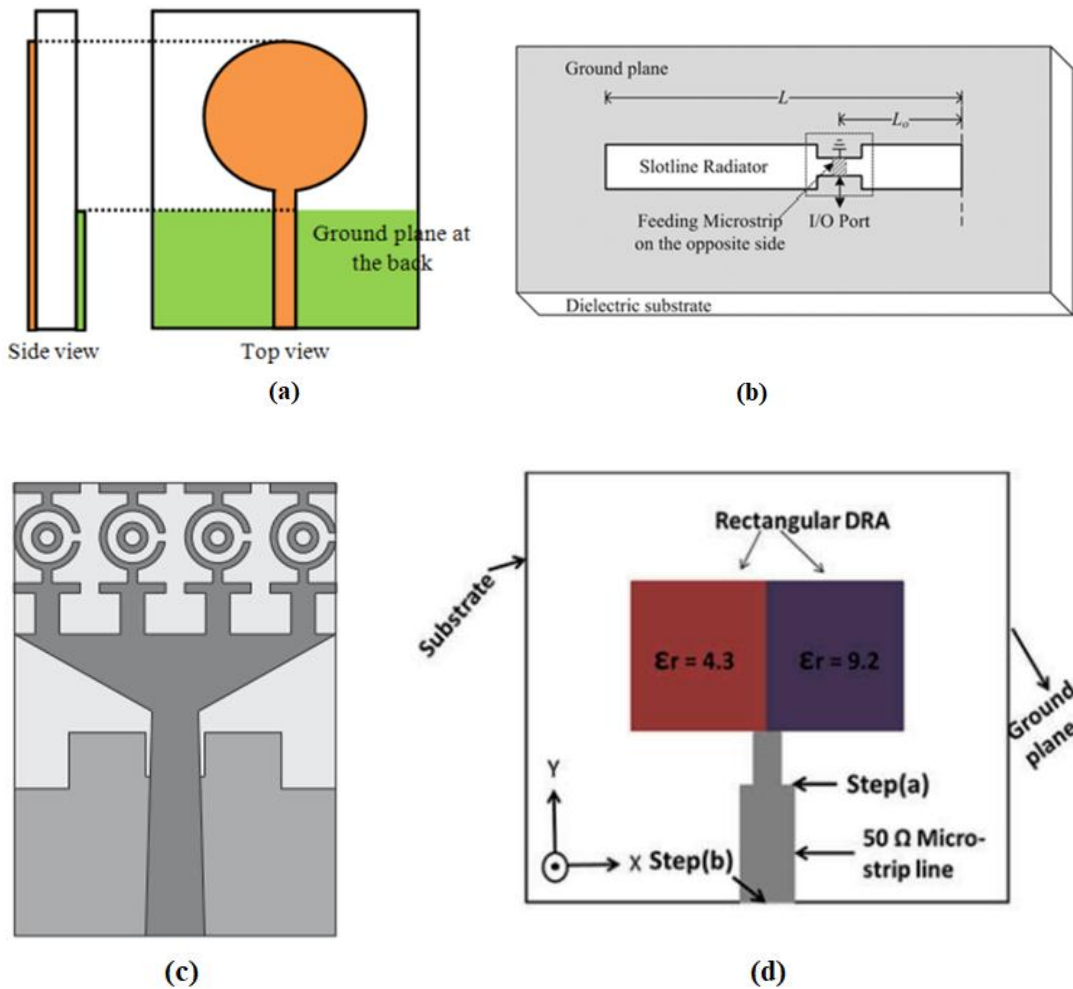


**Fig.1.7** Various types of UWB antennas (a) Printed antenna [24], (b) Slot antenna [25], (c) Metamaterial loaded antenna [26], and (d) Dielectric Resonator Antenna (DRA) [27].

In recent years, printed slot antennas are now being considered for usage in UWB applications, and they are growing in popularity because to their advantages of wide

frequency bandwidth, low profile, lightweight, low cross-polarization, ease of manufacturing, and integration with RF devices [28]. Different slot antennas have achieved wideband or UWB performance by utilising various feeding techniques or slot shapes [28]. A detailed literature review of the same is carried out in the second chapter of this thesis.

### **1.3 Motivation and Objectives**

Above discussions proved that there is a growing interest for the UWB technology for its extremely wide bandwidth and coexistence with other wireless technologies. As it was detailed before, printed antennas are becoming increasingly popular due to the inherent advantages of microstrip technology. Like the patch antennas, slot antennas are also effective radiators with low profile, small size, conformability, and low cost [28]. The slot antenna can however provide wider impedance bandwidth than the patch antenna through simpler designs. High gain and directional antenna designs are also easily implemented with slot antennas. It has been identified that very less work is available on the use of microstrip slot antennas for UWB applications, and also that the 6.0 – 8.5 GHz spectrum which covers both the Indian and European UWB spectra are not sufficiently investigated with respect to any antenna technology. Also, some Asian countries, such as the United Arab Emirates (UAE), Australia, Malaysia, and New Zealand etc., use the same ECC-assigned European UWB frequency band.

The above inferences inspire the author to framing the following research objectives leading to the development of a directional UWB for 6-8.5 GHz,

1. To investigate the impedance and radiation properties of rectangular slot antennas for 6.0 – 8.50 GHz UWB band.
2. To transform the bidirectional slot antenna to directional antenna over the same band.
3. To stabilize the radiation pattern and gain of the slot antenna over the band.
4. To validate the time domain performance of the developed antenna for UWB applications.

### **1.4 Methodology**

The research methodology adopted in this thesis comprises the antenna modelling, simulation, fabrication, and experimental characterization.

#### ***1.4.1 Antenna Modelling and Simulation***

Modelling and simulation of practical antennas has become easier and more effective, thanks to the innovations in digital computer technology and computational

electromagnetics. Commercial electromagnetic simulators such as ANSYS HFSS [29] and CST Microwave Studio [30] are very popular among antenna designers to model the antenna geometry, perform parametric analysis, optimize designs, visualise modal fields, and generate inferences about the antenna performance.

ANSYS HFSS (High Frequency Structure Simulator) is a 3D electromagnetic simulation software that uses the Finite Element Method (FEM) to model and simulate high-frequency consumer devices like antennas, RF, or microwave elements, high-speed interlinks, sensors, waveguides, filters, mixers, intelligent surfaces, amplifiers, connectors, integrated circuit (IC) packages, and printed circuit boards. ANSYS HFSS is used to develop high-frequency, high-speed electronics that may be used in communications systems, radar systems, intelligent transportation systems (ITS), spacecraft, internet-of-things (IoT) gadgets, and other RF and microwave devices. HFSS is mainly a frequency domain solver but also has an eigen mode solver. The utilisation of tetrahedral mesh elements that accommodate to geometries of arbitrary complexity, as well as adaptive mesh refinement that creates an approximate solution depending on the physics of the design, are key components in HFSS simulations producing accurate results. The meshing algorithm iteratively adds mesh elements in locations where a finer mesh is required due to localised electromagnetic field behaviour, and iteratively refines the mesh across the geometry.

CST MICROWAVE STUDIO is a powerful 3D electromagnetic (EM) analysis software suite for creating, evaluating, optimizing, and improving EM components and systems. Antenna and RF components performance and overall efficiency, electromagnetic compatibility, and interference (EMC/EMI), human body contact to EM fields, electro-mechanical effects in motors and generators, and thermal effects in high-power devices are all examples of common uses. CST MWS is dependent on the finite integration technique (FIT), which expresses Maxwell's equations on a grid space in both time and frequency domains and is not confined to a specific grid type. Therefore, frequency domain, time domain, and eigen solvers are all available with MWS. The perfect boundary approximation (PBA), a distinct in-built ability, allowing the user to properly depict curves and inclines.

The following EM CAD procedures in general are followed in the antenna simulation – choose the appropriate solver, define the antenna shape, describe the material characteristics, apply excitations, allocate the radiation box and run the solver. Once the

solution is completed, visualisations of the antenna characteristics in different 1D, 2D, and 3D formats, as well as animated forms, may be created, providing insight into the antenna's behaviour.

#### 1.4.2 Antenna Fabrication and Characterization

Antenna fabrication and experimental characterization of the impedance and radiation characteristics of the antenna under test (AUT) are completely carried out in the Department of Electrical and Electronics Engineering (EEE) of the parent institute. Photolithography facility as shown in Figure 1.8 is used to fabricate the antenna prototypes on microwave substrate. When high precision in dimensions is required, this approach is used. The antenna geometry is first produced as a negative mask on transparent sheet using a laser printer. To remove the oxide layer on the surface of a copper clad sheet of acceptable size, acetone-based surface cleaning is conducted at first. The copper clad is then coated with a thin layer of photo resist material and allowed to dry. After affixing the mask on the substrate side where copper clad is to be removed, it is subjected to UV rays. The exposed layer of photo resist material hardens, whereas the unexposed area is removed by dipping in the liquid photo resist (LPR) developer solution. After that, the substrate is rinsed in water. The undesired copper is now etched with a solution of ferric chloride ( $\text{FeCl}_3$ ). The board is then washed with water to get rid of the hardened negative photo resist. SMA connector is soldered to the antenna port and the antenna is ready for measurements.

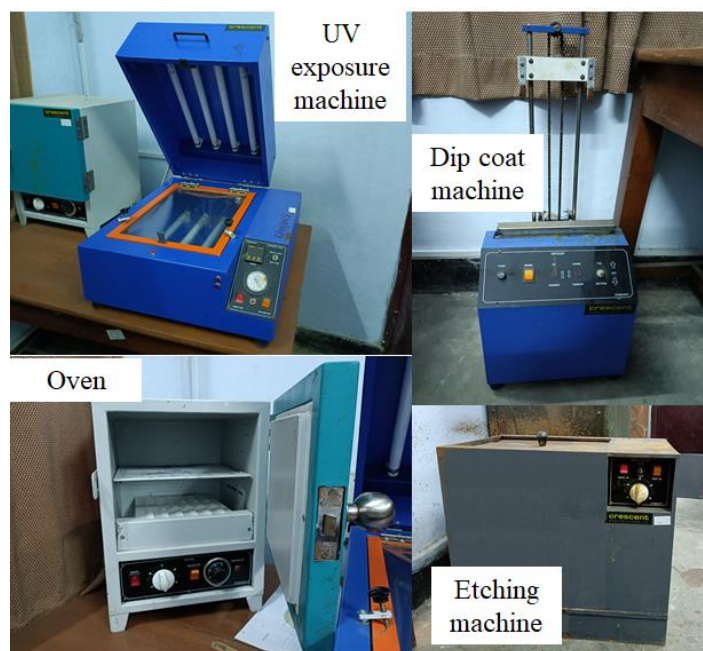


**Fig.1.8** Antenna fabrication facility at the parent institution



**Fig.1.9** Antenna characterization facility at the parent institution

The basic measurement setup consists of the following apparatuses: a vector network analyzer (VNA) (Keysight N9928A, 30 kHz to 26.5 GHz), power meter (Agilent E4418B, -90 to + 90 dBm), power sensor (Agilent E4412A, -70 to +20 dBm), RF signal generator (Keysight N5173B, 9 kHz to 20 GHz), a standard broadband horn antenna (1 to 18 GHz) and a compact anechoic chamber with pyramidal absorbers. Figure 1.9 depicts an image of the facility. The VNA is used to verify the frequency band of the fabricated AUT before and after mounting it inside the anechoic chamber. The radiation pattern of the antenna is then measured using the remaining apparatus. To prevent the use of long cables from the VNA ports to each of the Tx-Rx antennas placed inside the anechoic chamber, the RF signal generator and power meter combination is used as two individual apparatus placed closer to the respective antennas. The former is attached to the transmitting antenna (broadband horn) and the Rx-AUT is placed on a rotating platform controlled externally. The transmitter antenna is injected with 0 dBm power at the desired frequency and the received power from the AUT port is recorded on power meter through the power sensor. After that, the AUT gain is calculated using the Friis-transmission equation [31] given below,

$$\frac{P_r}{P_t} = \left( \frac{\lambda}{4\pi R} \right)^2 G_t G_r L_t L_r \quad (1.1)$$

Where,  $P_t$  = input power of the transmitter antenna,  $P_r$  = output power of the receiver antenna,  $G_t$  = gain of the transmitter antenna i.e., standard broadband horn antenna gain

from its gain vs frequency plot,  $G_r$  = gain of the AUT,  $L_t$  = cable loss at the transmitter,  $L_r$  = cable loss at the receiver and  $\lambda$  is the free space wavelength. The cable losses are monitored independently by connecting the signal generator and the power metre directly through the cable.

## 1.5 Thesis outline

This thesis is organised into 6 chapters as follows:

**Chapter 2:** This chapter explores the literature on various slot antenna designs for wideband, ultra wideband, high gain and directional applications, as well as flattening the gain response across the whole operating band. The performance of ultra wideband antennas in the time domain is also studied.

**Chapter 3:** This chapter discusses the approaches for widening the frequency band of the basic bidirectional slot antenna in the European/Indian UWB i.e., 6–8.5 GHz and for improving the gain of the slot antenna throughout the entire frequency band. These are respectively achieved through offset microstrip feeding and conducting side sheet loading. Resulting antenna performance is experimentally validated.

**Chapter 4:** In this chapter, the basic wideband antenna design from the previous chapter is modified for directional-high gain radiation pattern using conducting reflector-superstrate sheets loading. Additionally, a pair of conducting side sheets are then used to achieve the flattening the gain response throughout the band, as described in Chapter 3. The resulting wide gain-band antenna is experimentally characterized.

**Chapter 5:** This chapter presents the numerical analysis of the time domain performance of the basic offset microstrip fed slot antenna and the conducting sheets loaded slot antenna. The effect of gain flatness, group delay and fidelity factor in the operating band of 6–8.5 GHz on the antenna's suitability for UWB applications is analysed.

**Chapter 6:** This chapter highlights the major findings of the thesis, conclusions, and future research possibilities.

## **1.6 Conclusion**

This chapter provided an overview of ultra wideband (UWB) technology, covering its background, benefits, regulations, and applications. Subsequently UWB antennas are explored and the understanding of its importance motivated the author to frame the thesis objectives. To execute these objectives required research methodology involving UWB antenna modelling, simulation, fabrication, and characterization, is explained. Finally, the thesis outline is presented briefly.

## Chapter 2

### Literature Review

This chapter reviews the advancements in slot antennas for compact, directional, high gain and wideband applications. Slot antenna is an excellent candidate for the above applications for its low profile, simple construction and easy integration [28,31-33]. When compared to a basic patch antenna, a basic slot antenna offers wider impedance bandwidth, lower cross-polarized radiation, and bidirectional radiation pattern [28]. Several techniques have been proposed for achieving wide bandwidth, high gain/directivity and high gain-bandwidth or gain flatness. In the following sections the literatures are discussed in detail.

#### 2.1 Wideband and UWB slot antenna

Wide bandwidth from slot antennas is achieved through techniques such as the use of wide slots, tuning stubs and offset microstrip feed. A conventional narrow slot antenna has limited bandwidth, whereas wide-slot antennas exhibit wider bandwidth [28]. A rotated wide square slot fed by a  $50\ \Omega$  microstrip line is designed for bandwidth enhancement [34]. It has been found that, the impedance bandwidth of a wide slot antenna can significantly be improved by optimizing the rotating angle of slot and length of microstrip line. By selecting the rotating angle from  $40^\circ$  to  $50^\circ$  and length of microstrip line from 31.5 to 32 mm at 4.5 GHz operating frequency, a (-10 dB) impedance bandwidth of 2.2 GHz (about 3400–5600 MHz) is achieved which is four times of conventional microstrip line fed wide slot antenna. Also, the antenna gain within the operating band is measured and studied, and a 2-dB gain bandwidth of at least 1 GHz is achieved [34].

Later, by modifying the slot shape from rotated square to rhombus-like wide-slot excited by offset microstrip feed line loaded with circular stub, the bandwidth further increased. This slot antenna reached an operating bandwidth of 3.23 GHz (2.68-5.91GHz) which is about six times that (543 MHz) of a conventional microstrip line fed printed wide-slot antenna. Also, the gain variations were less than 3 dBi, with a peak gain of about 4.5 dBi [35]. When the rhombus slot fed by microstrip line loaded with a pair of parasitic strips, 4.29 GHz (1.80-6.09 GHz) bandwidth was achieved with gain variation of around 3 dB with a peak gain of 5 dBi [36].

The rotated square slot by embedding a parasitic patch into the centre of slot was reported. The rotated square slot exhibits two resonances and after loading the parasitic patch within slot the lower resonance was decreased and the higher frequency was



increased. Therefore, wide-slot antenna with broadband bandwidth of 2.23-5.35 GHz (80%) with peak gain of 4.5 dBi was achieved [37]. Another approach of using the pair of parasitic patches along the microstrip feed line was reported to have an additional resonance for bandwidth enhancement [38]. Here, the enhanced impedance bandwidth, defined by voltage standing wave ratio (VSWR) less than 2, is about 136% ranging from 2.1 to 11.1 GHz with gain variation of around 3 dB with a peak gain of 5 dBi [38].

A hexagonal wide slot excited by a 50  $\Omega$  microstrip line with hexagonal tuning stub was proposed for bandwidth enhancement. This hexagonal slot antenna exhibits the 2:1 VSWR bandwidth of 1.75 GHz (1.92 to 3.67 GHz), which is about four times larger than the reference antenna [39].

A wide slot antenna fed with fork shaped microstrip line was designed to achieve UWB band (3.1 GHz to 10.6 GHz). By optimizing the length of the tuning stubs of fork like feed, an ultra-wideband performance can be achieved [40]. The measured -10 dB in impedance band from 2.5 GHz to 11.3 GHz is covered the whole UWB band. The radiation pattern is characterized by a quasi-Omnidirectional pattern in the XZ-plane and the radiation is vertical polarized. And it is observed that a 4 dB gain variation and phase linearity are achieved within the UWB band. In [33], a 1:1.5 VSWR bandwidth of 1 GHz is obtained at operating frequency around 2 GHz, which is approximately ten times comparable to the conventional microstrip line fed printed wide-slot antenna. It also achieved a 2 dB gain bandwidth of at least 0.5 GHz.

It has been seen that a properly designed, off-centered microstrip-fed [41-42], moderately wide slot antenna shows the wideband behaviour because dual resonances of similar radiation characteristics of a wide slot antenna are excited. This technique is based on manipulating the field distribution along an ordinary resonant slot structure using the feed line and creating a dual resonance behaviour. The field distribution along the slot at a frequency slightly above its natural resonance is manipulated by a narrow microstrip line feeding the slot near one of the two edges. By proper choice of the slot width, feed location, and microstrip feed line a fictitious second resonance can be created by establishing a null in the electric field distribution (through the so called fictitious short) along the slot near the feed line. This null is resulted from the superposition of the microstrip near field and the slot field. A wide bandwidth of 1.22 GHz (37%) with peak gain 2.5 dBi gain is achieved [41].

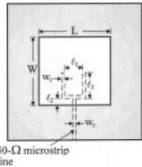
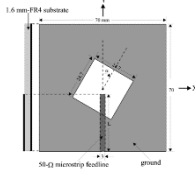
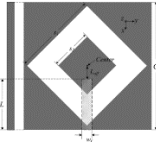
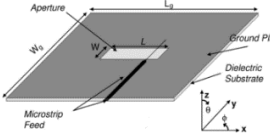
A multi-slot antenna fed by microstrip line is presented for bandwidth enhancement [43]. By employing the multi-slot configuration, multimode resonances with close

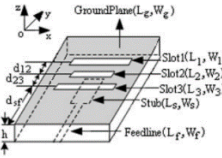
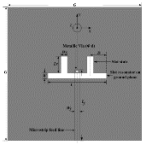
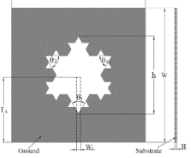
frequencies can be introduced and the impedance bandwidth of the antenna can be increased. it is shown in [43] that the -9.5 dB impedance bandwidth of the antenna is from 5.65 to 8.79 GHz (40%) with peak gain of 4dBi.

Another multi-mode resonance concept has been introduced in which two modes are excited in a single slot-line radiator by symmetrically introducing one or two pairs of slot stubs along the slot-line resonator near the nulls of electric field distribution of the second odd-order mode [44-45]. With the help of these stubs, the second odd-order mode can be gradually merged with its first counterpart, resulting in a wideband radiation characteristic with two resonances. This second mode is merged with the first one with the help of these stubs, in a wideband radiation characteristic with two resonances. The bandwidth of this reported slot-line antenna is increased up to 31.5% with 5.2 dBi peak in-band gain.

A slot antenna with fractal metasurface structures has been presented for wideband operation in [46]. In this structure the bandwidth is enhanced by selecting the suitable iteration angle, iteration factor, and iteration order. The reported results show the -10 dB impedance band of 1.45-4.86 GHz with maximum gain of 5.3 dBi. Table 2.1 compares a few of the reported wideband and ultrawideband slot antennas.

**Table 2.1** Performance comparison of existing wideband and ultra wideband antennas

Ref	Antenna design	Substrate ( $\epsilon_r$ , $\tan\delta$ , thickness (mm))	-10dB Impedance Band (GHz, %)	Overall dimension ( $\lambda_0$ )	Peak Gain (dBi)
[33]		4.4,0.02,0.8	1.82–2.91 (46.08)	$0.87\lambda_0 \times 0.87\lambda_0 \times 0.006\lambda_0$	4.5
[34]		4.4,0.02,1.6	3.40–5.60 (48.89)	$1.05\lambda_0 \times 1.05\lambda_0 \times 0.024\lambda_0$	5.2
[37]		4.4,0.02,1.6	2.23–5.35 (82.32)	$0.88\lambda_0 \times 0.88\lambda_0 \times 0.02\lambda_0$	4.5
[41]		3.4,0.003, 0.5	3.3–4.85 (37)	$2.03\lambda_0 \times 1.62\lambda_0 \times 0.006\lambda_0$	2.6

[43]		2.65, 0.001, 1	5.65–8.79 (40)	$1.20\lambda_0 \times 1.20\lambda_0 \times 0.024\lambda_0$	4
[45]		3.55, 0.0027, 0.813	2.30–3.20 (32.7)	$1.38\lambda_0 \times 1.38\lambda_0 \times 0.007\lambda_0$	4
[46]		3.5, NA, 1.6	1.45–4.86 (108)	$1.26\lambda_0 \times 1.26\lambda_0 \times 0.017\lambda_0$	5.3

In the present scenario a lot of efforts are put in the development of FCC-UWB antennas (range 3.1 - 10.6 GHz) but there exists no literature on antenna designs for the UWB spectrum provision in Europe/India (range 6.0 – 8.50 GHz) except [43,47].

## 2.2 Directional/high gain slot antenna

The basic slot antenna by default has bidirectional radiation pattern and possess gain range (2-5 dBi) in the wideband/UWB band frequencies [28,31-43]. There are a variety of applications where directional and high gain antennas are desirable, including wireless body area networks notably for medical surveillance, ground penetrating radar, and level probing radar. So, in this context, several approaches for achieving a directional and high gain antennas such as reflector loading, superstrate loading and combination of both have been reported, some of which are detailed below.

A bidirectional slot antenna can be converted into the directional slot by placing a plane reflector sheet at the one side of substrate parallel to the slot surface. The dependence of the input impedance and radiation characteristics of the slot on the reflector spacing has been discussed by Yoshimura [32] which suggests that the optimum spacing should be one quarter-wavelength from the slot. In order to minimize the effects of the human body proximity and body exposure to EM radiation or wireless body area network, a directional slot with an added plane reflector sheet is discussed. The reported results demonstrate a front-to-back ratio of more than 10 dB in a wide bandwidth ranging from 3.5 to 7 GHz, as well as increased efficiency and specific absorption rate (SAR) values [48].

An alternative approach for directivity enhancement of slot antenna using a grounded metamaterial slab is proposed [49]. This approach is applied for two different configurations. In first configuration two different dielectric layers are used for designing antenna and the metamaterial slab whereas in the second configuration only a single layer

of dielectric is used for both antenna and slab design. Despite the directivity enhancement, an improvement of impedance bandwidth of about 10.74% is observed for the first configuration whereas a significant compactness is achieved for the second configuration.

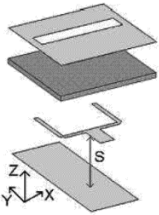
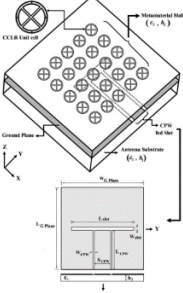
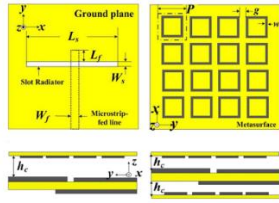
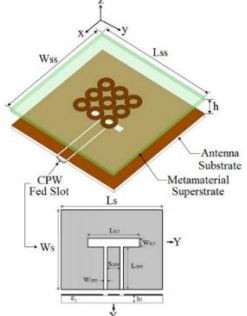
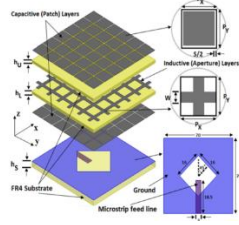
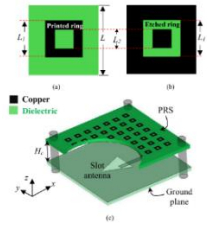
A mu-near-zero metasurface and zero index metamaterial as a superstrate consisting of a periodically square closed ring and circular ring have been proposed for gain and bandwidth enhancement of microstrip slot antennas [50-51]. It is found that using the metasurface above the slot antenna, we can obtain a unidirectional antenna and improve the gain by up to 9 dBi with a wide bandwidth of 25 % [50].

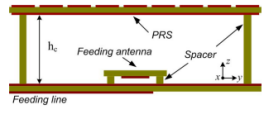
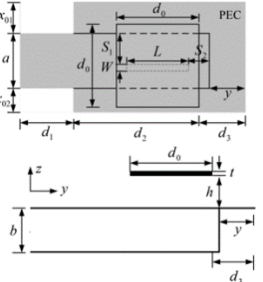
Dual layer bandpass as a superstrate allowing in-phase transmission and band stop frequency selective surfaces (FSS) as a reflector allowing in-phase reflection and metasurface combined with a wideband slot antenna for gain enhancement has been studied and demonstrated [52-55]. This dual layer bandpass FSS improves the 4dBi gain with peak gain of 9 dBi while the band stop FSS improves the 3 dBi with peak gain of 8.4 dBi over the entire -10 dB impedance band of 4-7 GHz.

Wideband Fabry-Perot antennas with gain enhancement using metamaterial based partially reflective surface (PRS) have been proposed [56-57]. The Fabry-Perot cavity is established between the single layer metamaterial based partially reflective surface (PRS) and simple feeding slot antenna. A  $6 \times 6$  array of the unit cells is optimized to produce a positive reflection phase gradient required for the gain enhancement. antenna demonstrate an impedance bandwidth of 13.1–15.3 GHz (15.5%) with a gain enhancement up to 8.2 dB [56] and an impedance bandwidth of 14.8–18.5 GHz (22.2%) with a gain improved to 11.2 dB [57]. The bandwidth enhancement of the Fabry-Perot resonator antenna is attributed to the positive reflection phase gradient of an electromagnetic band gap (EBG) structure, which is constructed by the combination of two complementary frequency selective surfaces (FSSs) [58].

An epsilon-very-large (EVL) based metasurface is loaded on top of the slot layer to improve its radiation characteristics and to reduce the physical size of the antenna. The effect of a metallic reflector and an artificial magnetic conductor (AMC) cavity on the metasurface based slot antenna is studied thoroughly to improve its forward gain and to reduce the back scattering. Finally, a wideband compact metasurface based antenna is proposed with two layers of metasurface having different permittivities [59-60]. Metasurface can also be used to design the frequency and/or polarization reconfigurable antennas which has also been discussed [61-64]. Table 2.2 compares a couple of the reported high gain and directional slot antenna designs.

**Table 2.2** Performance comparison of existing directional and high gain antenna designs.

Ref	Antenna design	Substrate ( $\epsilon_r$ , $\tan\delta$ , thickness (mm))	-10dB Impedance Band (GHz, %)	Overall dimension ( $\lambda_0$ )	Peak Gain (dBi)
[48]		2.2, NA, 1.58	4.00–6.50 (47)	$0.56\lambda_0 \times 0.77\lambda_0 \times 0.13\lambda_0$	8.5
[49]		Antenna: 4.4, 0.02, 1.6 Metamaterial slab: 3.55, 0.0027, 0.5	8.46–9.42 (10.74)	$1.79\lambda_0 \times 1.79\lambda_0 \times 0.626\lambda_0$	6.02
[50]		Antenna: 4.2, 0.02, 1.6 Metasurface slab: 4.2, 0.02, 0.8	2.25–2.75 (20)	$0.9\lambda_0 \times 0.9\lambda_0 \times 0.127\lambda_0$	9
[51]		Antenna: 3.38, 0.0027, 0.8 Metamaterial superstrate: 4, 0.005, 0.8	8.0–9.0 (11.76)	$2.55\lambda_0 \times 2.55\lambda_0 \times 0.13\lambda_0$	8.4
[52]		Antenna: 4.4, 0.02, 1.6 FSS superstrate: 4, 4, 0.02, 0.8	5.0–8.0 (42.86)	$1.63\lambda_0 \times 1.63\lambda_0 \times 0.75\lambda_0$	9
[56]		Antenna: 3.38, 0.003, 1.53 Meta superstrate: 3.38, 0.003, 1.53	13.1–15.3 (15.5)	$2.84\lambda_0 \times 2.84\lambda_0 \times 0.7\lambda_0$	13.78

[58]		Antenna: 2.2, 0.009, 0.787 EBG layer: 2.2, 0.0009, .787	8.6-11.2 (26.26)	$2.4\lambda_0 \times 2.4\lambda_0 \times 0.5\lambda_0$	13.8
[67]		Waveguide slot antenna with Metallic superstrate	7.7-9.7 (23)	$2.54\lambda_0 \times 3.06\lambda_0 \times 0.92\lambda_0$	12

Besides using the surfaces with some specific pattern such as metamaterial, frequency selective surfaces, and electronic band gap structure, simple conducting sheet can also be used as a superstrate to enhance the gain of the antennas due to the formation of resonant cavity [65-67]. The advantages of using simple conducting sheets allow looser tolerances of fabrication, assembly, and integration.

### 2.3 Wideband-flat gain slot antennas

Stable performance, such as gain flatness and radiation characteristics, is desirable over their entire impedance bandwidth for ultra wideband applications for meeting the time-domain requirements. Several antennas that extend the 3 dB gain bandwidth have been reported in the literature, mainly using three approaches. The first involves using array antennas as a radiating source [68-69]. Because the array source is used, the electric fields are more evenly distributed, resulting in more efficient radiation. As a result, the 3-dB gain bandwidth is increased. However, this approach may necessitate more space for the array source, resulting in a larger overall antenna size. Additionally, array sources use additional feed networks, which can complicate the design and result in more losses.

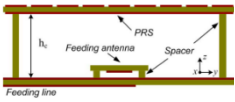
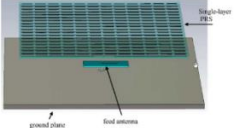
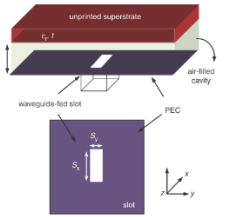
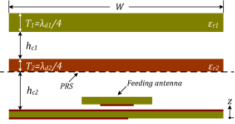
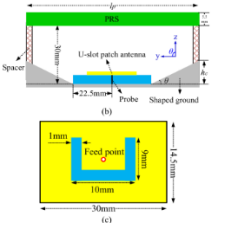
The second approach is to optimize the PRS structure by utilizing gradient index metamaterial-based superstrates [58,70-73], or multilayer superstrates with input reflection phases increasing with frequency [74-75]. The phase difference from the spherical wavefront can be adjusted, by employing dissimilar size PRS units, resulting in a 3-dB improvement in gain bandwidth from 7.99 % to 12.2 % [70].

The FPC antenna suggested in [71] uses a single-layer double-sided dipole-type PRS structure to produce a 3-dB gain bandwidth of 15.7%. In [74], a three-layer PRS superstrate is used to achieve a wideband FPC antenna with a 3-dB gain bandwidth of about 15%.

The antenna in [75] achieve a 3-dB gain bandwidth of 25.8% by employing a multi-layer all-dielectric PRS structure. The third approach is to modify the shape of the ground plane by altering the inner cavity, the cavity height is decreased gradually, and the reflection

phase differences can be compensated. This way, the resonance condition can be achieved in a broader operating frequency range. As a result, FPC antennas with shaped ground structures can reach a 3-dB gain bandwidth of more than 20 % [76]. Table 2.3 compares some of the reported antenna designs for flattening the gain response thereby providing a wide 3 dB gain-band. It is found that the techniques for flattening the gain response throughout entire operating band of the antenna have not been extensively investigated in the literature.

**Table 2.3** Performance comparison of existing antenna designs for gain flatness or wide 3dB gain-band

Ref	Antenna design	Substrate ( $\epsilon_r$ , $\tan\delta$ , thickness (mm))	-10dB Impedance Band (GHz, %)	Overall dimension ( $\lambda_0$ )	Peak Gain (dBi)	3 dB gain band (GHz, %)
[58]		Antenna:2.2,0.00 09,0.787 EBG layer: 2.2,0.0009,.787	8.6-11.2 (26.26)	$2.4\lambda_0 \times 2.4\lambda_0 \times 0.5\lambda_0$	13.8	8.6–11.4 (28)
[71]		Antenna:2.2, NA, 1.6 PRS layer: 2.2, NA, 1.6	11.7-15 (24.72)	$13.12\lambda_0 \times 13.12\lambda_0 \times$ $0.712\lambda_0$	16.2	11.1–13 (15.7)
[72]		Waveguide slot antenna with dielectric superstrate (9.2,0.0022,2.15)	10.3–16.4 (45.69)	$2.88\lambda_0 \times 2.88\lambda_0 \times$ $0.594\lambda_0$	16.5	10.43–12.37 (16.25)
[75]		Antenna:2.2,0.00 09,0.787 PRS layer: 6.15, 0.0019,1.9 Dielectric layer:2.2,0.0009, 3.175	13.8-19 (31.7)	$2.4\lambda_0 \times 2.4\lambda_0 \times 1.36\lambda_0$	15	13.5–17.5 (25.8)
[76]		Antenna:2.2, 0.0009, 3 PRS layer: 6.15, 0.0019, 5.5	4.96-6.02 (19.31)	$2.75\lambda_0 \times 2.75\lambda_0 \times$ $0.56\lambda_0$	16	5.10–6.3 (23)

In recent years, for enhancing the performance such as gain and bandwidth of antennas, various configurations of superstrate layers such as frequency selective surfaces [77-79], metamaterial and metasurfaces [80-85] are becoming more popular. Apart from that, metasurface lens layer loading [86-90] and lateral sheet loading [91] are other interesting ways to improve the antenna performance.

#### **2.4 Time domain analysis of UWB antenna**

Since UWB systems operate on pulsed mode than continuous wave carrier mode, the antenna's influence on the pulse both at the transmitter side and receiver side is also very critical in deciding the degree of distortion imparted to the pulse that carries the information. The information will not undergo serious distortion only if the antenna exhibits low dispersion. For this, UWB antennas should have flat magnitude of transfer function, linear phase response hence constant group delay over the band. Also, the fidelity factor (to be detailed in chapter 5) is an important attribute that implies the fidelity or correlation between transmitted pulse and received pulse. The fidelity factor achieves its maximum value of unity when the two pulses are equal, indicating that the transmitter-receiver antennas do not distort the pulse at all. In the worst-case scenario, where the two pulses are completely different in shape, the fidelity becomes to zero [4-5, 92]. Two different orientations of transmitter and reception antennas set at far-field separation, face-to-face and side-by-side, have been analysed for pulse distortion factor, or fidelity factor, which ranged from 70 % to 98 % [93-98].

The above literature analysis acts as a guideline for accomplishing the research objectives framed in Chapter 1. The research begins with a performance analysis of a wideband antennas, followed by an investigation of various approaches to improve its performance, such as bandwidth enhancement, gain and/or directivity enhancement, and gain flatness. Since UWB systems operate on pulsed mode than continuous wave carrier mode, the antenna's influence on the pulse both at the transmitter side and receiver side is critical in deciding the degree of distortion imparted to the pulse that carries the information. In other words, good time domain performance such as group delay and fidelity factor etc. is also one of the requirements of any UWB antenna. These findings lead to the development of a high gain directional slot antenna for ultrawide band applications.



## **2.5 Conclusion**

This chapter provided a thorough review of previous works published in the field of wideband slot antennas. Slot antenna designs were discussed from a variety of perspectives, including bandwidth enhancement, gain and/or directivity augmentation, gain flatness, and compact designs. Considering the above discussion, the next chapters propose and investigate a high gain directional slot antenna for directive ultra-wideband applications.

## Chapter 3

### Wide Band Bidirectional Slot Antenna Design

In this chapter, the radiation characteristics of microstrip slot antenna are investigated. Firstly, the design of a centred microstrip fed rectangular slot antenna is presented. Next discussed is the feed optimization for widening the impedance band i.e., frequency band with reflection coefficient  $(\Gamma_{in}) \leq -10$  dB for the European/Indian UWB recommendation of 6.0–8.5 GHz [2,4]. Following this, a design approach using conducting sheet loading to enhance the bidirectional gain uniformly throughout the operating band is demonstrated with the support of ANSYS HFSS simulations. Finally, all results are experimentally validated for a fabricated prototype and conclusions are drawn.

#### 3.1 Radiation characteristics of slot antennas

Microstrip slot antennas have gained popularity in recent years for usage in UWB applications because of their benefits of wide frequency bandwidth, low profile, lightweight, ease of manufacturing, and integration with other devices or RF circuitries. Compared to conventional patch antennas, slot antennas offer (i) larger bandwidth (ii) bidirectional radiation pattern (iii) low cross-polarization and (iii) less sensitivity to manufacturing tolerances [28]. Figure 3.1 depicts the conventional structure of a planar microstrip slot antenna using finite ground plane backed by a substrate, on which a rectangular slot of size  $L_{slot} \times W_{slot}$  is printed.

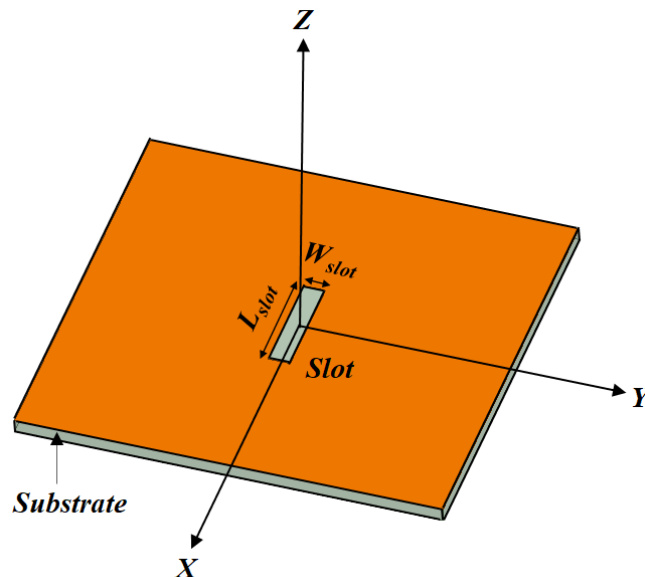


**Fig.3. 1** Structure of a conventional microstrip slot antenna with substrate and finite ground size.

Theoretically model of the slot antenna is derived from the theory of aperture antennas [31] wherein a rectangular aperture of size  $L_{slot} \times W_{slot}$  is placed on an infinitely conducting ground plane of infinite extent lying in the  $XY$ -plane as shown in Figure 3.2. As shown, the aperture is centred at the origin of the spherical coordinate system.

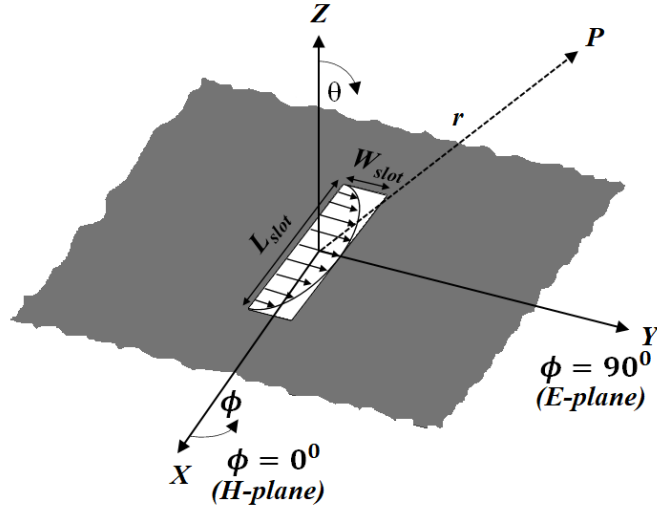


**Fig.3.2** Rectangular aperture placed on the infinite ground plane

### 3.1.1 Resonant frequency

The length of the slot (with respect to the feed position) decides the resonance frequency of the slot antenna. For the rectangular aperture, the resonant frequency of the  $TE_{mn}$ -like slot mode can be given approximately by the formula (eq. 3.1) [31].

$$f_r = \frac{c}{2\sqrt{\epsilon_{re}}} \sqrt{\left(\frac{m}{L_{slot}}\right)^2 + \left(\frac{n}{W_{slot}}\right)^2} \quad (3.1)$$

Where,  $m = 0, 1, 2, 3, \dots$  represents the number of half-wave field variation in the  $X$ -direction and  $n = 0, 1, 2, 3, \dots$  represents the number of half-wave field variation in the  $Y$ -direction of the slot,  $\epsilon_{re}$  is the effective relative permittivity of the medium surrounding the slot which can be calculated by using the same empirical formula (eq. 3.2) as that of a patch antenna which is valid in 3–10 GHz frequency range [99].

$$\epsilon_{re} = \frac{\epsilon_r + 1}{2} + \frac{\epsilon_r - 1}{2} \frac{1}{\sqrt{1 + 12t/W_{slot}}} \quad (3.2)$$

$$1 < \epsilon_{re} < \epsilon_r$$

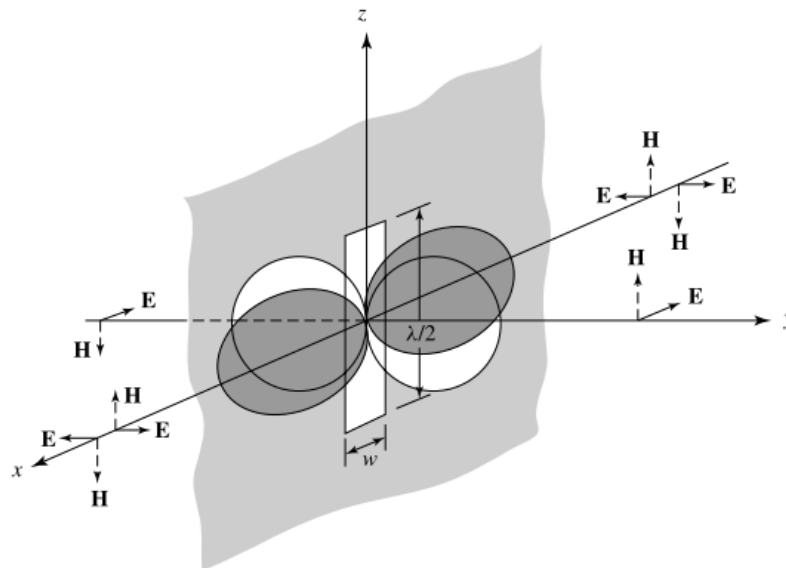
The  $\epsilon_r$  is the relative permittivity of the substrate material,  $t$  is the thickness of the substrate and  $W_{slot}$  is the width of the slot. Using equation (3.1), the length of the slot antenna can

be computed using the fundamental mode of the slot  $TE_{10}$  as shown in Figure 3.2. Therefore, the length of the slot  $L_{slot}$  is the half wavelength long  $\lambda_{eff}/2$ , where  $\lambda_{eff}$  is guided wavelength at resonant frequency  $f_r$  which depends on the relative effective permittivity  $\epsilon_{re}$  of the medium surrounding the slot.

$$L_{slot} = \frac{c}{2 f_r \sqrt{\epsilon_{re}}} = \frac{\lambda_{eff}}{2} \quad (3.3)$$

### 3.1.2 Radiation pattern

The radiation pattern is the magnitude of the far-zone field strength vs the angular position around the antenna, in the far-field of the antenna. Generally, for electrically small antennas, the region  $r < \lambda_0/2\pi$  ( $kr < 1$ ) is referred to as the near-field region, and  $r \gg \lambda_0/2\pi$  ( $kr \gg 1$ ) as the far-field region, where  $\lambda_0$  is the free-space operating wavelength. A more popular criterion for the far-field region of an antenna with the largest dimension  $D$  is  $r > 2D^2/\lambda_0$ , where  $D$  is the antenna's maximum overall dimension [31]. This criterion is set as the distance at which the spherical wave front of the transmitted waves illuminates the aperture of the receiving antenna with nearly uniform field intensity similar to that by a plane wave front [31]. The radiation pattern may be described in terms of the electric field strength in the far-field against the elevation angle ( $0 \leq \theta \leq \pi$ ) for appropriate azimuth angles ( $\phi = \text{constant}$  for 2D pattern) or for all azimuth angles ( $0 \leq \phi \leq 2\pi$  for 3D pattern). Babinet's Principle of optics [31,100] as extended to slot antennas [31] demonstrates that a slot will have the same radiation pattern as a dipole of the same dimensions and alignment, except that the  $E$ - and  $H$ -field distributions are interchanged as illustrated in figure 3.3.



(a)  $\lambda/2$  slot on a screen

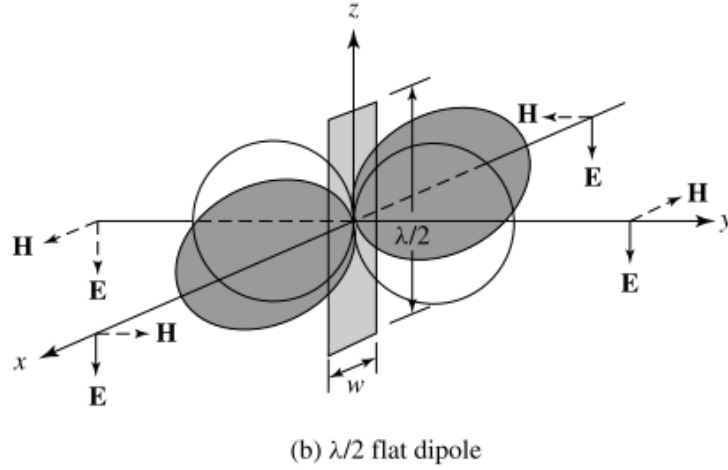


**Fig.3.3** Radiation fields of a half-wavelength (a) slot on an infinite sheet and (b) flat dipole in free space [31].

Assuming that the fundamental mode of the aperture fields (Fig.3.2) has  $TE_{10}$  distribution given by [31],

$$\mathbf{E}_a = \hat{\mathbf{a}}_y E_0 \cos\left(\frac{\pi}{L_{slot}} x'\right) \Bigg|_{-L_{slot}/2 \leq x' \leq L_{slot}/2}^{-W_{slot}/2 \leq y' \leq W_{slot}/2} \quad (3.4)$$

Where  $E_0$  is the maximum magnitude of the field and  $(x', y')$  represent the source coordinates. The aperture field in equation 3.4 is polarized along the  $y$ -direction with one half-wave variation in the  $x$ -direction, as seen in figure 3.2.

The far-field components radiated by the above aperture field can be written as [31],

$$E_r = H_r = 0 \quad (3.5)$$

$$E_\theta = -\frac{\pi}{2} C \sin \phi \frac{\cos X}{(X)^2 - \left(\frac{\pi}{2}\right)^2} \frac{\sin Y}{Y} \quad (3.6)$$

$$E_\phi = -\frac{\pi}{2} C \cos \theta \cos \phi \frac{\cos X}{(X)^2 - \left(\frac{\pi}{2}\right)^2} \frac{\sin Y}{Y} \quad (3.7)$$

$$H_\theta = -E_\phi / \eta_0 \quad (3.8)$$

$$H_\phi = E_\theta / \eta_0 \quad (3.9)$$

Where  $X$ ,  $Y$  and  $C$  are defined as follows,

$$X = \frac{kL_{slot}}{2} \sin \theta \cos \phi \quad (3.10)$$

$$Y = \frac{kW_{slot}}{2} \sin \theta \sin \phi \quad (3.11)$$

$$C = j \frac{L_{slot} W_{slot} k E_0 e^{-jkr}}{2\pi r} \quad (3.12)$$

Where  $r > 2D^2/\lambda$  the far-field distance.

From the figure 3.2, the principal plane co-polarized patterns can be defined as follows,

***E*- plane or *yz*-plane pattern ( $\phi = \pi/2$ ):**

$$E_r = E_\phi = 0 \quad (3.13)$$

$$E_\theta = -\frac{\pi}{2} C \sin \phi \frac{\cos X}{(X)^2 - (\frac{\pi}{2})^2} \frac{\sin Y}{Y} \quad (3.14)$$

***H*- plane or *xz*-plane pattern ( $\phi = 0$ ):**

$$E_r = E_\theta = 0 \quad (3.15)$$

$$E_\phi = -\frac{\pi}{2} C \cos \theta \cos \phi \frac{\cos X}{(X)^2 - (\frac{\pi}{2})^2} \frac{\sin Y}{Y} \quad (3.16)$$

The above pattern functions after normalization are plotted figure 3.4. As expected, the radiation pattern of the slot antenna is similar to that of a dipole antenna with the difference that the shapes of the *E*-plane and *H*-plane patterns are interchanged.

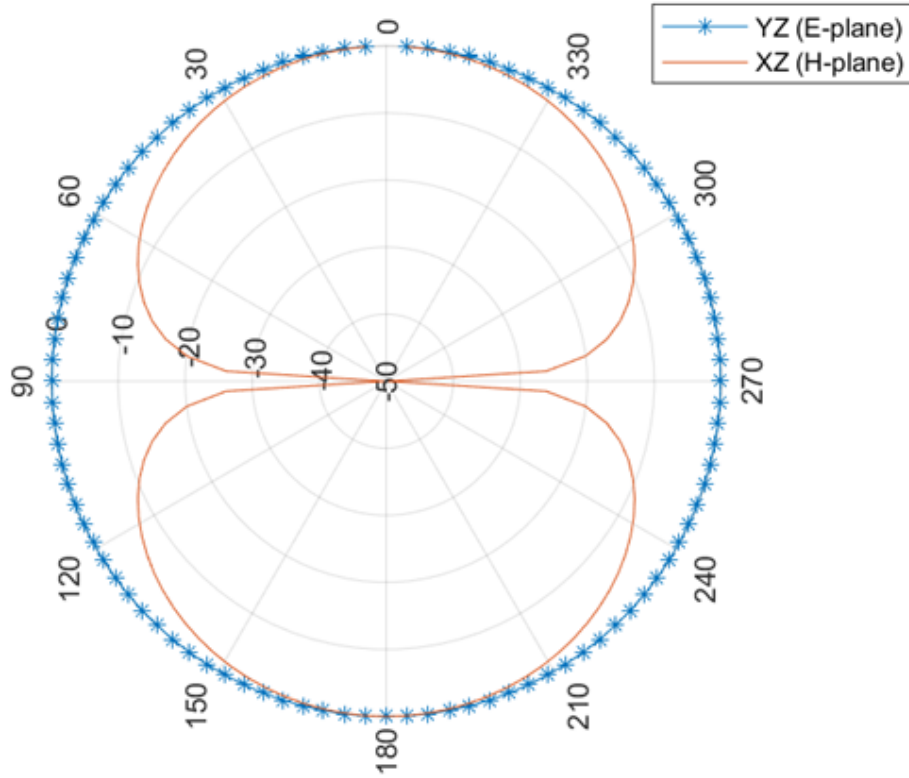


**Fig.3.4** Theoretical 2D radiation patterns of the rectangular aperture (in fig.3.1)

The directivity of the antenna ( $D$ ) is defined as the ratio of the maximum radiation intensity in the main beam to the average radiation intensity through all space [31].

$$D = \frac{U_{max}}{U_{av}} = 4\pi \frac{U_{max}}{P_{rad}} \quad (3.17)$$

$$\text{where } P_{rad} = \int_{\theta=0}^{\pi} \int_{\phi=0}^{2\pi} U(\theta, \phi) \sin \theta d\theta d\phi \quad (3.18)$$

where  $P_{rad}$  is the radiated power and  $U_{max}$  is maximum the radiation intensity (W/unit solid angle). An isotropic antenna transmits the same amount of energy in all directions hence holds  $D = 1$  or 0 dB, the absolute lower limit for any antenna. Thus, the directivity is frequently expressed in relation to the isotropic radiator's directivity, using the unit dBi. The antenna gain ( $G$ ) considers the antenna's efficiency along with its directional capabilities. It is defined as the ratio of the radiation intensity in a given direction to the radiation intensity that would be produced if the antenna's input power was emitted isotropically. The expression for the gain is given by

$$G = 4\pi \frac{U(\theta, \phi)}{P_{in}} \quad (3.19)$$

Where  $U(\theta, \phi)$  denotes the radiation intensity and  $P_{in}$  is the antenna's total input power.

The radiation efficiency ( $\eta_{rad}$ ) is the ratio of the total radiated power ( $P_{rad}$ ) to the total input power ( $P_{in}$ ) fed to the antenna as,

$$P_{rad} = \eta_{rad} P_{in} \quad (3.20)$$

where ( $\eta_{rad}$ ) is the antenna radiation efficiency, which is affected by the antenna's losses such as dielectric and conductor losses. And the gain-directivity relationship is defined by,

$$G(\theta, \phi) = \eta_{rad} D(\theta, \phi) \quad (3.21)$$

The pair of orthogonal polarization components, i.e., co-polarization and cross-polarization on each point of the radiation sphere, may be used to further describe the radiation characteristics. The desired polarization of the radiated wave is represented by co-polarization, whereas the orthogonal or undesired polarisation is represented by cross-polarization. For a linearly polarised antenna, the isolation between the co-polarization and cross-polarization components should be 10 dB or above in general.

### 3.2 Slot antenna design using ANSYS HFSS

In the practical implementation of the slot antenna, the aperture field of (eq. 3.4) is excited by using a suitable feeding mechanism such as a y-directed-open ended-microstrip line constructed on the same dielectric substrate but on the opposite side. Microstrip line feed is chosen as it is compatible with planar structures and easily fabricated. Such a practical slot antenna will experience feed perturbation and finite ground plane effects [28,31,99] which are not accounted by the above theoretical model. Thus, for the correct judgement of the resonant frequency, pattern shape and polarization purity of the antenna we need full-wave simulation techniques such as ANSYS HFSS.

Microstrip slot antennas can be designed with narrow slots or wide slots. The so-called slot aspect ratio is defined as the ratio of the slot width to slot length. Wide-slot antennas

generally provide wider bandwidth than narrow slots [28,42]. Although wide-slots have higher cross-polarization [28], careful design can keep the cross-polarization within tolerable levels. Generally, slot antennas are resonant structures hence exhibit limited bandwidth. To enable wideband or ultra-wideband bidirectional communication, various bandwidth enhancement designs such as offset fed slot, fork-like microstrip fed wide slot, and stub loaded slot are discussed before in the chapter 2. Among these, the offset feeding of the wide slot is the simplest technique to achieve wideband bidirectional radiation. Also, various superstrate loading techniques for gain enhancement such as dielectric sheet, metamaterial, frequency selective surface, electronic bandgap structure and fully conducting surface have also been effectively discussed in chapter 2 for patch antennas, dielectric resonator antennas, and directional slot antennas.

Superstrate based antennas often face frequency detuning issues due to the capacitive loading from the resonant cavity formed between the superstrate sheet and the ground plane of the primary antenna. This limits the gain-bandwidth of superstrate based wideband antennas [65,101]. Such frequency sensitive antenna designs are also unfriendly from fabrication, assembly, and integration points of view. Besides, the frequency dependent field distribution on the superstrate surface causes non-uniform gain enhancement in the band, and also causes increased side lobe radiation [65,67].

The above discussion motivates the author to investigate a new approach for improving the gain of a wideband slot antenna. Therefore, following section discusses two slot antenna designs for (i) bandwidth enhancement through feed optimization and (ii) gain enhancement through conducting sheet loading. The antenna design is optimized using ANSYS HFSS wherein standard FR4 material ( $\epsilon_r = 4.4$ ,  $\tan\delta = 0.02$  and thickness ( $t$ ) = 1.6 mm) and perfect electric conductor (PEC) sheets are adopted respectively for the substrate and metallic parts of the antenna.

### **3.2.1 Center fed Slot Antenna**

Figure 3.5 shows the geometry of the centre fed slot antenna that uses a square ground plane backed substrate of size  $L=W=50$  mm on which a rectangular slot of size  $L_{slot} \times W_{slot}$  is printed. The slot is fed by a simple  $50 \Omega$  microstrip line of length ( $L_f$ ) and width ( $W_f$ ), printed on the opposite side of the substrate. In the antenna, the location of the microstrip feed line is the center of the slot itself and the length ( $L_f$ ) is used to tune the impedance matching for a given slot size.



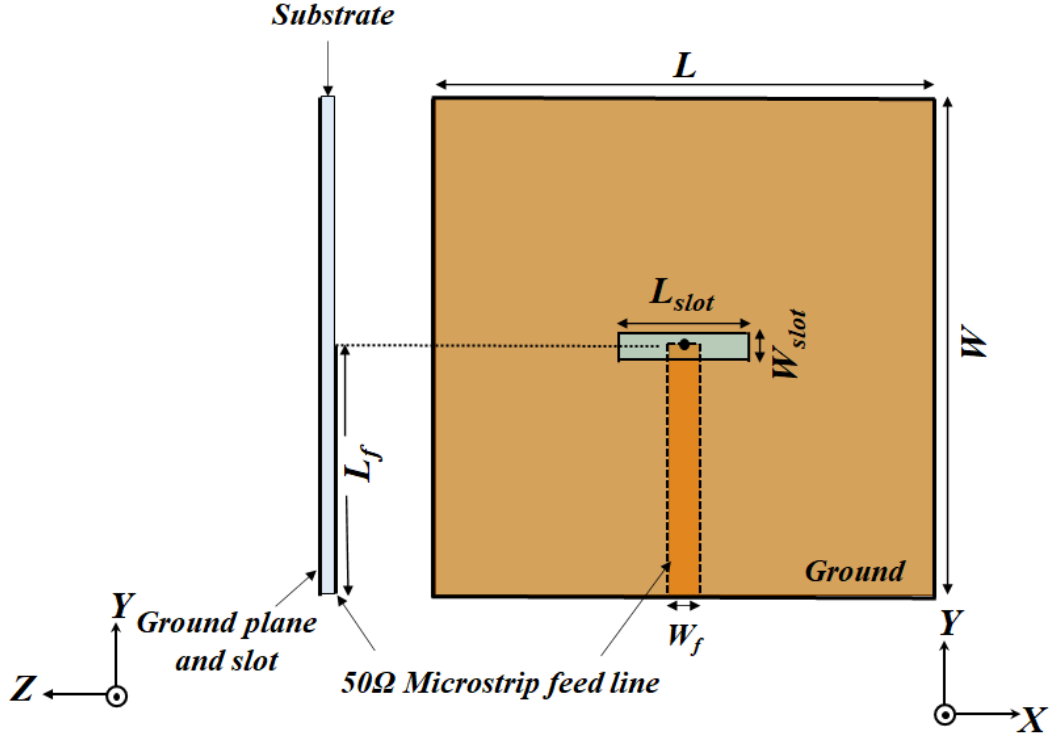


**Fig.3.5** Geometry of the center-fed slot antenna in the Side view (XZ-plane) and Top view (XY-plane).

To start modelling a basic slot antenna for the fundamental mode ( $TE_{10}$ ) resonant frequency of  $f_r = 6$  GHz, the length of the slot ( $L_{slot}$ ) is calculated by using the expression (3.22) where the effective relative permittivity  $\epsilon_{re}$  can be calculated from empirical equation (3.23) which is valid in 3-10 GHz frequency range [31,99].

$$L_{slot} = \frac{c}{2 f_r \sqrt{\epsilon_{re}}} = \frac{\lambda_{eff}}{2} \quad (3.22)$$

$$\epsilon_{re} = \frac{\epsilon_r + 1}{2} + \frac{\epsilon_r - 1}{2} \frac{1}{\sqrt{1 + 12 t / W_{slot}}} \quad (3.23)$$

As per the above equations, the effective permittivity  $\epsilon_{re}$  depends on  $W_{slot}$ , hence  $L_{slot}$  will also depend on  $W_{slot}$ . So, to find out the correct resonant length of the slot, at a constant frequency  $f_r = 6$  GHz, the equations are calculated in the range  $2 \text{ mm} \leq W_{slot} \leq 16 \text{ mm}$ , and the results are furnished in Table 3.1. As the table shows,  $\epsilon_{re}$  ranges from 3.22 to 3.85, with an average value of 3.62. Theoretically, the length of the slot  $L_{slot}$  corresponds to  $\epsilon_{re} = 3.62$  is obtained from equation (3.22) which is 13.14mm. Thus, to begin,  $L_{slot} = 13 \text{ mm}$  was chosen and figure 3.6 shows the reflection coefficient ( $|\Gamma_{in}|$ ) for an arbitrary aspect ratio

$W_{slot}/L_{slot} = 0.25$ , showing resonant frequency of 6.16 GHz. Figure 3.7 illustrates the electric field distribution in the slot aperture confirming the fundamental or  $TE_{10}$ -like mode excitation as mentioned in section 3.1. For the resonant frequency, the radiation pattern is shown in Figure 3.8 which is bidirectional as predicted by the theoretical pattern of Figure 3.4. The deviations in the simulated radiation pattern from the theoretical one are due to the feed perturbation, effect of substrate and finite ground plane effects as discussed before.

**Table 3.1** Calculated effective permittivity  $\epsilon_{re}$  at  $f_r = 6$  GHz using equations (3.23)

$W_{slot}$ (mm)	$\epsilon_{re}$ (Theoretical (Eq.3.23))
2	3.22
4	3.41
6	3.53
8	3.62
10	3.69
12	3.75
14	3.80
16	3.85

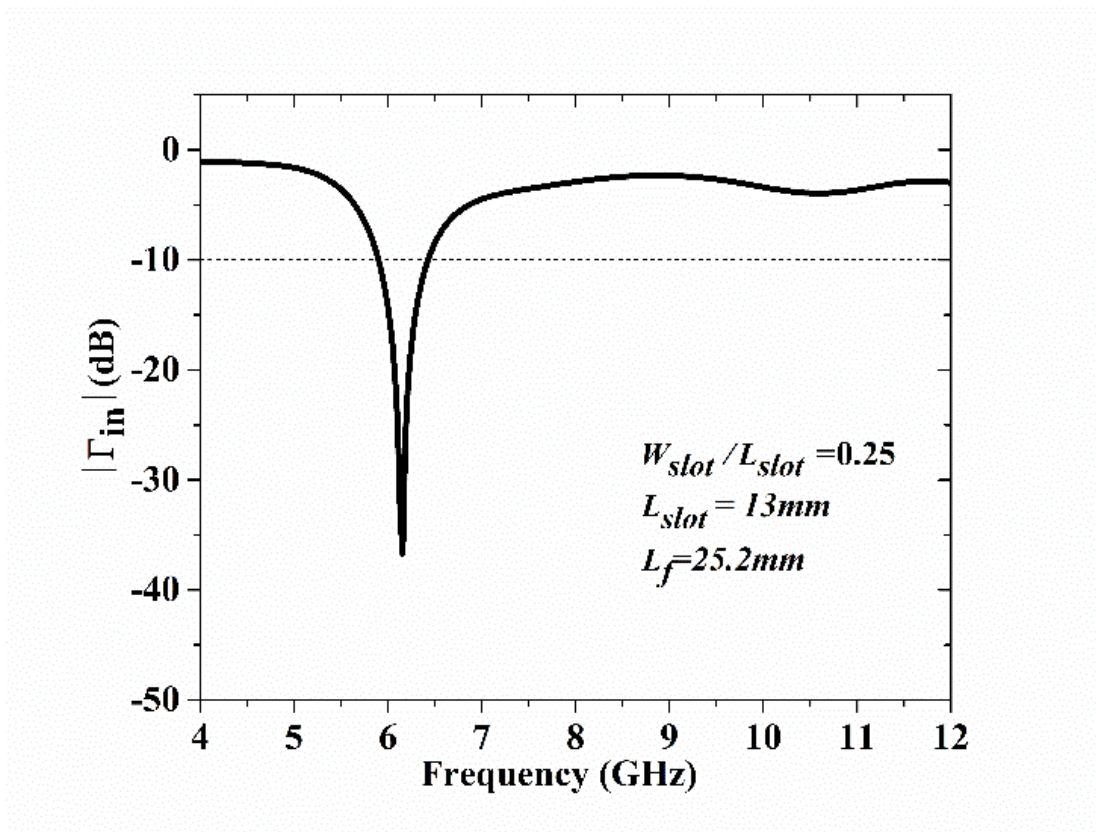


**Fig.3.6** Reflection coefficient of the microstrip slot antenna for  $L_{slot} = 13$  mm and  $W_{slot}/L_{slot} = 0.25$ .

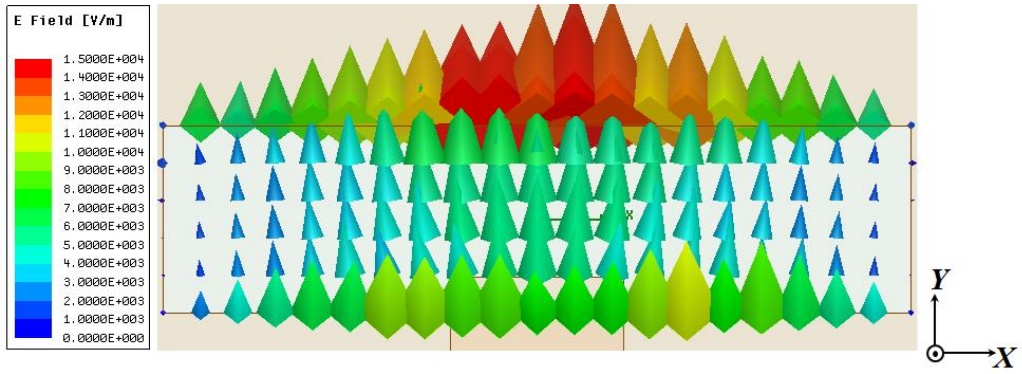


**Fig.3. 7** Simulated  $E$ -field distribution within the slot at 6.16 GHz

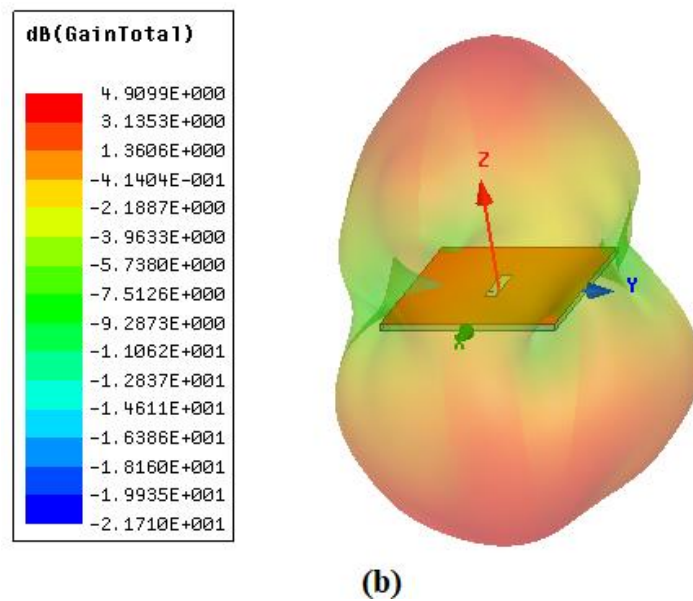
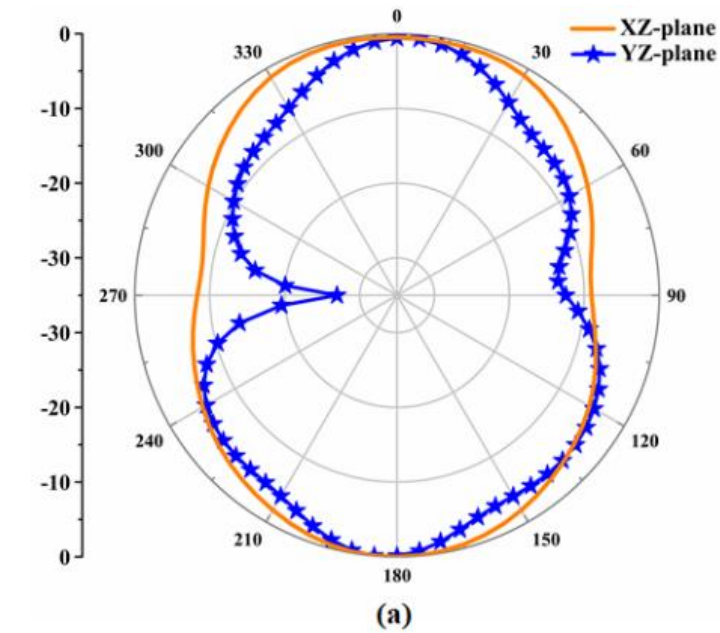


**Fig.3.8** Simulated radiation pattern of conventional rectangular slot antenna with (a) 2D and (b) 3D at 6.16 GHz

In the next section, a systematic parametric analysis for selecting the right aspect ratio of the slot by monitoring the impedance matching and radiation pattern is presented.

### 3.2.1.1 Slot size and aspect ratio ( $W_{slot}/L_{slot}$ ) selection

The effect of aspect ratio of the slot ( $W_{slot}/L_{slot}$ ) on the reflection coefficient ( $|\Gamma_{in}|$ ) of the microstrip slot antenna is simulated. Corresponding curves are shown in Figure 3.9. For each  $W_{slot}/L_{slot}$ , the microstrip length ( $L_f$ ) is re-optimized to achieve good impedance matching ( $|\Gamma_{in}| < -30$  dB at  $\sim 6$  GHz). Extracted antenna performance parameters are shown in Table 3.2 for comparison. As shown in Table 3.2, the resonant frequency  $f_r$  for all aspect ratios ( $W_{slot}/L_{slot}$ ) is almost constant at the design frequency of  $\sim 6$  GHz, showing that the slot impedance is mostly decided by  $L_{slot}$  than the width  $W_{slot}$ . As the aspect ratio is increased or when the width of the slot is increased for a fixed length, the impedance bandwidth of the primary resonance also increases, and the higher order resonant frequency significantly decreases. This second resonance is thus attributed to the half-wave variation along the slot width. For the range of aspect ratios ( $1 \geq W_{slot}/L_{slot} \geq 0.125$ ), the co-polar gain in both XZ and YZ- planes are higher than 4 dB. But cross-polar level, especially in the XZ-plane increases with slot width as understood from the Table 3.2. This is the direct effect of the higher order mode with X-polarized fields in the slot giving rise to high cross-polarization.

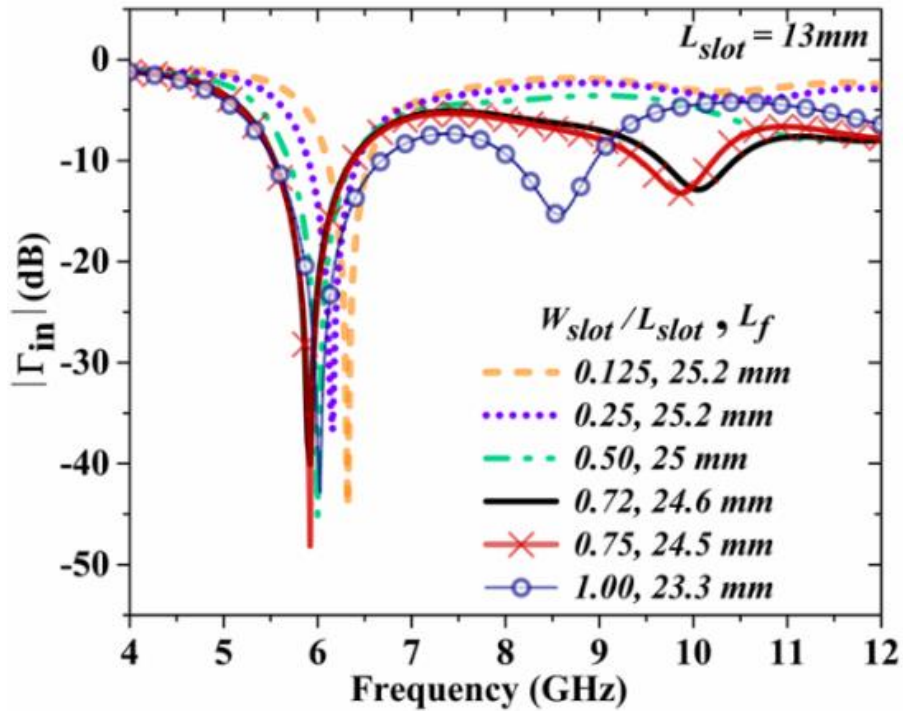


**Fig.3.9** Reflection coefficients for the center-fed slot antenna ( $L_{slot} = 13$  mm) for various slot width ( $W_{slot}$ ).

**Table 3.2** Performance characteristics of the of the center-fed slot antenna ( $L_{slot}=13$  mm) for various aspect ratios ( $W_{slot}/L_{slot}$ ).

$W_{slot}/L_{slot}$	$L_f$ (mm)	$ I_{in} $ (dB)	Resonant		Higher		Bandwidth (GHz, %)	Boresight Co-gain (dBi)		Peak cx-polar gain (dBi)		Peak cx-polar level (dB)	
			freq. $f_r$ (GHz)	Lower -10 dB freq. $f_l$ (GHz)	Higher -10 dB freq. $f_h$ (GHz)	$\phi=0^\circ$ (XZ- plane)		$\phi=90^\circ$ (YZ- plane)	$\phi=0^\circ$ (XZ- plane)	$\phi=90^\circ$ (YZ- plane)	$\phi=0^\circ$ (XZ- plane)	$\phi=90^\circ$ (YZ- plane)	
0.125	25.2	-44.28	6.32	6.1	6.55	0.45, 7.11	4.05	4.05	-14.52	-26.69	-18.57	-30.74	
0.25	25.2	-36.71	6.16	5.9	6.43	0.53, 8.60	4.3	4.3	-10.37	-18.60	-14.67	-22.09	
0.50	25	-45.16	6	5.69	6.37	0.68, 11.28	4.92	4.92	-9.97	-16.04	-14.89	-20.96	
<b>0.72</b>	<b>24.6</b>	<b>-40.09</b>	<b>5.92</b>	<b>5.54</b>	<b>6.36</b>	<b>0.82, 13.78</b>	<b>5.28</b>	<b>5.28</b>	<b>-9.41</b>	<b>-24.24</b>	<b>-14.69</b>	<b>-29.52</b>	
0.75	24.5	-48.14	5.92	5.54	6.37	0.83, 13.94	4.16	4.16	-7.61	-19.23	-11.77	-23.39	
1.00	23.3	-42.76	6.02	5.53	6.68	1.15, 18.84	4.78	4.78	-5.46	-19.31	-10.24	-24.09	

The effective permittivity ( $\epsilon_{re}$ ) of the antenna is now calculated using the simulated resonant frequency and eq. (3.22) and compared with that given by the empirical formula of (3.23) in Table 3.3. The simulated values are in decent matching with analytical ones for slot aspect ratio  $\leq 1$ .

An aspect ratio  $W_{slot}/L_{slot} = 0.72$  or ( $W_{slot}=9.36$  mm for  $L_{slot}=13$  mm) is chosen as a trade-off among the bandwidth (13.78 %), boresight gain (5.28 dBi), and cross-polar level ( $< -14$  dB) in both principal planes.

**Table 3.3** Calculated vs simulated effective permittivity for the center-fed slot antenna ( $L_{slot} = 13$  mm) for various aspect ratios ( $W_{slot}/L_{slot}$ ).

$W_{slot}/L_{slot}$	$W_{slot}$	$L_f$ (mm)	$f_r$ (GHz) (simulated)	$\epsilon_{re}$ (simulated (Eq.3.22))	$\epsilon_{re}$ (Theoretical (Eq.3.23))	$\epsilon_{re}$ Error (%)
0.125	1.625	25.2	6.32	3.33	3.17	4.99
0.25	3.25	25.2	6.16	3.51	3.35	4.83
0.5	6.5	25	6	3.70	3.55	4.03
<b>0.72</b>	<b>9.36</b>	<b>24.6</b>	<b>5.92</b>	<b>3.80</b>	<b>3.67</b>	<b>3.42</b>
0.75	9.75	24.5	5.92	3.80	3.69	3.05
1	13	23.3	6.02	3.67	3.78	-2.82
1.25	16.25	21.8	6.21	3.45	3.85	-10.35

### 3.2.1.2 Effect of Slot length for slot width =9.36mm

The impact of changing the slot length ( $L_{slot}$ ) while keeping the slot width ( $W_{slot}=9.36$  mm) constant on the slot antenna's reflection coefficient is analysed. Figure 3.10 depicts the corresponding reflection coefficient ( $|\Gamma_{in}|$ ) plots. The microstrip feed length ( $L_f$ ) is re-optimized for each length of slot to ensure good impedance matching. As expected, the resonant frequency decreases with increasing slot length, as shown in Figure 3.10. Table 3.4 compares the retrieved resonant frequency from the simulation to the theoretical resonant frequency derived using the formula above (equation 3.22) and shows that they are quite near to each other for each length of the slot.

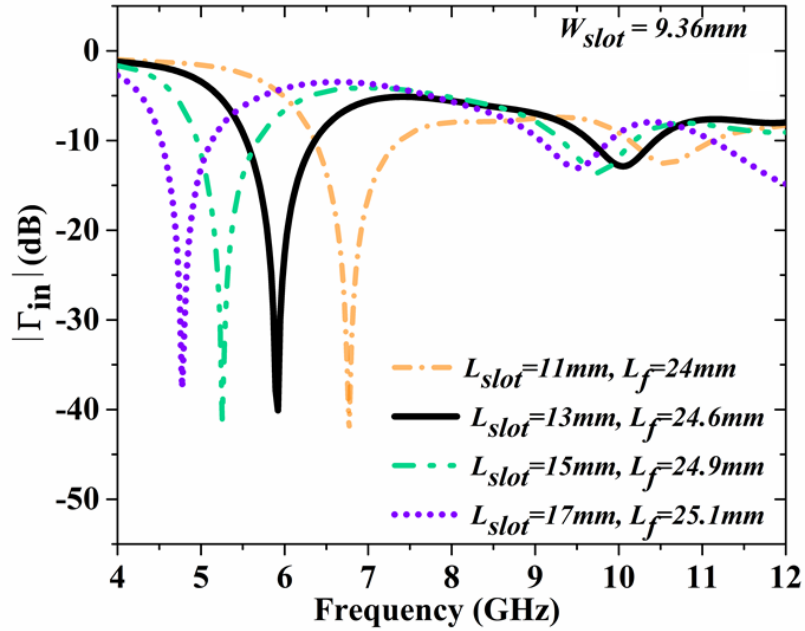


**Fig.3.10** Reflection coefficients for the center-fed slot antenna for the varying slot length

**Table 3.4** Comparison between the simulated and theoretical resonant frequencies as a function of slot length for constant slot width ( $W_{slot}=9.36$  mm).

$L_{slot}$ (mm)	$L_f$ (mm)	$f_r$ (GHz) (Simulated)	$f_r$ (GHz) (Eq. (3.22))	Error (%)
11	24	6.77	7.11	4.7
13	24.6	5.92	6.02	1.7
15	24.9	5.25	5.22	-0.5
17	25.1	4.77	4.61	-3.4

### 3.2.2 Off-center fed Slot Antenna for Wideband Operation

Based on the former analysis, a centre-fed microstrip slot of aspect ratio of  $W_{slot}/L_{slot} = 0.72$  and  $L_{slot}=13$  mm is chosen for the wideband design. The geometry is shown in Figure 3.11 in which the offset location of the microstrip feed is denoted by  $d$ . Figure 3.12 illustrates simulated variation in reflection coefficients for distinct off-centre parameter  $d/L_{slot}$ . In each scenario, the microstrip feed length  $L_f$  is re-optimized to provide good impedance matching. Table 3.5 summarizes the performance of the offset fed slot. Bandwidth optimization is achieved through adjustments of the microstrip feed parameters ( $L_f$  and  $d$ ). For  $W_{slot}/L_{slot} = 0.72$ ,  $L_f=25.2$  mm, and  $d/L_{slot}=0.35$  or  $d=4.55$  mm, the impedance bandwidth achieved is 5.92–8.56 GHz (36.46%) with peak boresight gain of  $\sim 3$  dBi within



the band. This frequency band covers the desired European/Indian UWB band i.e., 6–8.5 GHz. Figures 3.13 and 3.14 respectively show the reflection coefficient response and the near- aperture field in the slot at three unique dips 6.45 GHz, 7.52 GHz, and 9.52 GHz. Corresponding radiation patterns are shown in Figure 3.15.

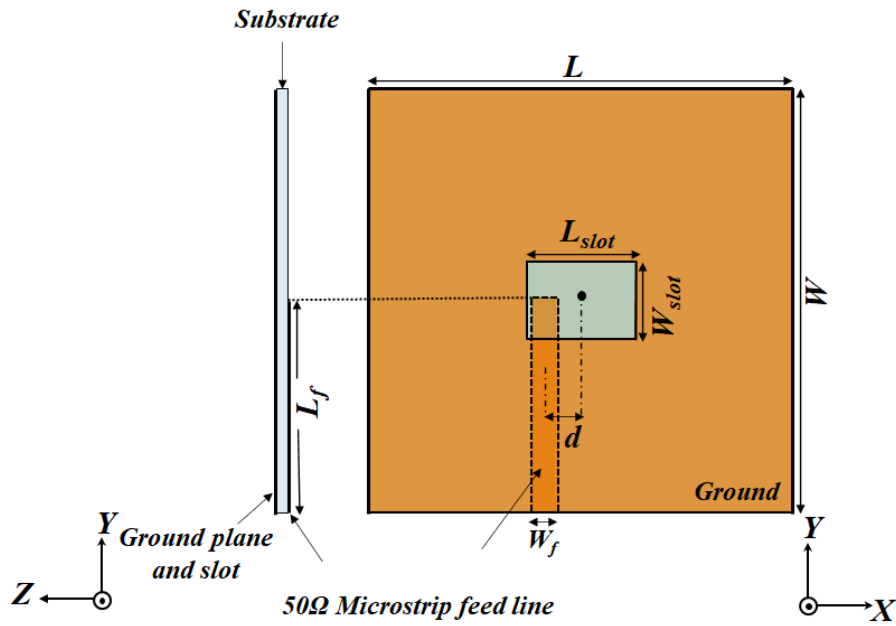


**Fig.3.11** Geometry of the offset-fed slot antenna with  $W_{slot}/L_{slot} = 0.72$ ,  $L_{slot} = 13$  mm.

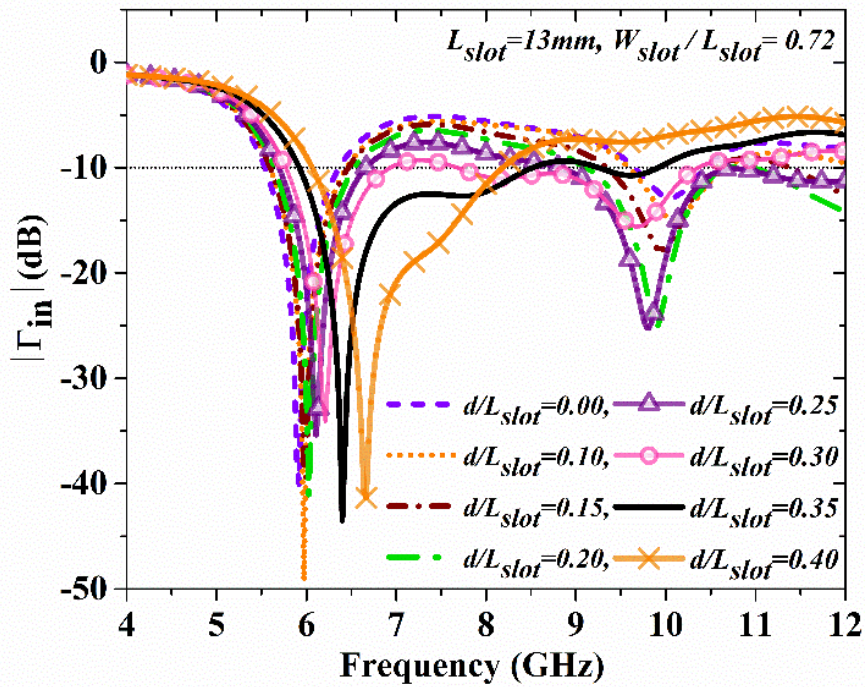


**Fig.3.12** Effect of offset parameter  $d/L_{slot}$  on the reflection coefficient of rectangular slot antenna



**Table 3.5** Performance characteristics of the slot antenna ( $W_{slot}/L_{slot} = 0.72$ ,  $L_{slot} = 13$  mm) with various offset parameter ( $d/L_{slot}$ )

$d/L_{slot}$	$L_f$ (mm)	$f_l$ (GHz)	$f_h$ (GHz)	$f_h/f_l$	BW (GHz, %)	Peak boresight gain (dBi)
0.00	24.6	5.54	6.36	1.15	0.82,13.78	5.28
0.10	24.5	5.6	6.45	1.15	0.85,14.11	2.89
0.20	24.8	5.65	6.54	1.16	0.89,14.60	2.18
0.25	24.9	5.7	6.66	1.16	0.96,15.53	4.75
0.30	25.1	5.77	6.94	1.20	1.17,18.41	3.29
<b>0.35</b>	<b>25.2</b>	<b>5.92</b>	<b>8.56</b>	<b>1.45</b>	<b>2.64,36.46</b>	3.02
0.40	25.5	6.07	8.19	1.35	2.12,29.73	3.66

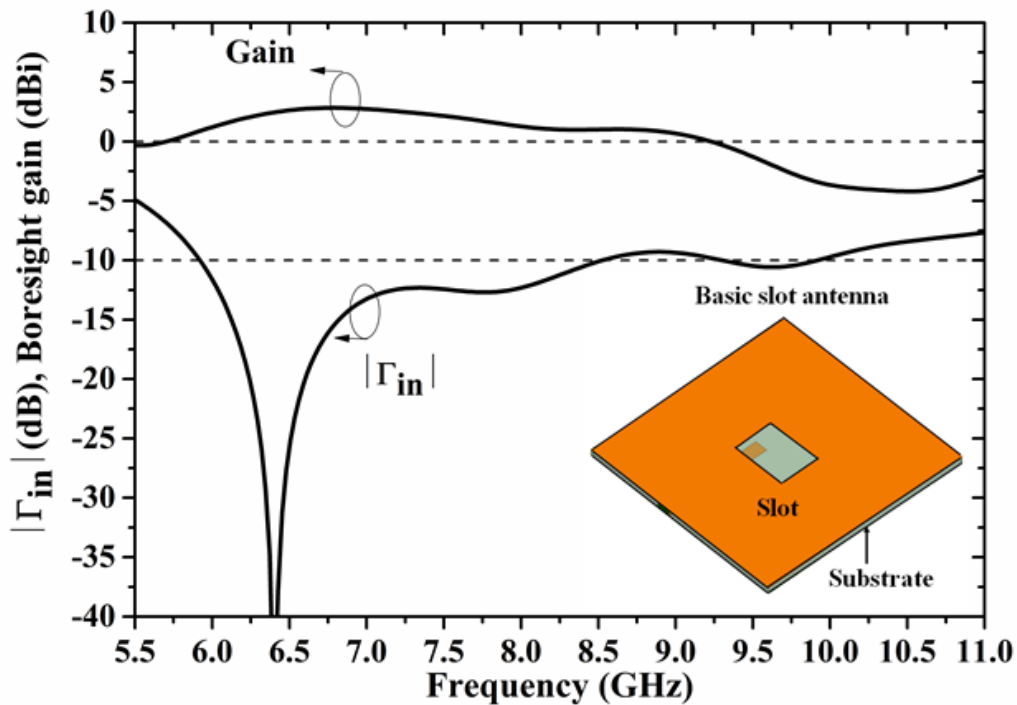


**Fig.3.13** Reflection coefficient and boresight gain Vs frequency of optimized offset-fed slot antenna ( $W_{slot}/L_{slot}=0.72$ ,  $L_f=25.2$  mm,  $d/L_{slot}=0.35$  and  $d=4.55$  mm).

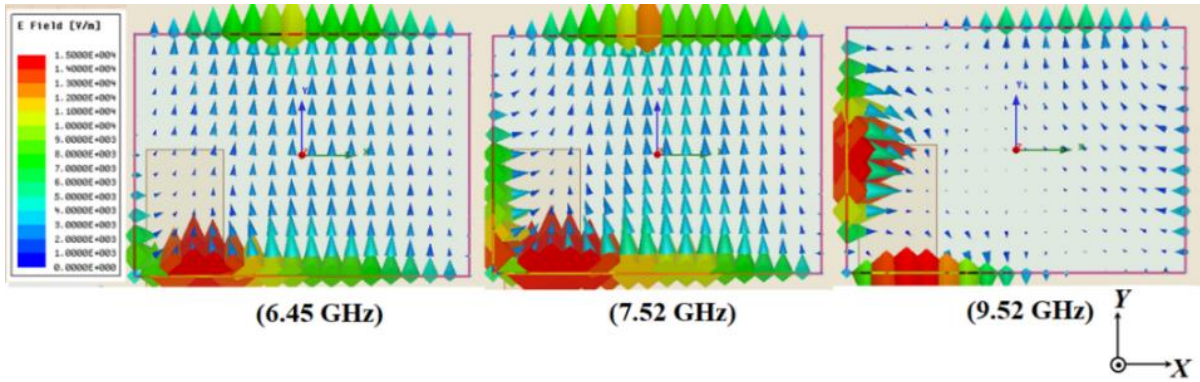


**Fig.3.14** Simulated electric-field distributions for a basic slot at 6.45 GHz, 7.52 GHz, and 9.52 GHz.

The electric field patterns of Figure 3.14(a) and (b) reveal  $y$ -polarized  $TE_{10}$ -like electric field variation respectively for the first and second modes. The variation of the electric field along the slot length is about  $\lambda/2$  for the first mode while it is less than  $\lambda/2$  for the second mode due to the fictitious short placed by the microstrip [41]. This is the cause of bandwidth enhancement by the offset feed that allows the merging of these two modes of identical polarization. The same effect is observed in the radiation patterns also wherein well-defined bidirectional patterns are observed for the first two modes whereas for the third mode, it is distorted.

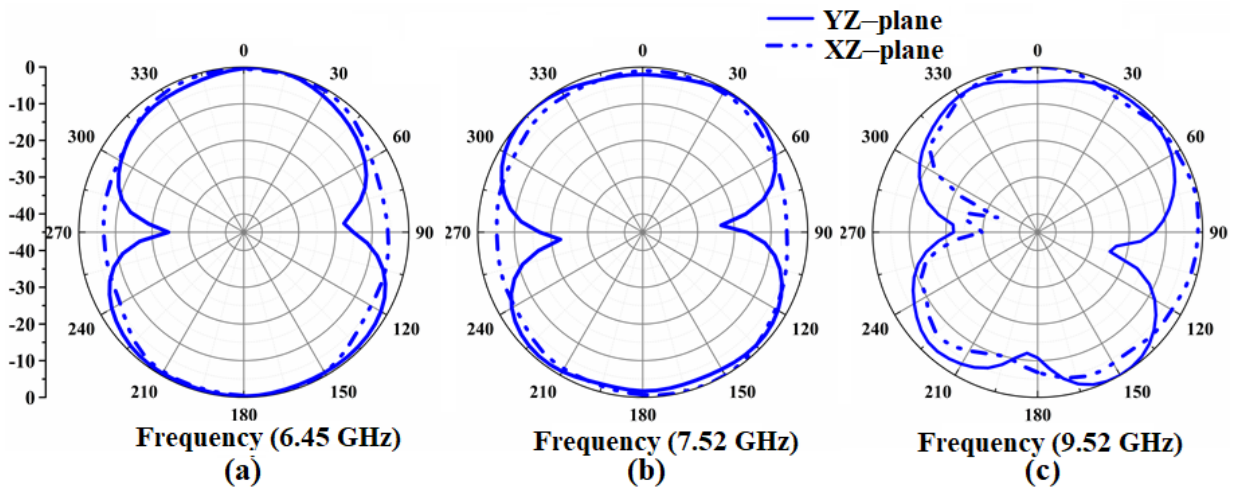


**Fig.3.15** Radiation patterns at (a) 6.45 GHz, (b) 7.52 GHz, and (c) 9.52 GHz for the optimized basic slot.

As the slot length was fixed in all the former optimizations, its variation is simulated here. Figure 3.16 shows the curves which are summarized in Table 3.6. It is found that for any slot length proper offset feed location gives wideband behaviour. As expected, the frequency band shifts to the lower side as the slot length increases, while the ratio of the

upper band frequency  $f_h$  to the lower band frequency  $f_l$  stays nearly constant. However, the desired operating band is achieved at  $L_{slot}=13$  mm which justifies its initial selection.

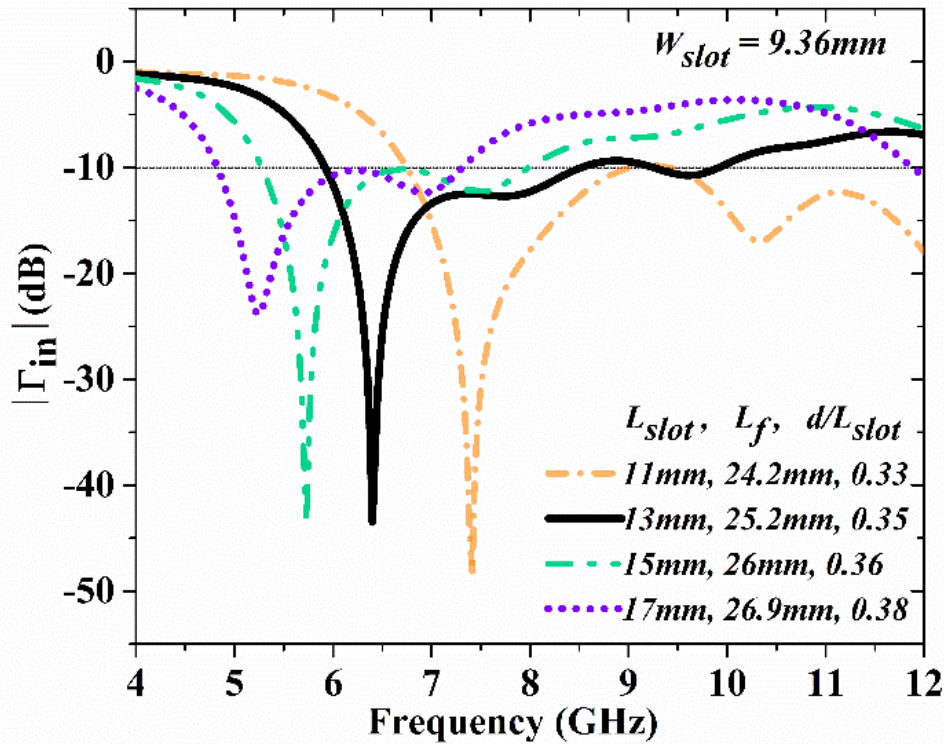


**Fig.3.16** Reflection coefficients for the offset fed slot antenna for the varying slot length  $L_{slot}$

**Table 3.6** Effect of slot length variation ( $L_{slot}$ ) of the offset-fed slot antenna with  $W_{slot}=9.36\text{mm}$

$L_s$ (mm)	$d/L_{slot}$	$L_f$ (mm)	$f_l$ (GHz)	$f_h$ (GHz)	$f_h/f_l$	BW (GHz, %)
11	0.33	24.2	6.75	9.41	1.40	2.66,32.92
<b>13</b>	<b>0.35</b>	<b>25.2</b>	<b>5.92</b>	<b>8.56</b>	<b>1.45</b>	<b>2.64,36.46</b>
15	0.36	26	5.28	7.99	1.51	2.71,40.84
17	0.38	26.9	4.83	7.31	1.51	2.48,40.85

### 3.2.3 Conducting Sheet Loading for Gain Enhancement

The primary aim of the proposed design is to enhance the gain of the wideband slot antenna over the original frequency band of 6–8.5 GHz. This is possible through a non-resonant design unlike existing resonant designs with superstrate loading [65,67]. In the proposed non-resonant design, a pair of conducting sheets is loaded in the vertical (XZ or YZ) plane of the slot on the two opposing ground plane edges. The proposed antenna structure is shown in figure 3.17.

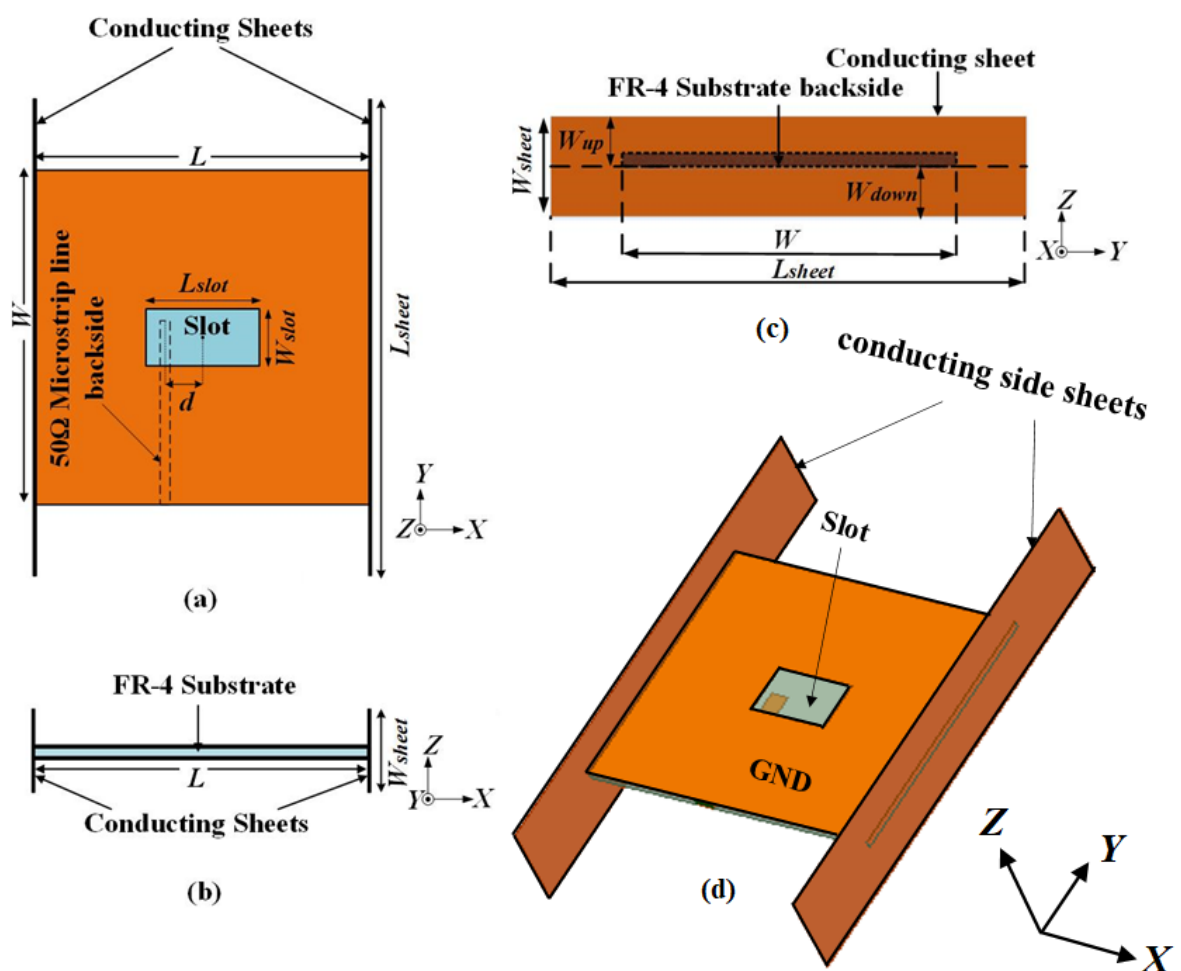


**Fig.3.17** Geometry of proposed antenna in (a) top view, (b&c) side views, and (d) 3D view.

In Figure 3.18, the illustrations of the rays and corresponding fields generated by the basic slot antenna are shown. The oblique rays ( $0 < \theta < 90^\circ$ ) give rise to the broad XZ-plane

pattern for the slot antenna (Figure 3.15). If the oblique rays can be converged towards the broadside direction ( $\theta = 0^\circ$ ), naturally the directivity can be increased. Thus, in the proposed design, a pair of conducting sheets is loaded in the  $YZ$ -plane of the slot on the opposing edges of the ground plane to form a parallel plate structure (Figure 3.17).

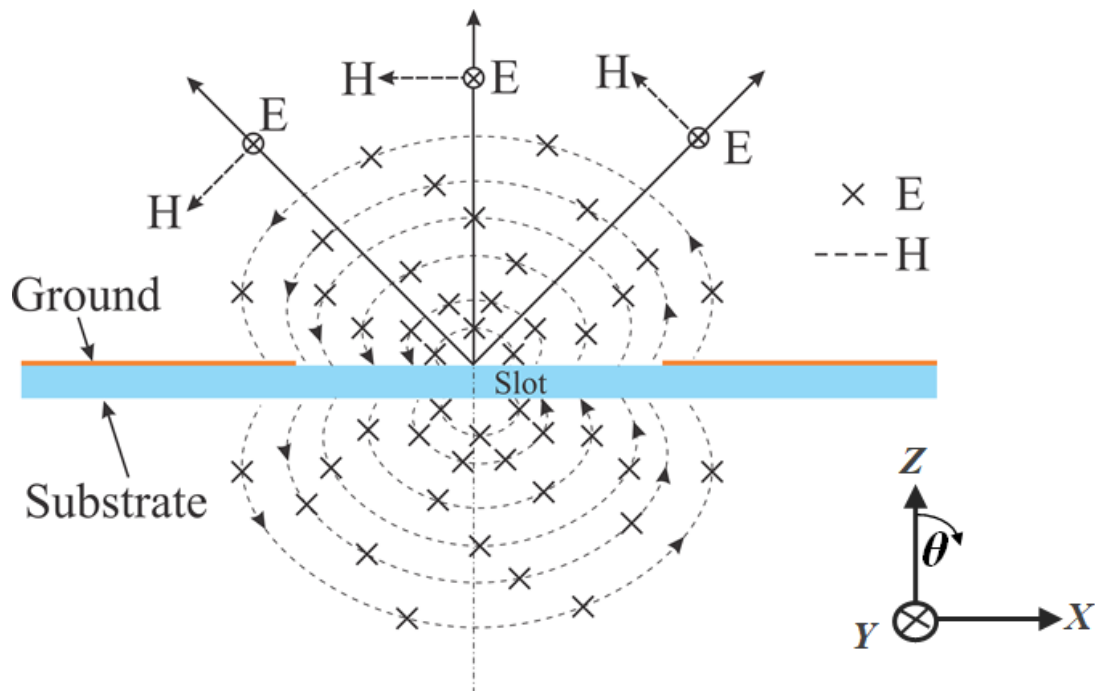


**Fig.3.18** Typical rays and corresponding  $E$  and  $H$ -fields radiated by the slot in vertical plane ( $XZ$ -plane) (Due to symmetry, the same applies in the backward direction which is not shown).

For the optimum size ( $L_{slot} \times W_{slot}$ ) and spacing between the sheets ( $L$ ), the oblique rays will converge in the broadside direction with a path difference of  $n\lambda_0$ , ( $n=1,2,3$ , etc.) among the rays for constructive interference. The sheet optimization for maximizing the boresight gain is carried out with ANSYS HFSS, and the results are summarized in Table 3.7.

The table shows that  $L=50$  mm ( $\sim 1.2 \lambda_0$  at mid-band frequency of 7.25 GHz) and  $L_{sheet} \times W_{sheet} = 90$  mm  $\times$  20 mm ( $\sim 2.2 \lambda_0 \times 0.48 \lambda_0$ ) gives the maximum gain improvement of 4.75 dB in the band with gain variation of only 1.1 dB. The required 6–8.5 GHz band is also fully covered in this optimum design, although the band remains nearly identical for any sheet spacing. Also, the simulated magnitude of  $E$ -field (V/m) distribution in the vertical plane of the antenna is compared between the basic slot antenna and the side sheets loaded slot antenna in Figure 3.19. As shown, the side sheets loaded slot antenna has higher field intensity in the broadside direction, giving higher gain.



**Table 3.7** Conducting sheet optimization for in-band gain improvement of the proposed antenna (side sheets loaded slot antenna) relative to the basic slot antenna (common parameters:  $L_{slot} \times W_{slot} = 13 \text{ mm} \times 9.36 \text{ mm}$ ,  $L_{strip} = 25.2 \text{ mm}$ ,  $d = 4.55 \text{ mm}$ , and  $W = 50 \text{ mm}$ ).

$L$ (mm)	$W_{sheet}, L_{sheet}$ (mm)	-10dB Impedance band (GHz–GHz)	In-band gain Improvement (dB)	
			Max	Min
40	16,90	5.98–8.48	4.10	3.23
45	20,100	5.94–8.48	4.15	2.97
50	20,90	5.97–8.53	4.75	3.65
55	20,90	6.02–8.64	4.63	2.78
60	20,80	6.02–8.64	4.12	2.68

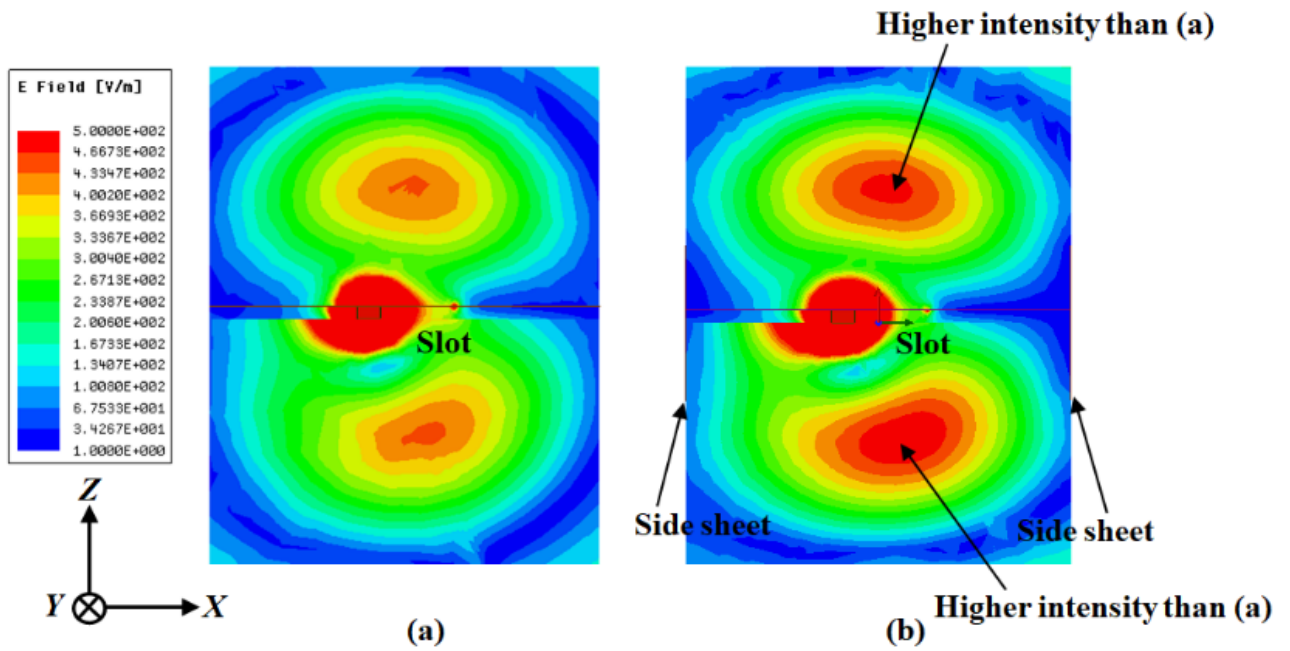


**Fig.3.19** Electric field distribution (HFSS) in the XZ plane of the (a) basic slot antenna (b) proposed antenna (side sheets loaded slot antenna).

### 3.2.3.1 Ray-trace analysis

A ray-trace analysis with the help of illustrations of Figure 3.20 is carried out to estimate the path difference between various rays.

A ray-trace analysis is performed to calculate the path difference between distinct rays using the illustrations in Figure 3.20. A fictitious plane  $C-C'$  is defined at a height of  $W_{sheet}/2$  away from the slot (the side sheets terminate here), where the oblique rays after undergoing reflection from the sheets converge. Although there can be an infinite number of rays reflected at various angles (heights) from the sheet, in the present model, three

representative rays are considered which are reflected from point  $Q$  on the sheet and fall at point  $P'$  on  $C-C'$ . As indicated in Figure 3.20 (a), (b) and (c) respectively, point  $Q$  lies at three different locations on the sheet separated by  $W_{sheet}/8$ . In Fig.6(b), note that as  $Q$  is in the upper half of the sheet,  $P' \neq P$ .

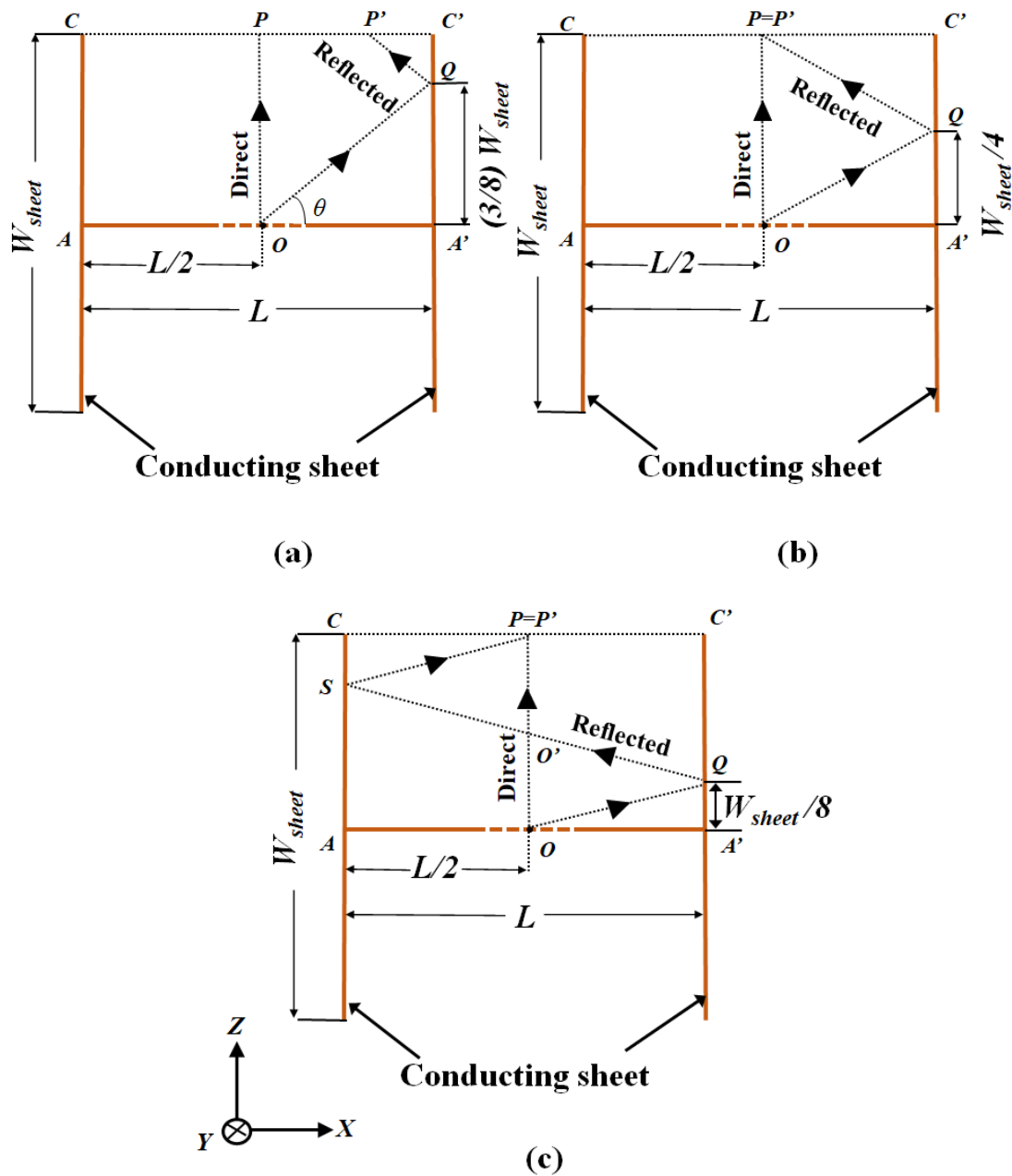


**Fig.3.20** Ray trace models for three representative rays reflected from the conducting side sheet with the point of reflection  $Q$  lying (a) above the sheet centre (b) at the sheet centre (c) below the sheet centre (Due to symmetry, the same applies in the backward direction which is not shown).

In all the cases of Figure 3.20, the direct ray's path is constant i.e.,  $R_{OP} = W_{sheet}/2$ , and the reflected ray's total path depends on  $Q$ . The path differences for these cases can be expressed as follows,

**Case 1:  $Q$  located at  $3W_{sheet}/8$  (Fig 3.20(a))**

The reflected ray's path is  $R_{OQ} + R_{QP}$ . Therefore, the path difference ( $\delta$ ) between the direct ray and the reflected ray can be expressed by equation (1)

$$\delta = (R_{OQ} + R_{QP}) - R_{OP} = \left[ R_{OQ} + \frac{R_{OP} - R_{A'Q}}{\sin \theta} \right] - R_{OP} \quad (3.24)$$

$$\text{Where } R_{OQ} = \sqrt{(R_{A'Q})^2 + (R_{OA'})^2} \quad (3.25)$$

$$R_{A'Q} = \frac{3}{8}W_{sheet}, R_{OA'} = \frac{L}{2}, \theta = \tan^{-1} \left( \frac{R_{A'Q}}{L/2} \right)$$

**Case 2:  $Q$  located at  $W_{sheet}/4$  (Fig 3.20(b))**

Here the reflected ray's path is  $R_{OQ} + R_{QP}$  or  $2R_{OQ}$  because  $R_{OQ} = R_{QP}$  (law of reflection). Thus, we can write,

$$\delta = 2R_{OQ} - R_{OP} \quad (3.26)$$

$$\text{Where } R_{OQ} = \sqrt{(R_{A'Q})^2 + \left( \frac{L}{2} \right)^2} \quad (3.27)$$

$$R_{A'Q} = \frac{W_{sheet}}{4}$$

**Case 3:  $Q$  located at  $W_{sheet}/8$  (Fig 3.20(c))**

In this case, the reflected ray's path is  $R_{OQ} + R_{QO'} + R_{O's} + R_{SP}$  or  $4R_{OQ}$  because  $R_{OQ} = R_{QO'} = R_{O's} = R_{SP}$  (law of reflection). Thus,

$$\delta = 4R_{OQ} - R_{OP} \quad (3.28)$$

$$\text{Where } R_{OQ} = \sqrt{(R_{A'Q})^2 + \left( \frac{L}{2} \right)^2} \quad (3.29)$$

$$R_{A'Q} = \frac{W_{sheet}}{8}$$

Using the optimum parameters of Table 3.7 in equations (3.24)–(3.29), the path differences can be calculated in terms of free-space wavelength at the lower, middle, and upper frequencies of the operating band (6–8.5 GHz), as summarized in Table 3.8.



**Table 3. 8** Path difference (in unit of  $\lambda_o$ ) at C–C’ plane for the three different rays of Figure 3.20 in the band ( $W_{sheet} \times L_{sheet} = 20 \text{ mm} \times 90 \text{ mm}$ ,  $L = 50 \text{ mm}$ , and  $R_{OP} = W_{sheet}/2$ ).

Case, Fig., Path difference ( $\delta$ )	Lower frequency, 6 GHz	Midband frequency, 7.25 GHz	Higher frequency, 8.50 GHz
1, Fig 3.20(a), Eq.3.24	$0.70 \lambda_o$	$2.2 \lambda_o$	$0.99 \lambda_o$
2, Fig 3.20(b), Eq.3.26	$0.82 \lambda_o$	$\lambda_o$	$1.16 \lambda_o$
3, Fig 3.20(c), Eq.3.28	$1.80 \lambda_o$	$0.84 \lambda_o$	$2.56 \lambda_o$

It can be observed from Table 3.8 that the path difference at the midband frequency of 7.25 GHz is close to  $n\lambda_o$  for all the three rays under consideration. This implies that at the midband frequency, the gain enhancement is resulted mainly by the rays which are reflected from all over the sheet. Similarly, it can be observed that at the lower frequency i.e., 6 GHz, rays of cases 2 and 3 are dominant, while at the higher frequency i.e., 8.5 GHz, rays of cases 1 and 2 makes major effect. Thus, the plane C–C’ represents nearly a constant phase aperture leading to improved radiation.

### 3.2.3.2 Poynting vector analysis

The Poynting flux density ( $\text{W}/\text{m}^2$ ) distribution in the principal planes are generated for the basic slot antenna and the proposed antenna as shown in Figure 3.21(a) and (b) respectively. Both the plots are shown with identical scaling ( $0.2\text{--}250 \text{ W}/\text{m}^2$ ) where the dark red region represents the highest density and dark blue region represents the lowest density. A comparison between the corresponding patterns of Figure 3.21(a) and 3.21(b) reveals that the side sheet loaded slot has most of its power flow focused in the boresight direction ( $\theta = 0^\circ$  and  $\theta = 180^\circ$ ). In addition, the lateral radiation ( $\theta = 90^\circ$  and  $\theta = 270^\circ$ ) in the XZ-plane is significantly reduced in Figure 3.21(b) compared to Figure 3.21(a) as expected.

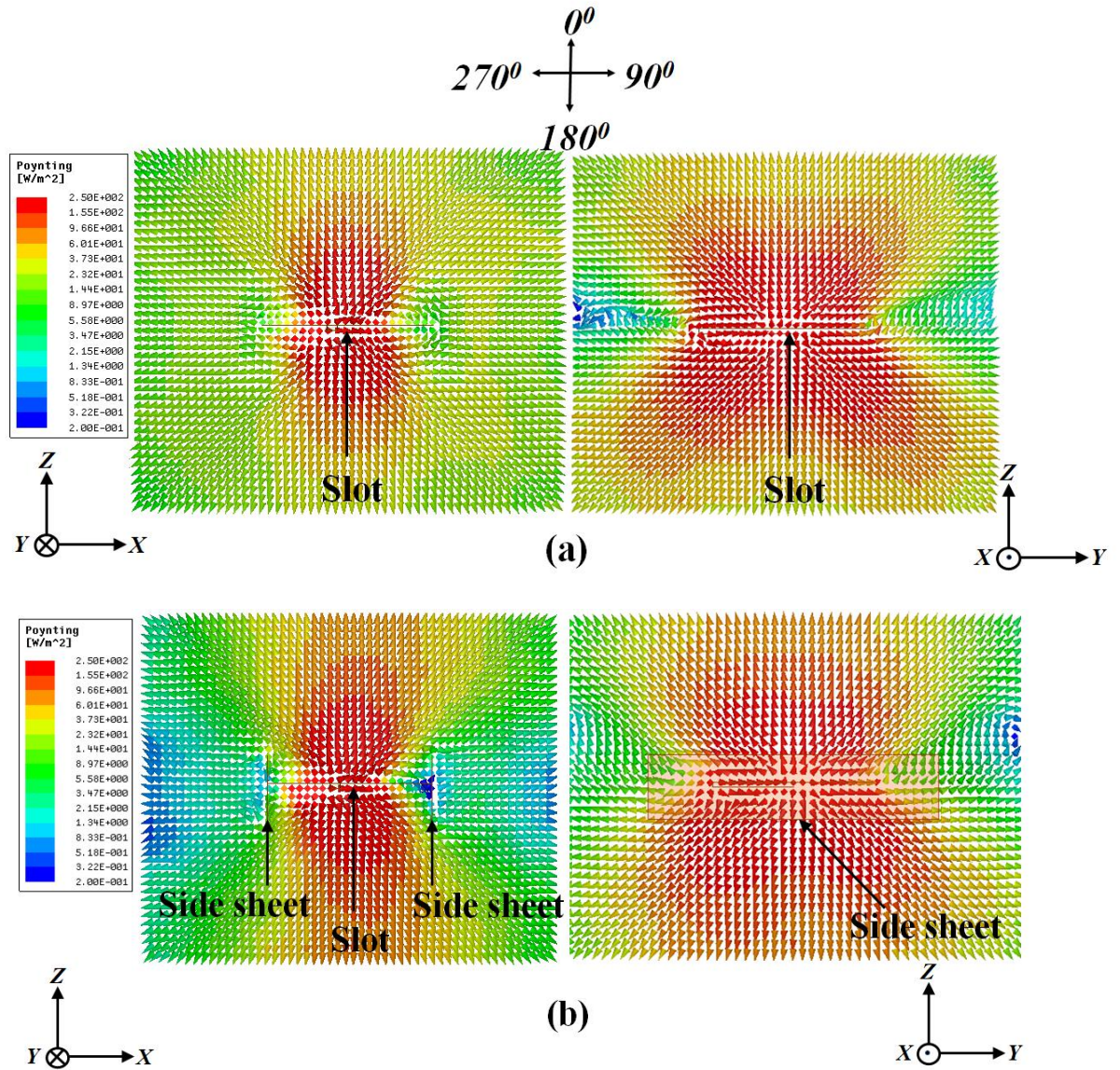


**Fig.3.21** Real Poynting vector distribution (HFSS) in the XZ and YZ-planes of the (a) basic slot antenna (b) proposed antenna (slot with side sheets).

### 3.3 Prototype fabrication, measurements, and discussion

The fabricated prototype of the proposed antenna is shown in Figure 3.22. Here, the design parameters are identical to those in simulations, except the metallic parts which are made of copper. Simulated versus measured reflection coefficients before and after the sheet loading of the basic slot antenna are shown in Figure 3.23. All the curves in the figure show good matching among one another. The measured impedance bandwidth of the basic slot antenna is 5.92–8.56 GHz or 36.46 %, whereas that of the proposed antenna is 5.97–8.53 GHz or 35 %, about the center frequencies of the respective bands. A comparison of the radiation patterns (normalized) in two principal planes (XZ and YZ-planes) of the

basic slot and the sheet loaded slot antennas at 7.25 GHz is illustrated in Figure 3.24. The figures show that for the sheet loaded case, the directivity in the XZ-plane is increased, as a result, the boresight gain is enhanced by 3.51 dB at 7.25 GHz identically in both directions ( $\theta = 0^\circ, 180^\circ$ ).

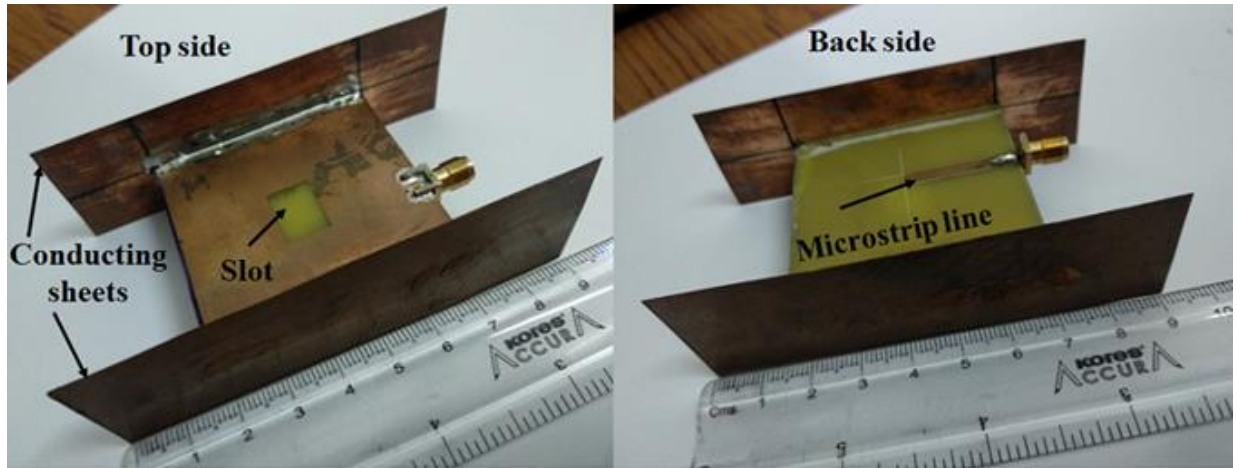


**Fig.3.22** Photograph of the fabricated antenna ( $L=W=50$  mm,  $L_{slot}=13$  mm,  $W_{slot}=9.36$  mm,  $L_{strip} = 25.2$ mm,  $d = 4.55$  mm,  $L_{sheet} = 90$  mm,  $W_{sheet} = 20$  mm).

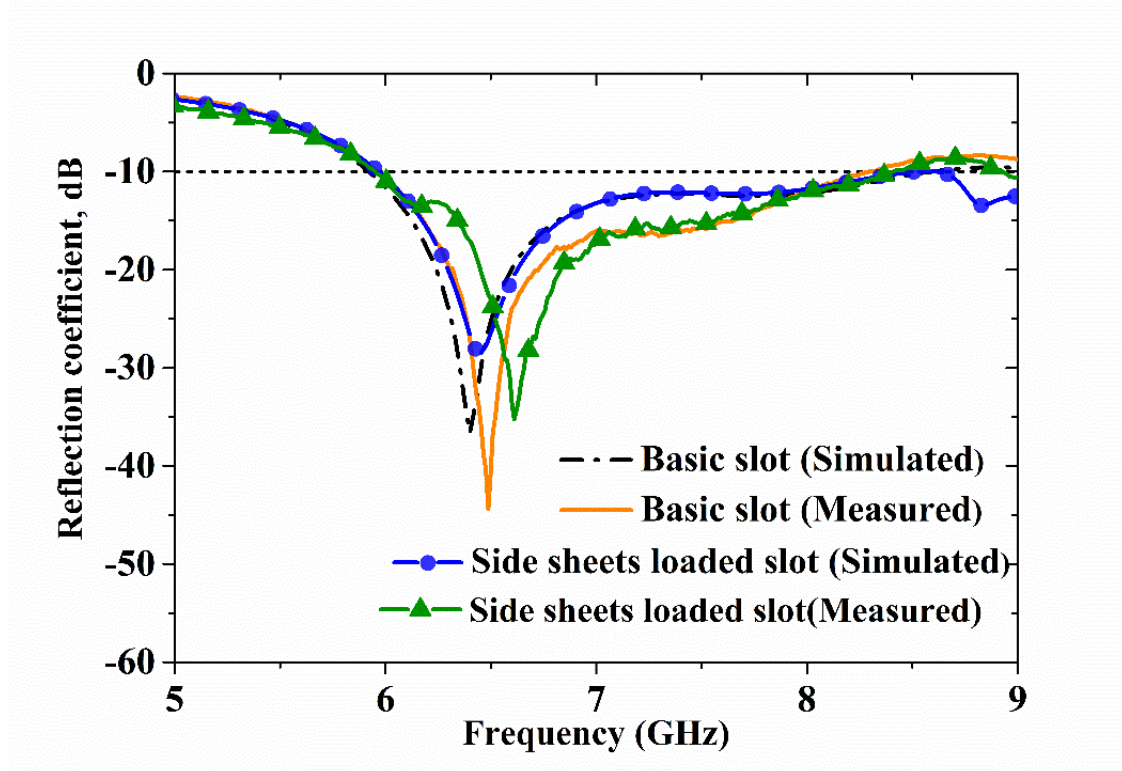


**Fig.3.23** Simulated and measured reflection coefficients of the basic slot antenna and the proposed antenna (slot with side sheets).



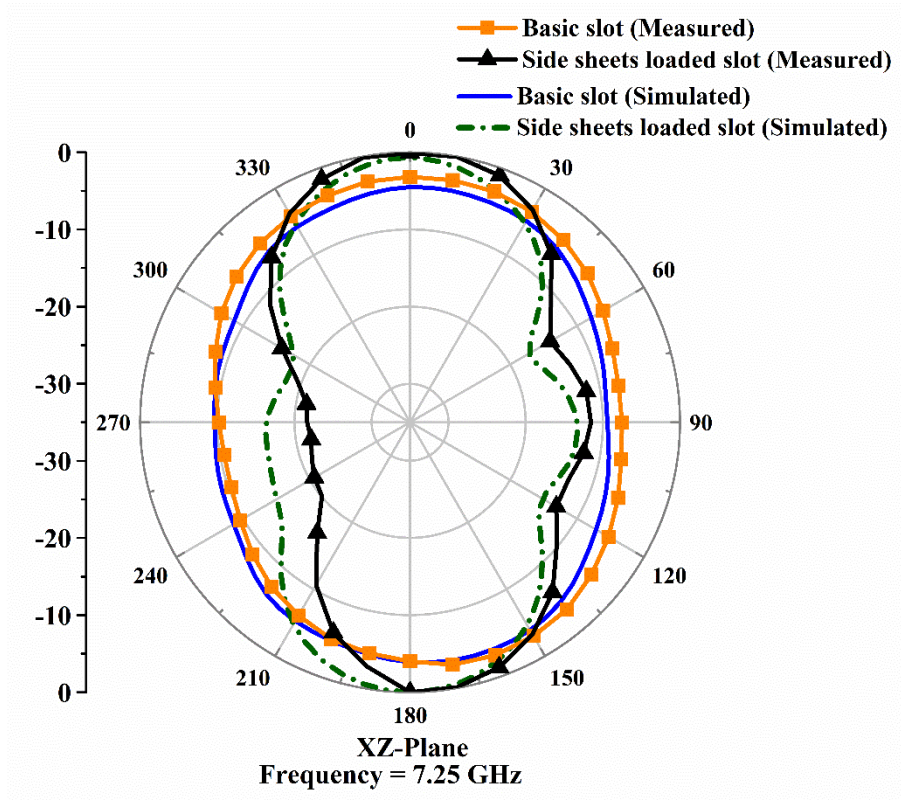
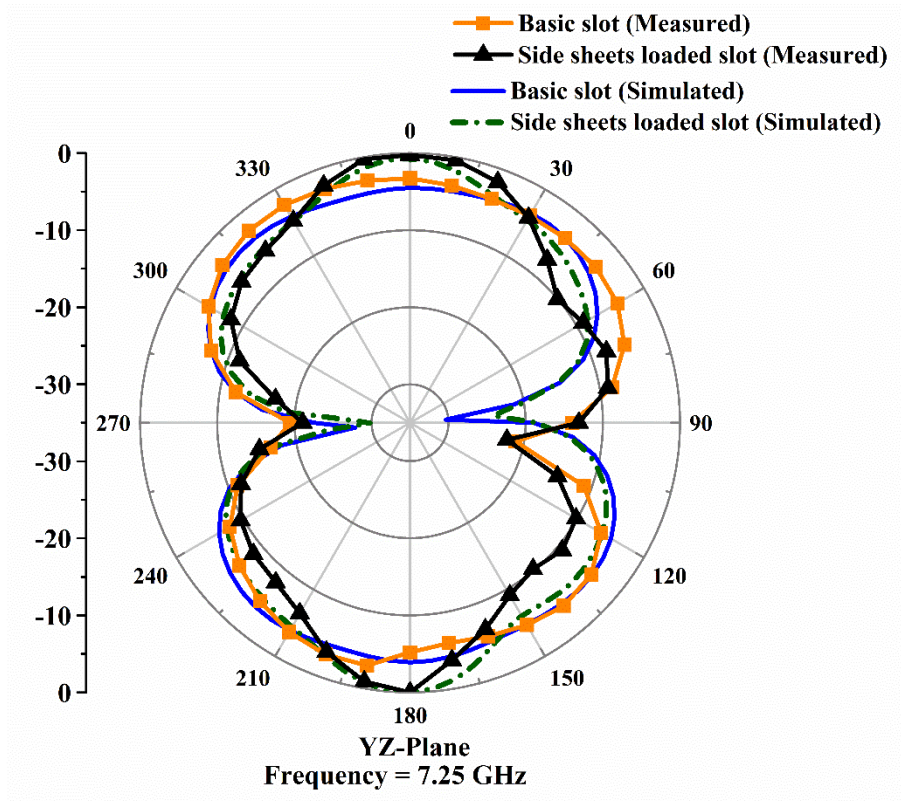


**Fig.3.24** Simulated Vs measured radiation patterns of the basic slot antenna and the proposed antenna (slot with side sheets) at the center frequency of 7.25 GHz, in the principal planes (XZ and YZ-planes).

Figure 3.25 shows the boresight gain versus frequency for the sheet loaded slot antenna in comparison with the basic slot antenna. The maximum in-band gains are 5.52 dBi and 2.59 dBi respectively for the sheet loaded and the basic slot antennas. The variation between measured and simulated gains in Figure 3.25 is attributed to fabrication and measurement errors. The in-band gain improvement obtained from Figure 3.25 are plotted in Figure 3.26. From this, a peak gain improvement of 5.92 dB (at 8.26 GHz) and an average improvement of 3.99 dB can be observed.

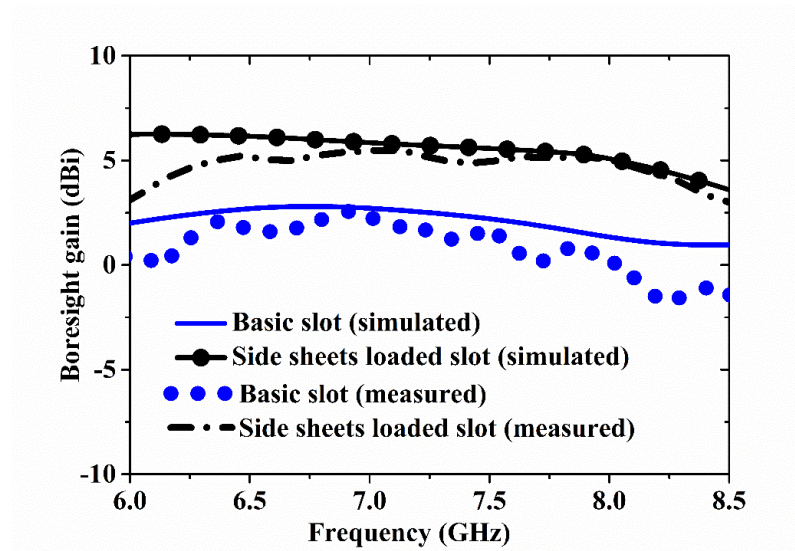


**Fig.3.25** Simulated vs measured gains versus frequency for the basic slot antenna and the proposed antenna (slot with side sheets)

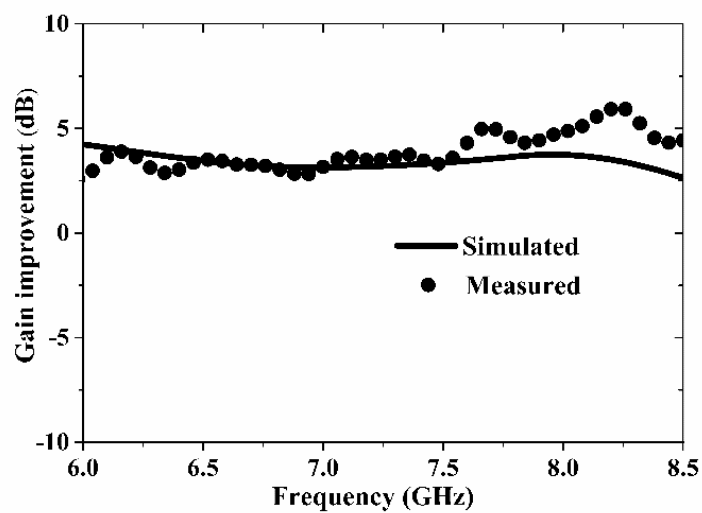


**Fig.3.26** Simulated and measured gain improvement within the operating band of the proposed antenna (slot with side sheets), relative to the basic slot antenna.

**Table 3.9** Comparison of the proposed antenna with previously reported superstrate loaded antennas

Ref.	Antenna design / directionality	Frequency band (GHz, %)	Dimensions (length $\times$ breadth $\times$ height)	Antenna volume ( $\lambda_0^3$ )	Peak gain improvement (dB)	Peak gain improvement per volume ( $\text{dB}/\lambda_0^3$ )
[103]	Aperture coupled microstrip patch antenna with dielectric superstrate/directional.	4.65–6.16 (27.94)	$2.80\lambda_0 \times 2.80\lambda_0 \times 0.98\lambda_0$	$7.68 \lambda_0^3$	7.23	0.94
[65]	Dielectric resonator antenna loaded with conducting superstrate/directional.	3.50–4.40 (23)	$2.60\lambda_0 \times 2.60\lambda_0 \times 0.5\lambda_0$	$3.38 \lambda_0^3$	6	1.77
[67]	Waveguide slot antenna loaded with conducting superstrate/directional.	7.70–9.70 (23)	$2.54\lambda_0 \times 3.06\lambda_0 \times 0.92\lambda_0$	$7.15 \lambda_0^3$	5.3	0.74
[104]	Aperture coupled microstrip antenna with FSS superstrate layer/directional.	8.6–11 (24.49)	$2.35\lambda_0 \times 2.35\lambda_0 \times 0.6\lambda_0$	$3.31 \lambda_0^3$	6	1.81
[105]	Waveguide slot antenna loaded with parasitic patch's cover/directional.	7.7–9.3 (19)	$2.33\lambda_0 \times 3.03\lambda_0 \times 0.79\lambda_0$	$5.58 \lambda_0^3$	10	1.79
[56]	Triangular slot antenna loaded with metamaterial-based superstrate/directional.	13.1–15.3 (15.5)	$2.84\lambda_0 \times 2.84\lambda_0 \times 0.7\lambda_0$	$5.65 \lambda_0^3$	8	1.42
[106]	Slot antenna loaded with artificial magnetic conductor (AMC) meta-surface/directional.	10.8–12.4 (13.79)	$3\lambda_0 \times 3\lambda_0 \times 0.1\lambda_0$	$0.9 \lambda_0^3$	2.7	3
This work	Offset fed slot antenna loaded with conducting sheets / bidirectional	5.97–8.53 (35.31)	$2.2\lambda_0 \times 1.2\lambda_0 \times 0.5\lambda_0$	$1.32 \lambda_0^3$	5.92 (3.99 dB average)	4.48 (3.02 average)

**Table 3.10** Performance comparison of existing bidirectional antennas with the proposed antenna

Ref	Substrate ( $\epsilon_r$ , $\tan\delta$ , thickness (mm))	-10dB Impedance Band (GHz, %)	Overall dimension ( $\lambda_0$ )	Peak Gain (dBi)
[41]	3.4,0.003, 0.5	3.3–4.85 (37)	$2.03\lambda_0 \times 1.62\lambda_0 \times 0.006\lambda_0$	2.6
[33]	4.4,0.02,0.8	1.82–2.91 (46.08)	$0.87\lambda_0 \times 0.87\lambda_0 \times 0.006\lambda_0$	4.5
[102]	3.4,0.003, 0.5	3.00–5.40 (57.14)	$1.61\lambda_0 \times 1.40\lambda_0 \times 0.007\lambda_0$	2.5
[45]	3.55,0.0027, 0.813	2.30–3.20 (32.7)	$1.38\lambda_0 \times 1.38\lambda_0 \times 0.007\lambda_0$	4
This work	4.4,0.02,1.6	5.97–8.53 (35.31)	$2.2\lambda_0 \times 1.2\lambda_0 \times 0.5\lambda_0$	5.52

Overall performance of the proposed antenna in comparison with that of existing superstrate loaded antennas is furnished in Table 3.9. Here, a one-to-one comparison is not possible as these designs operate at different frequency bands, and produce directional radiation patterns, whereas the proposed antenna is bidirectional. Hence a logical comparison would use two performance parameters, namely the electrical size, and the gain improvement per unit antenna volume (dB/  $\lambda_0^3$ ). As shown in Table 3.9, the proposed antenna offers the smallest volume except [106], and the highest gain improvement per unit volume of all the designs. Table 3.10 further compares the performance of the proposed antenna with existing bidirectional antennas. The proposed design offers the highest peak gain of all the designs as seen in the table.

### 3.4 Conclusion

This chapter presented the investigation on the performance of a wide slot offset fed slot antenna for wideband operation in 6-8.5 GHz. Subsequently, a non-resonant method for improving the bidirectional gain of the antenna was also discussed. The gain improvement relies on the focusing action of a pair of fully conducting sheets that are loaded vertically with respect to the plane of the basic slot antenna. The design preserves both the original operating band and the bidirectional characteristics of the radiation pattern of the wideband slot antenna. The fabricated prototype exhibits an impedance band from 5.97–8.53 GHz (35.31%) with a maximum boresight gain of 5.52 dBi. The average in-band gain improvement is 3.99 dB while the peak gain improvement is 5.92 dB, relative to the primary antenna. The proposed design is attractive for its (i) flexibility to control the gain independent of the bandwidth through the size selection of the sheets, and (ii) easy fabrication and integration due to the loose tolerances set by the simple conducting sheets.

Such bidirectional antennas are suitable for specialized applications such as tunnel communication. It may be added that this method can be implemented for directional antennas also, adding about 3 dB more gain. Such a design for a high-gain directional antenna for the same 6-8.5 GHz band will be investigated in the next chapter.



## Chapter 4

### Wide Gain-Band Directional Slot Antenna Design

Previous chapter demonstrated the design technique to improve the bandwidth and bidirectional gain of a wide rectangular microstrip slot antenna by using simple offset feeding and conducting side sheet loading of the microstrip slot antenna. In this chapter, additional design through reflector-superstrate loading is incorporated in the previous antenna to convert the bidirectional radiation to directional radiation over the same European/Indian UWB band (6–8.5 GHz). The design also ensures high gain with gain flatness over the entire band implying a 3 dB gain-band as high as 47.34 % (6.03–9.77 GHz) with peak gain of 12.04 dBi. Results are presented for both simulation (ANSYS HFSS) and measurement of the impedance band, radiation pattern, and gain.

#### 4.1 Conducting sheet loading in the horizontal and vertical planes of the slot

Compact antennas with directional radiation pattern, high gain, wide impedance bandwidth, and gain flatness across the band are essential parameters in a variety of communication applications such as wireless body area networks, wireless personal area networks, non-destructive assessment, ground penetrating radar, and level probing radar etc [48]. But achieving all these with a single design pose significant challenges for antenna designers. Slot antennas have a wider bandwidth and a bidirectional radiation pattern than traditional patch antennas. Because of the wider bandwidth of slot antennas, various wideband and ultra wideband antenna designs have been developed employing simple techniques such offset fed slot, wide slot fed with fork-like microstrip, and stub loaded slot as discussed before in chapter 2. The design followed to achieve the above has the following stages,

- (i) The basic bidirectional slot antenna is loaded with a conducting reflector sheet to generate a directed beam towards the upper hemisphere ( $\theta=0^\circ$ ).
- (ii) Next, a conducting superstrate is loaded on the radiating side of the slot to achieve high peak gain in the band.
- (iii) The conducting side sheet loading of previous chapter is then employed in the vertical plane of the slot antenna to further increase and flatten the gain throughout the band.

### 4.1.1 Reflector sheet loading

The basic offset fed rectangular slot antenna designed for the 6–8.5 GHz band in the previous chapter is used as the starting design element. Note that the side sheets are not included at this stage. This bidirectional slot antenna can be converted into a directional antenna by adding a reflecting surface at a quarter-wave distance below the slot [28,32]. As shown in Figure 4.1, a conducting sheet of size  $L_{ref} \times W_{ref}$  is located at  $h_{ref} = \frac{\lambda_0}{4\sqrt{\epsilon_{re}}} \cong 7$  mm (at  $\lambda_0$  corresponding to 6 GHz) from the plane containing the microstrip, where  $\epsilon_{re}$  is the relative effective permittivity surrounding the slot, which is computed using equation 3.23 (Ch3). For  $h_{ref} = 7$  mm, the reflector size is varied, and the results are shown in Figure 4.2. For  $L_{ref} = 40$  mm, and  $W_{ref} = 70$  mm a peak boresight gain of 9.75 dBi is achieved. Figure 4.3 shows the directional radiation pattern at three resonant frequencies of 6.45 GHz, 7.52 GHz, and 9.52 GHz for the reflector sheet loaded slot antenna. It can be noticed that the first two resonances are radiating while the third one is non radiating. Although the impedance band appears to have increased, the radiating band (where boresight gain  $\geq 0$  dBi) is only 6.06–7.53 GHz (22.07 %). As observed for the basic slot antenna (Ch3, figure 3.15), here too the third non-radiating resonance around 9.5 GHz remains. The near-field electric field distributions corresponding to the radiation patterns (Figure 4.3) are shown in figure 4.4, which are very similar to that of the basic slot antenna (Ch3, Figure 3.14).

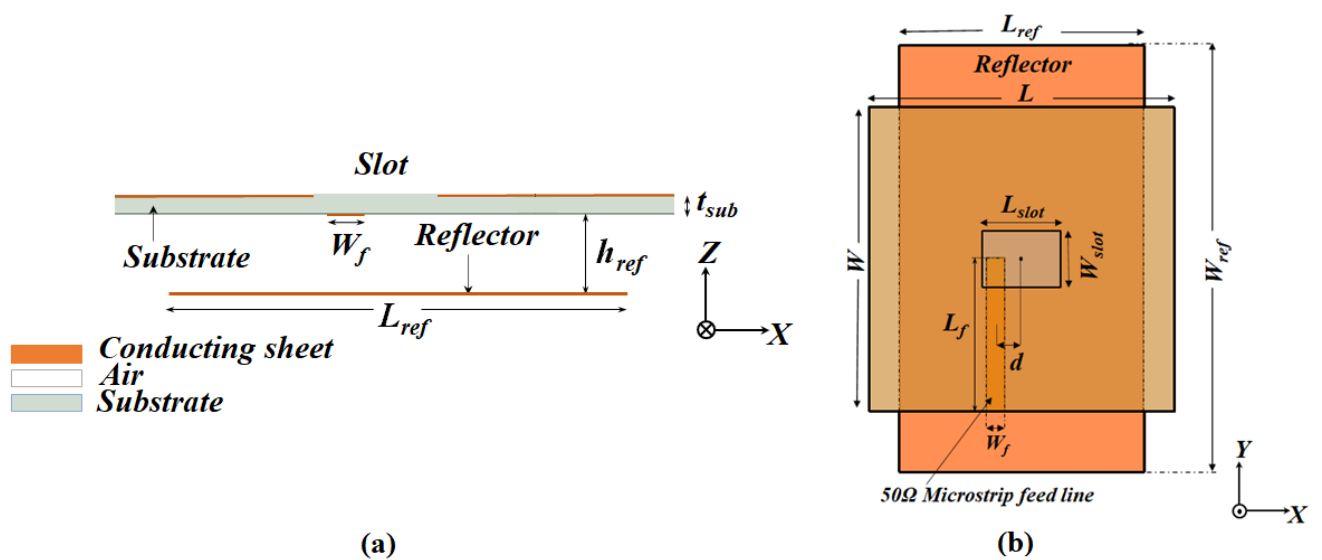


**Fig.4.1** Geometry of the reflector loaded slot antenna (a) Side view (XZ-plane) (b) Top view (XY-plane).

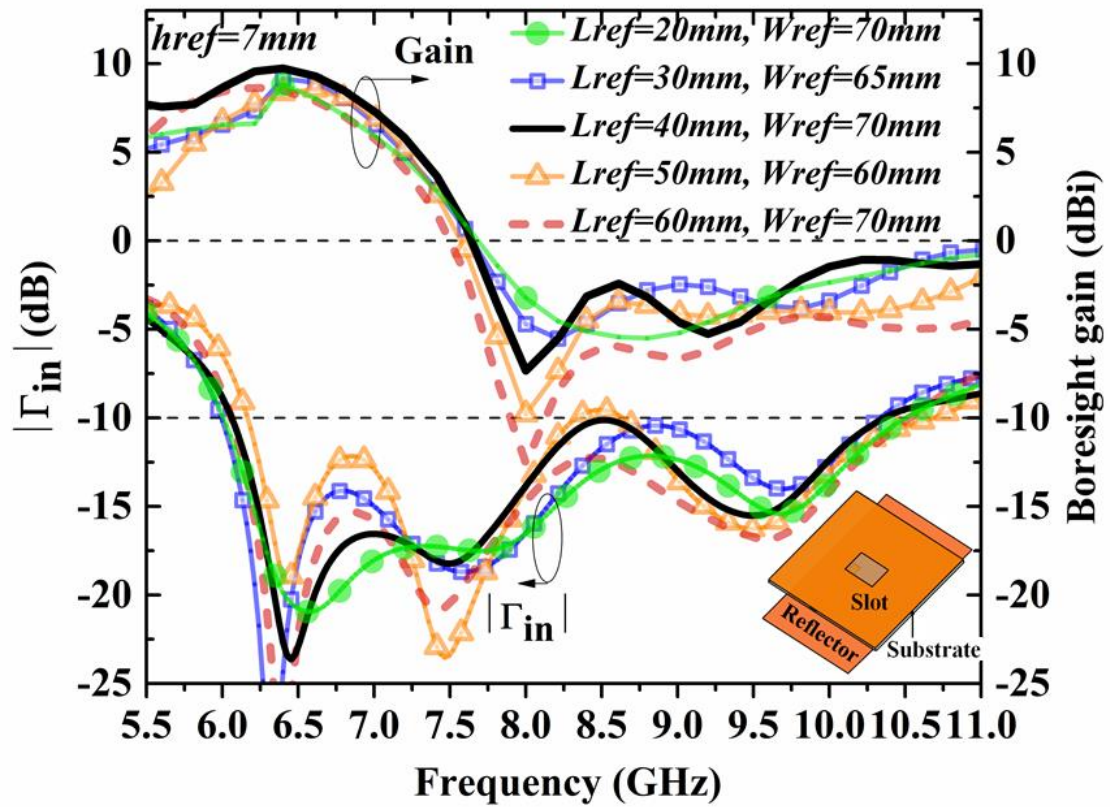
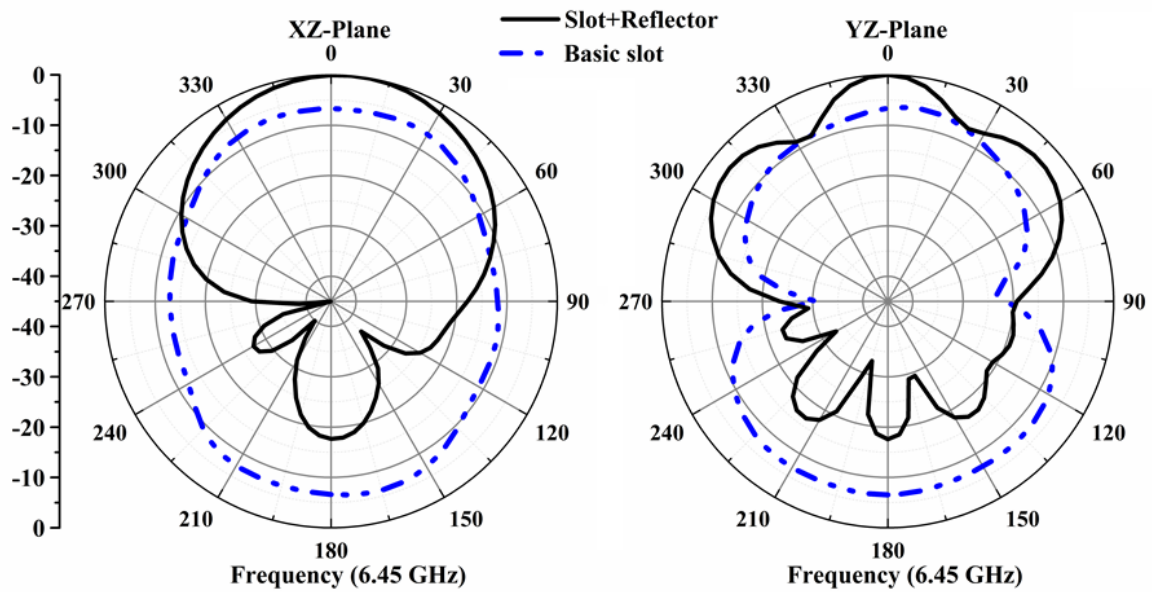
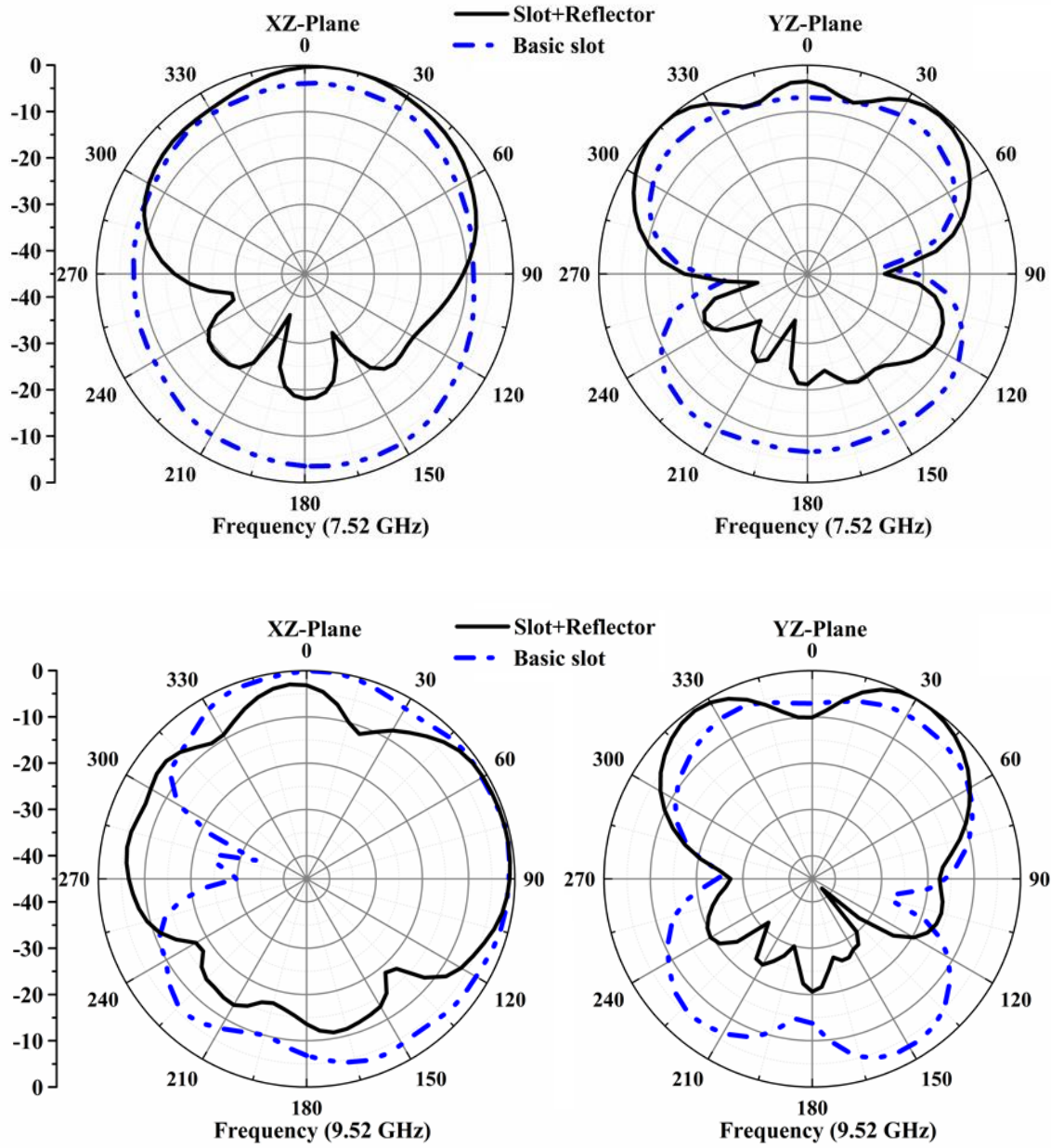
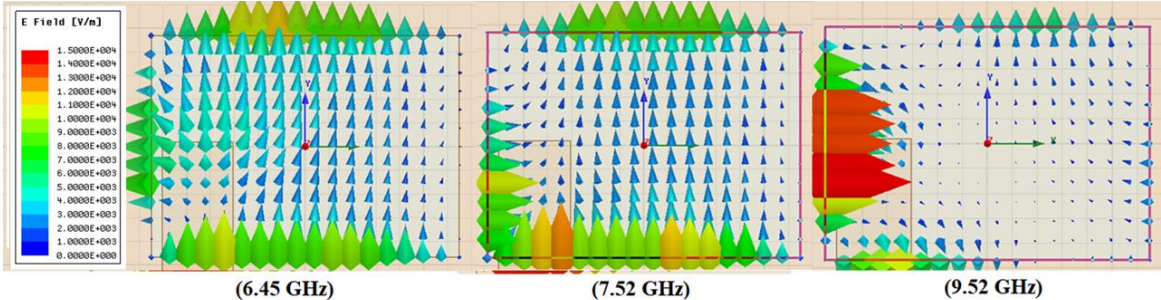


Fig.4.2 Reflection coefficient and boresight gain vs frequency of reflector loaded basic slot antenna for the varying reflector sheet size.





**Fig.4.3** Radiation patterns at (a) 6.45 GHz, (b) 7.52 GHz, and (c) 9.52 GHz for the optimized reflector loaded basic slot.



**Fig.4.4** Simulated electric-field distributions for reflector-loaded basic slot at 6.45 GHz, 7.52 GHz, and 9.52 GHz.

### 4.1.2 Superstrate sheet loading

The technique of various superstrate loading such as frequency selective surfaces, dielectric sheets, electronic band gap structures and metallic sheets have been discussed in chapter 2 to improve the gain of the antennas. Superstrate loaded antennas, also known as the resonant cavity antennas, produce high gain through multiple reflections between itself and the ground plane through the Fabry-Perot cavity effect [107]. Among these, the use of simple conducting sheets as superstrates [65-67] for bandwidth and gain enhancement allows looser tolerances of fabrication, assembly, and integration of the antenna compared to those with specific patterns.

Therefore, a conducting superstrate ( $L_{sup} \times W_{sup}$ ) is loaded above the slot at a spacing of  $h_{sup}$  from the microstrip plane as shown in figure 4.5. Resulting structure can be modelled as a Fabry-Perot cavity antenna formed between the superstrate and the reflector with the slot at the center serving as the primary source. The fundamental resonance of the cavity occurs for half-wave separation between the superstrate and the reflector ( $h$ ), while the superstrate geometry decides the gain response [65,67]. The fundamental frequency of the Fabry-Perot cavity can be written as [65],

$$f_r = \frac{c}{2h\sqrt{\epsilon_{re}}} \quad (4.1)$$

$$\text{where } h = h_{sup} + h_{ref} \quad (4.2)$$

Here in Figure 4.5, the plane containing the microstrip line is taken as reference for calculating  $h$ . In the above equations,  $c$  is the speed of light in vacuum,  $\epsilon_{re}$  is the effective relative permittivity of the medium filling the cavity, and  $f_r = f_0 = \frac{c}{2h}$  when the medium inside the cavity is a vacuum. In (4.1), the effective permittivity appears due to the presence of the wide slot ( $L_{slot} = 13\text{mm}$ ,  $W_{slot} = 9.36\text{mm}$ ,  $\epsilon_r=4.4$ ,  $t_{sub}=1.6 \text{ mm}$ ) present between the plates making the medium heterogeneous. In simple terms, the effective permittivity can be conveniently expressed as a weighted average of the permittivities of the three regions lying between the plates as, [108,109],

$$\epsilon_{re} = \frac{\sum_{i=1}^3 V_i \epsilon_{ri}}{\sum_{i=1}^3 V_i} \quad (4.3)$$

Where  $V_i$  and  $\epsilon_{ri}$  respectively are the volume and relative permittivity of region  $i=1-3$ . The first, second, and third regions, respectively, are the air gap between the superstrate sheet and slot ground ( $h_{sup} - t_{sub}$ ), substrate thickness ( $t_{sub}$ ), and air gap between the slot and

reflector sheet ( $h_{sup}$ ). By limiting the volume of interest to  $L_{slot} \times W_{slot} \times h$ , for each of the three regions, (4.3) can be expanded as,

$$\epsilon_{re} = \frac{(h_{sup} - t_{sub}) \epsilon_{r(air)} + t_{sub} \epsilon_{r(sub)} + h_{ref} \epsilon_{r(air)}}{(h_{sup} + h_{ref})} \quad (4.4)$$

By adjusting the superstrate location above the slot ( $h_{sup}$ ), the Fabry-Perot resonant frequency  $f_r$  can be chosen appropriately to enhance the gain bandwidth beyond that of the reflector loaded antenna (Figure 4.1). As the reflector-loaded slot has a non-radiating resonance at 9.5 GHz (Figure 4.2), we can choose  $f_r = 9.5$  GHz. By substituting (4.2) in (4.1) we get,

$$f_r = \frac{c}{2(h_{sup} + h_{ref})\sqrt{\epsilon_{re}}} \quad (4.5)$$

Now by simultaneously solving (4.4) and (4.5), both the superstrate spacing, and effective permittivity can be obtained as  $h_{sup} = 6.51$  mm and  $\epsilon_{re} = 1.403$ . As the superstrate spacing is nearly equal to that of the reflector ( $h_{ref} = 7$  mm) for fabrication easiness,  $h_{sup} = h_{ref} = 7$  mm is chosen.

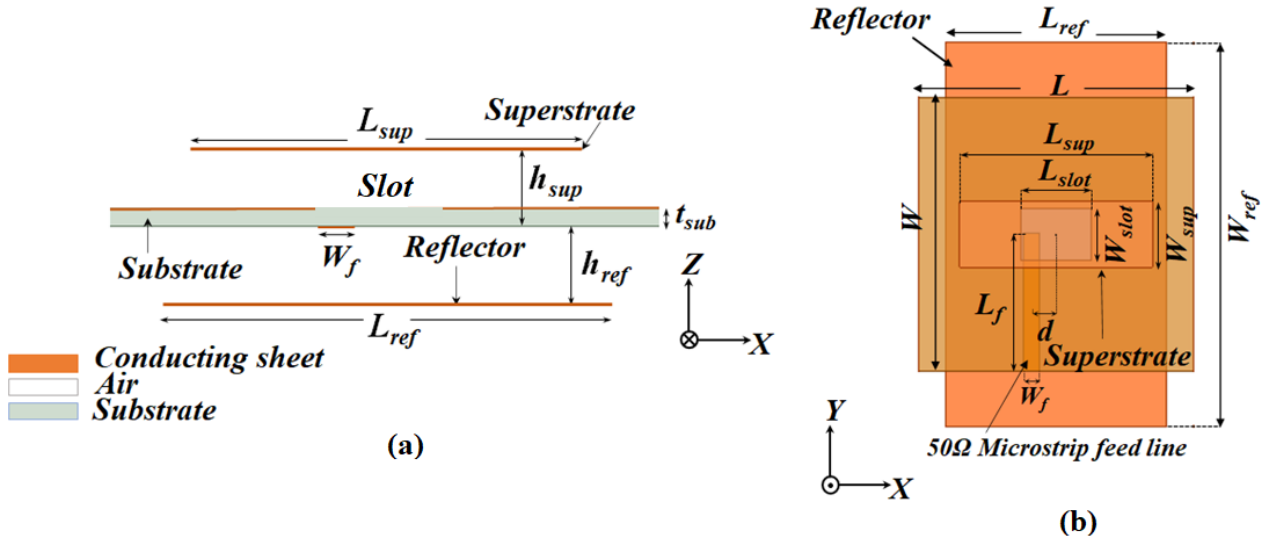


**Fig.4.5** Geometry of the superstrate and reflector loaded basic slot antenna (a) Side view (XZ-plane) (b) Top view (XY-plane).

Next, the superstrate size is optimized for gain enhancement, as shown by the curves of Figure 4.6. As the figures shows, for the optimized superstrate size of  $L_{sup} = 35$  mm and  $W_{sup} = 12$  mm, an impedance band of 6.03–10.33 GHz (52.57 %) with a peak boresight gain of 10.33 dBi is achieved. As seen, the gain throughout the band is also improved due to the merging of the gain bands around 6.45 GHz (reflector loaded slot mode) and 9.5



GHz (Fabry-Perot mode) giving rise to a nearly flat mid-band gain response. For the same, the 3 dB gain-band is calculated as 6.03–8.50 GHz (33.40 %), which is 64 % of the impedance band. The improvement in the gain-band is also reflected by the improved near-field pattern of the electric field distribution at the third resonance of 9.5 GHz as shown in Figure 4.7. This improvement at 9.5 GHz is caused by the y-polarized Fabry-Perot mode.

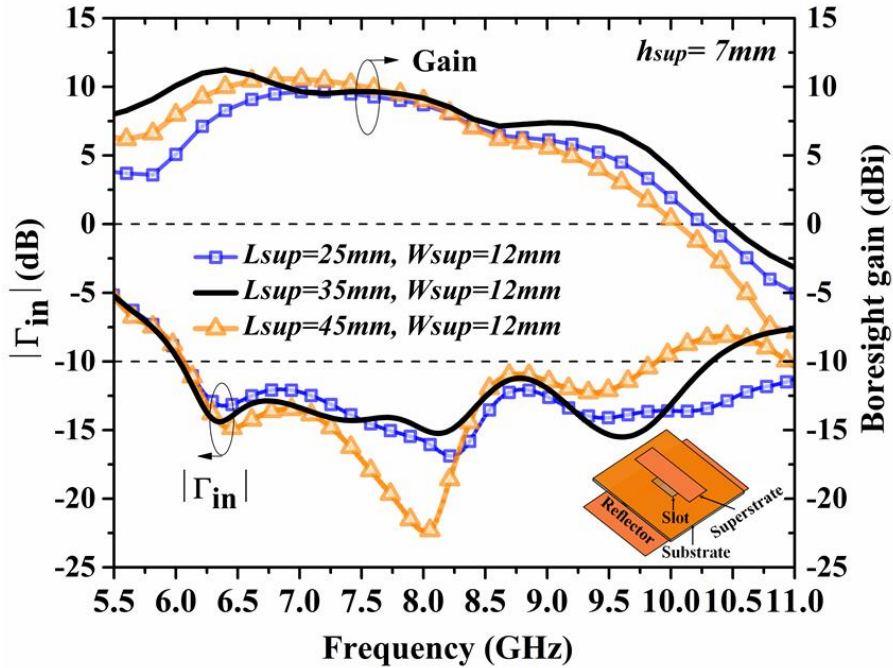


**Fig.4.6** Reflection coefficient and boresight gain vs frequency of superstrate and reflector loaded basic slot antenna for varying superstrate size.

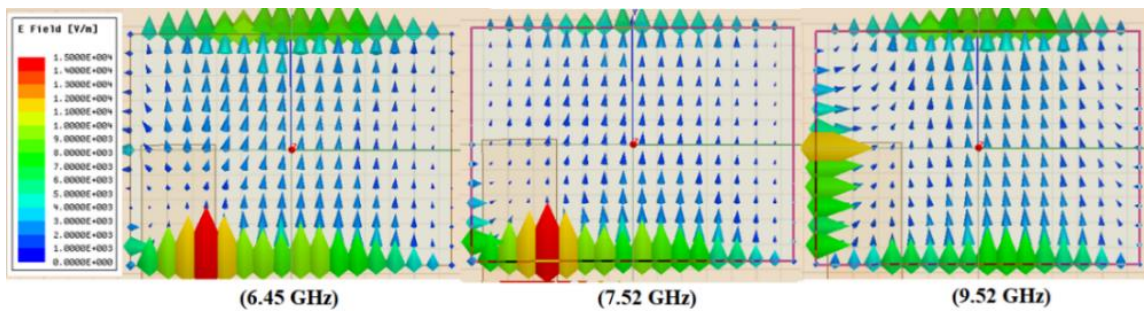


**Fig.4.7** Simulated electric-field distributions for superstrate and reflector loaded basic slot at 6.45 GHz, 7.52 GHz, and 9.52 GHz.

#### 4.1.3 Side sheet loading

It is observed in the previous section that although the impedance band extends up to 10.33 GHz, the 3 dB gain-band is limited to 8.5 GHz. If the gain at 9.5 GHz can be further enhanced, the higher 3 dB frequency of the gain-band can also be increased. For this, as shown in Figure 4.8, a pair of conducting side sheets are loaded in the vertical (YZ) plane

of the slot on the two opposing ground plane edges of the previous superstrate and reflector-loaded slot antenna. These side sheets reflect the oblique radiations ( $0 < \theta < 90^\circ$ ) from the slot and converge them towards the broadside direction ( $\theta = 0^\circ$ ) or into the Fabry-Perot cavity to increase the field intensity inside the cavity hence to further enhance the gain. Results for the optimized side sheet size  $L_{sheet} = 85$  mm and  $h_{sheet} = 12$  mm are shown in Figure 4.9. The impedance band of 5.94–10.53 GHz (55.74 %) with 12.52 dBi peak boresight gain and a 3 dB gain-band of 5.94–10.08 GHz (51.68 %) are achieved. This gain-band is about 93 % of the impedance band. It can also be noted that loading of side sheets does not affect the impedance band of the previous reflector–superstrate loaded antenna as it was justified for the bidirectional design of previous chapter.

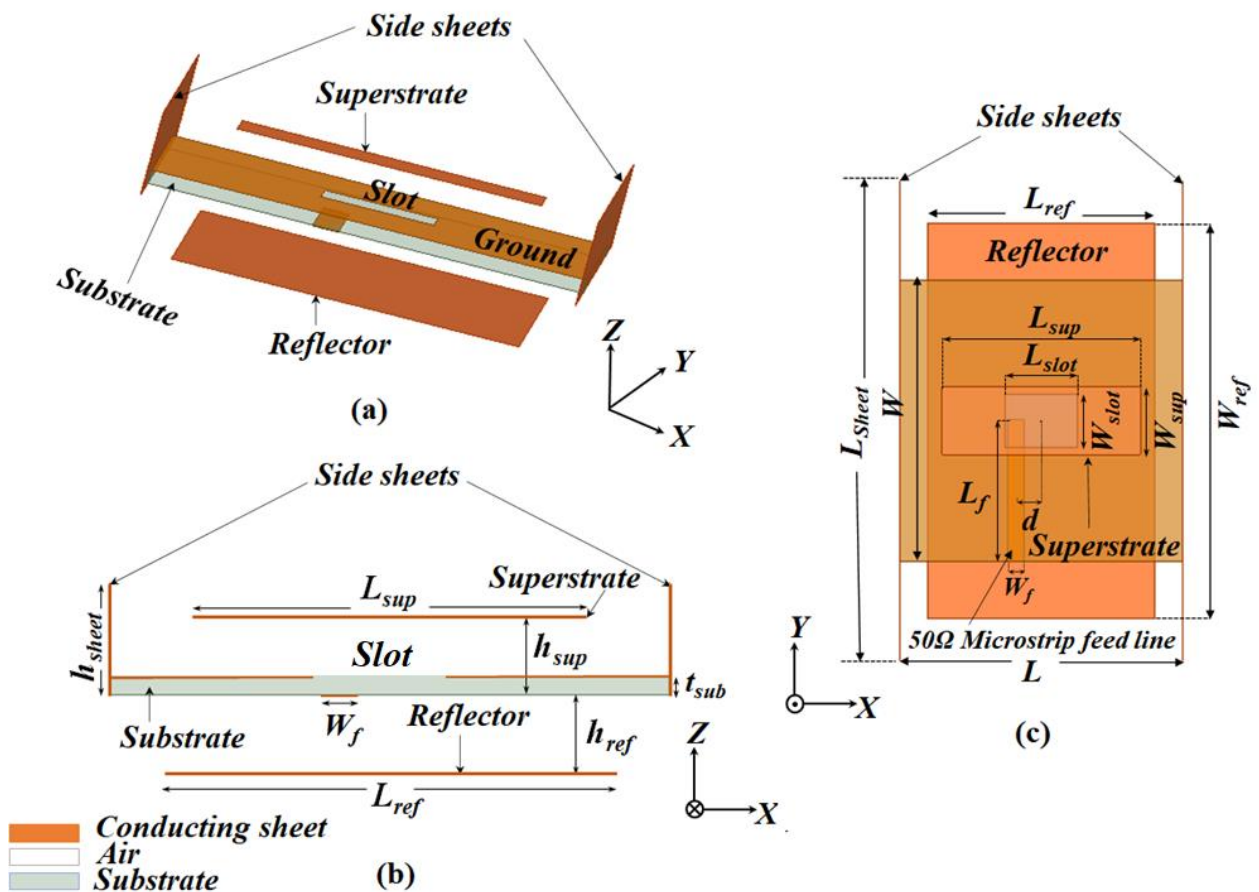


**Fig.4.8** Geometry of the proposed antenna (a) 3-D view (b) Side view (XZ-plane) (c) Top view (XY-plane).



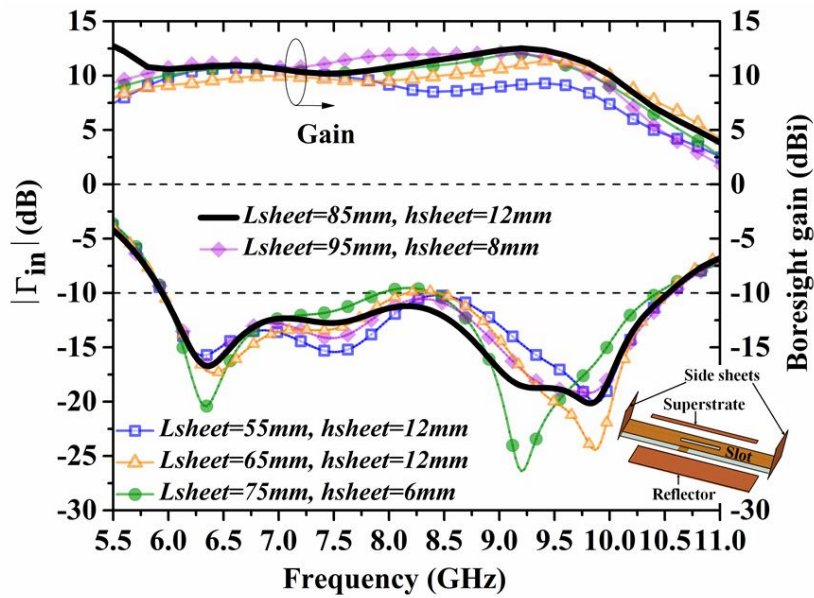
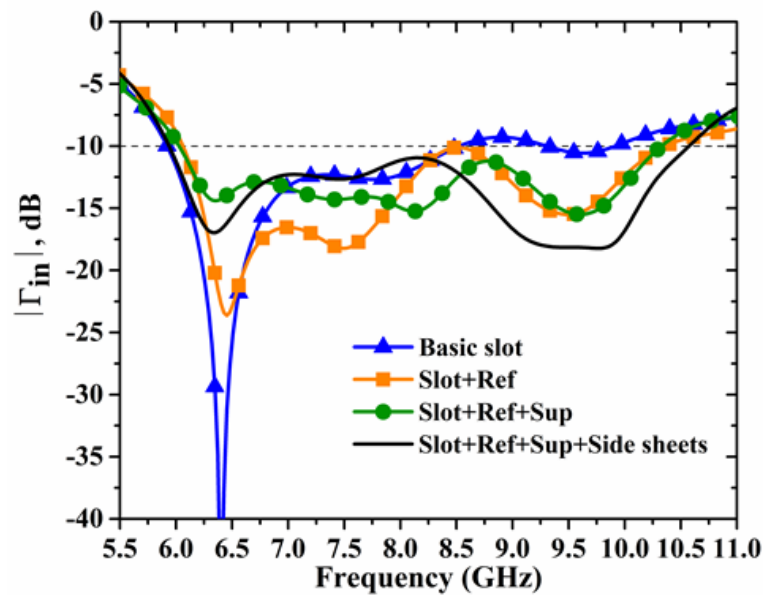


**Fig.4.9** Reflection coefficient and boresight gain vs frequency of basic slot antenna loaded with side sheet, superstrate, and reflector, for the varying side sheet size.

Figure 4.10 compares the reflection coefficients and the gain spectra of all the designs, and Figure 4.11 shows the respective radiation patterns in  $XZ$  and  $YZ$ -planes at three different frequencies of 6.50 GHz, 8.50GHz and 9.50 GHz. Resulting radiation patterns show that the basic slot antenna produces bidirectional pattern while the reflector-superstrate loaded slot and reflector-superstrate-side sheets loaded slot (final antenna) gives the directional pattern. Apart from that the final antenna generates more directive pattern of all the designs. Table 4.1 summarizes the important performance characteristics extracted from the figure 4.10.



(a)

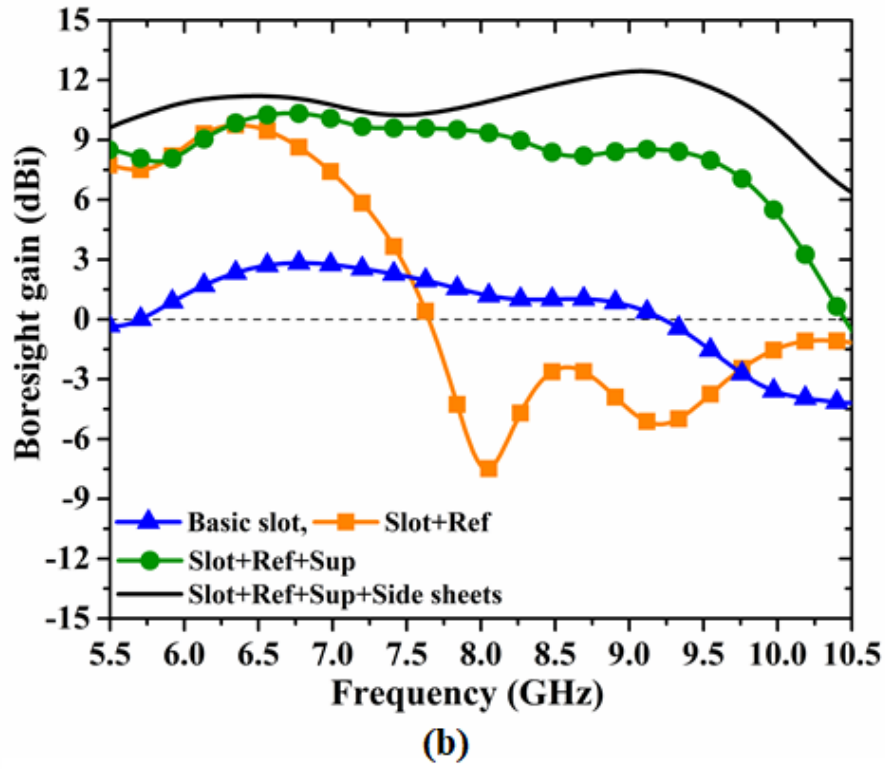
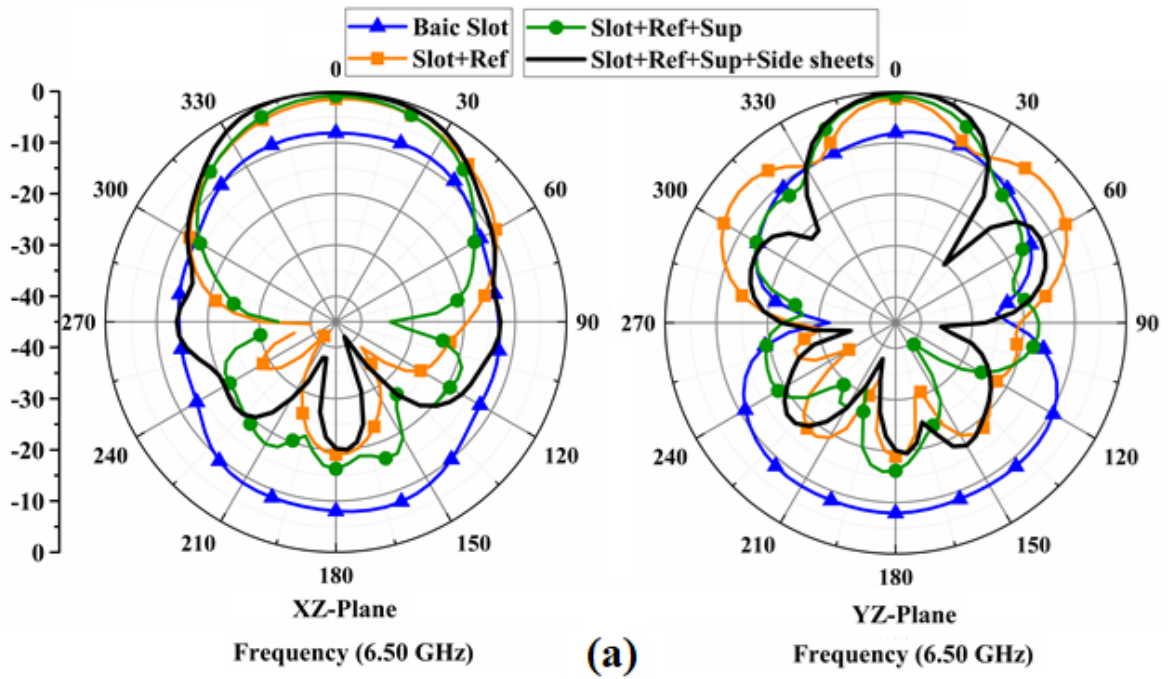
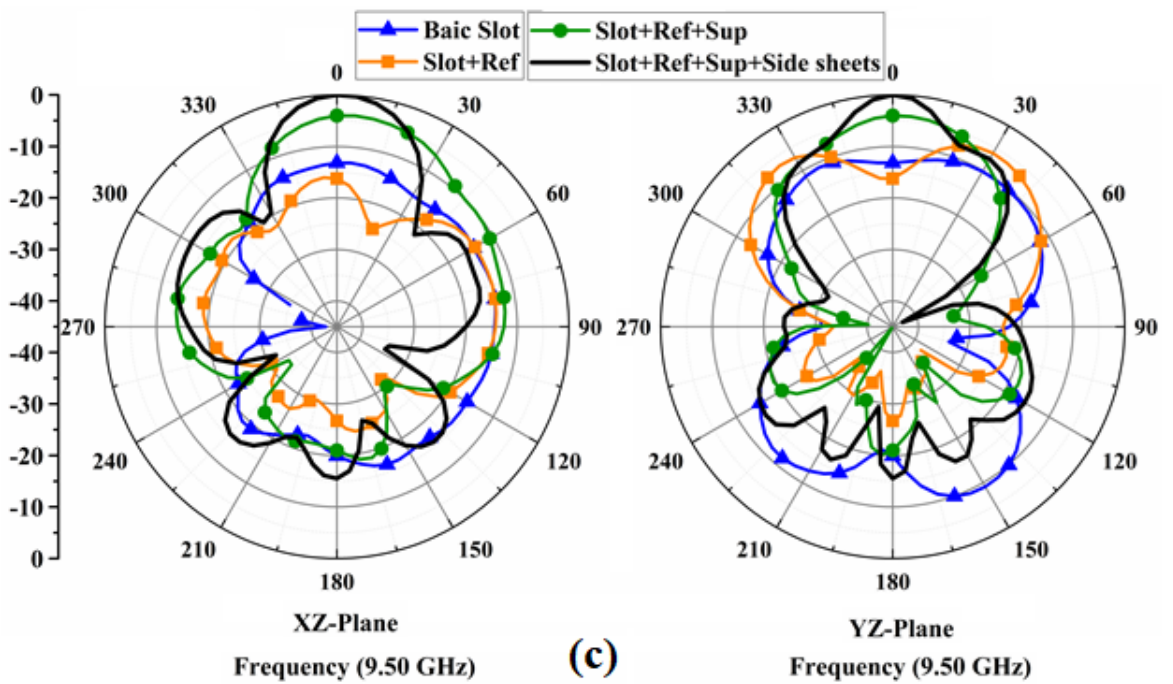
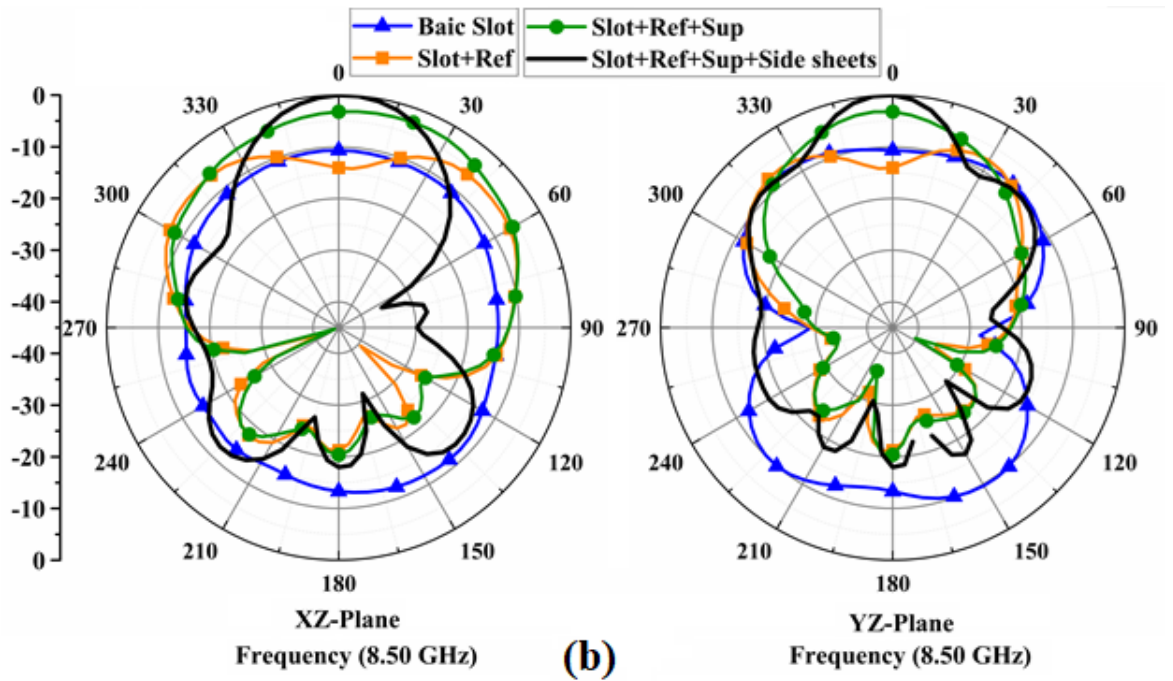


Fig.4.10 Comparison of (a) reflection coefficients and (b) boresight gains of antennas under various sheet loaded cases.



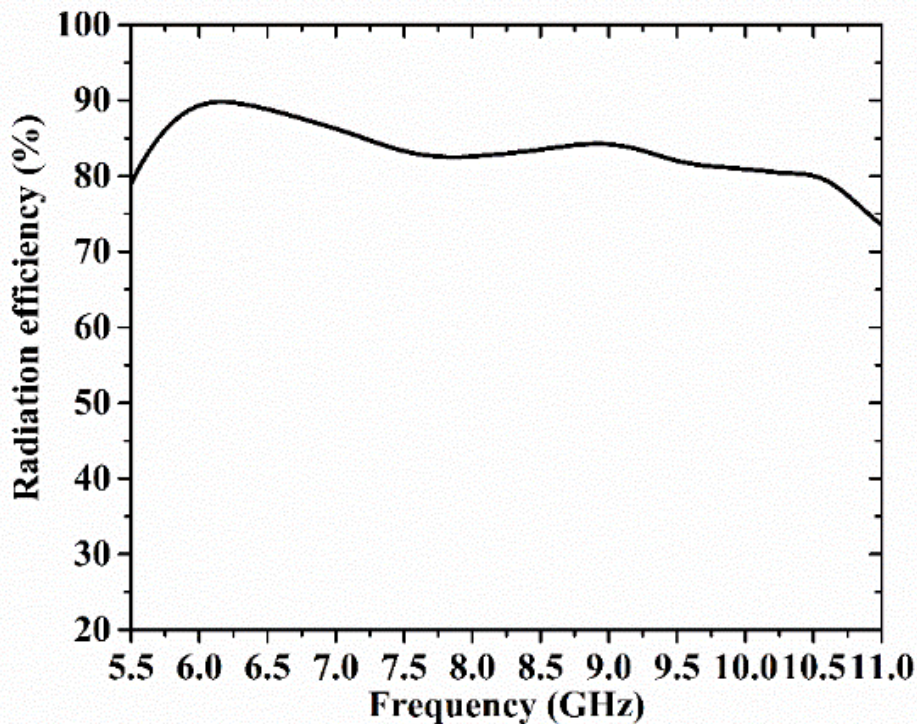


**Fig.4.11** Comparison of radiation patterns of all the antenna designs at (a) 6.50 GHz, (b) 8.50 GHz, and (c) 9.50 GHz.

**Table 4.1** Performance comparison of various antennas discussed

Antenna	-10 dB Impedance band (GHz, %), Band-1	Peak boresight gain (dBi)	3 dB gain band (GHz), Band-2	3 dB gain band (Intersection of band-1 and band-2) (GHz, %)
Slot	5.94–8.54, 35.91%	2.83	NA (as peak gain is < 3 dBi)	
Slot+Ref	6.06–10.36, 52.37%	9.75	5.00–7.08	6.06–7.08, 15.52%
Slot+Ref+Sup	6.03–10.33, 52.57%	10.33	5.99–8.50	6.03–8.50, 33.40%
Slot+Ref+Sup+ Side sheets (Final antenna)	5.94–10.53, 55.74%	12.52	4.73–10.08	5.94–10.08, 51.68%

Moreover, the radiation efficiency of the final antenna i.e., the basic slot antenna loaded with reflector, superstrate, and side sheets is shown in Fig 4.12. It shows a maximum radiation efficiency of 90 % and a minimum of 75 %.

**Fig.4.12** Radiation efficiency of the final antenna.



## 4.2 Prototype fabrication, measurements, and discussion

To verify the simulation findings, a prototype of the optimized proposed antenna is fabricated as shown in Figure 4.13. Teflon spacers affixed by glue are used to separate the sheets from the substrate and the conducting side sheets are soldered to the ground plane of the basic slot antenna.

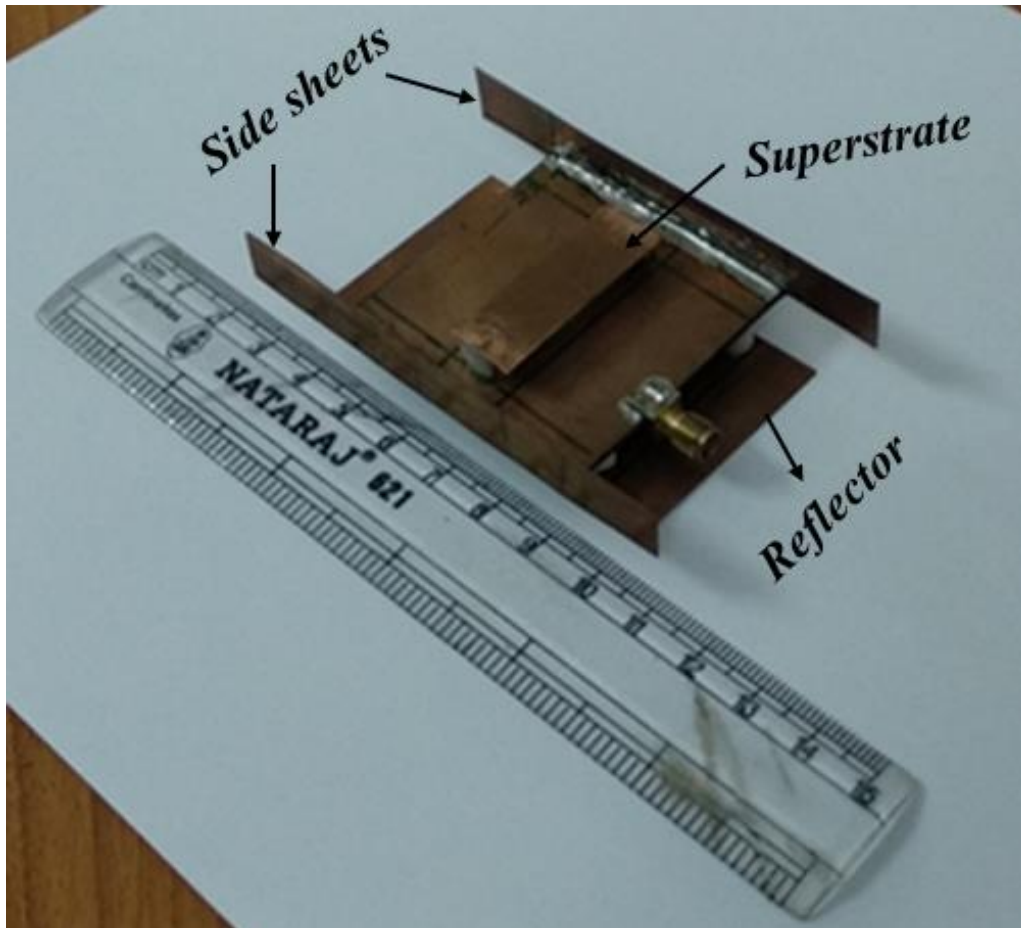


**Fig.4.13** Photograph of fabricated final antenna

Measurements are conducted in an anechoic chamber using Keysight Technologies N9928A Vector Network Analyzer. Figure 4.14 shows the measured reflection coefficient and boresight gain vs frequency of the proposed antenna. Major performance parameters are furnished in Table 4.2. Measured impedance band of 6.03-10.12 GHz (50.56%), 12.04 dBi peak boresight gain and an operating 3dB gain-band of 6.03-9.77 GHz (47.34%) are achieved. Also, measured radiation patterns (normalized) at three different frequencies 6.50 GHz, 8.50 GHz, and 9.50 GHz in the impedance band are shown in Figure 4.15. All the measured results are in decent matching with the simulated results, except for minor mismatches caused by fabrication errors.

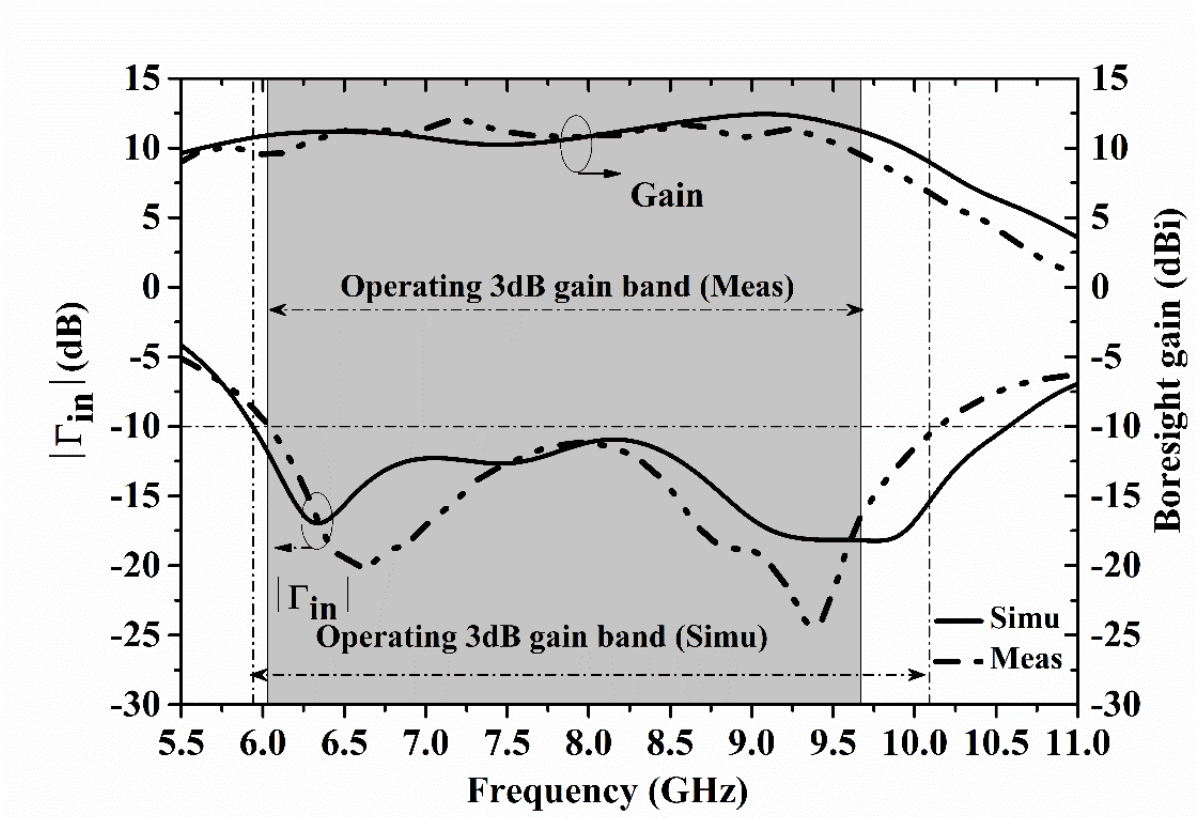
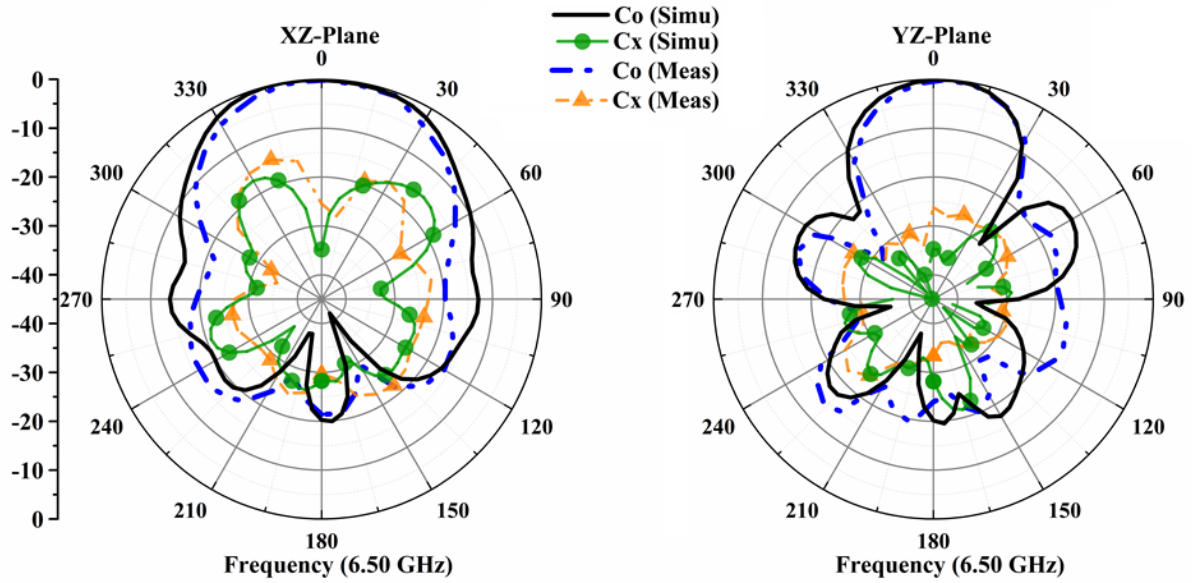
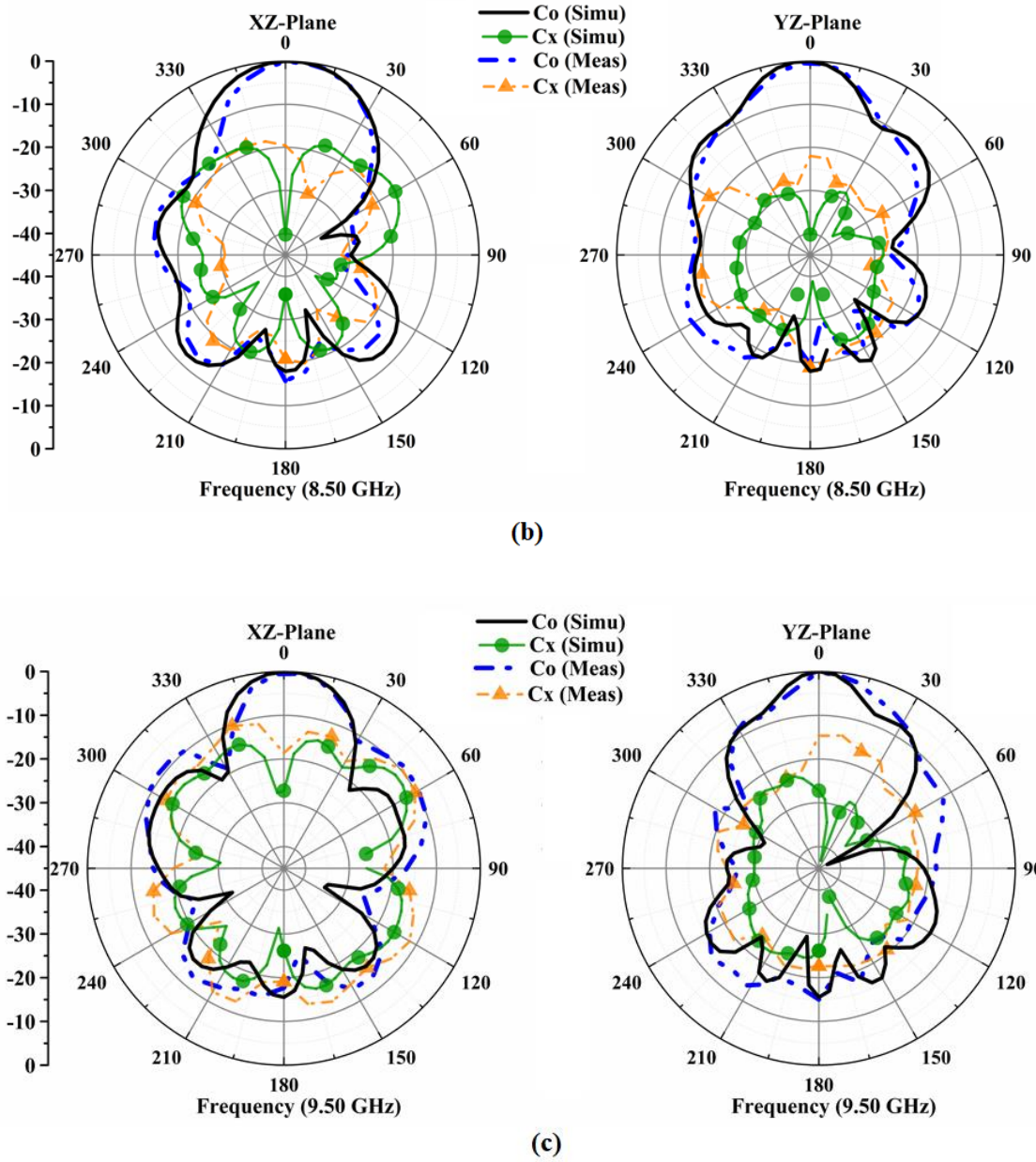


Fig.4.14 Reflection coefficient and boresight gain vs frequency for the final antenna.



(a)



**Fig.4.15** Measured vs simulated radiation pattern of the final antenna at (a) 6.50 GHz, (b) 8.50 GHz, and (c) 9.50 GHz.

**Table 4.2** Simulated and measured performance characteristics of the final antenna

Result	-10 dB Impedance band (GHz, %), Band-1	Peak boresight gain (dBi)	3 dB gain band (GHz), Band-2	Operating 3dB band (Intersection between band-1 and band-2) (GHz, %)
Simulated	5.94-10.53, 55.74%	12.52	4.73-10.08	5.94-10.08, 51.68%
Measured	6.03-10.12, 50.65%	12.04	5.40-9.77	6.03-9.77, 47.34%

**Table 4.3** Performance comparison of the proposed antenna with existing broadband-high gain antennas

[Ref] Antenna design	-10 dB Impedance band (GHz, %)	Antenna dimension (length $\times$ breadth $\times$ height)	Peak gain (dBi)	Peak rad. efficiency (%)	Peak Gain/Area (dBi/ $\lambda_0^2$ )	Peak Gain/Vol. (dBi/ $\lambda_0^3$ )	Gain improvement w.r.t to basic antenna (dB)	3 dB gain band (GHz, %)
[65] Dielectric resonator antenna loaded with conducting superstrate.	3.5–4.4 (23)	$2.60\lambda_0 \times 2.60\lambda_0 \times 0.5\lambda_0$	12	96.5	1.77	3.55	6	$\sim 3.5\text{--}4.4^*$ (23)
[67] Waveguide slot antenna loaded with conducting superstrate.	7.7–9.7 (23)	$2.54\lambda_0 \times 3.06\lambda_0 \times 0.92\lambda_0$	12	NA	1.54	1.67	5.3	$\sim 7.8\text{--}9.6^*$ (20.68)
[105] Waveguide slot antenna loaded with parasitic patch's cover.	7.7–9.3 (19)	$2.33\lambda_0 \times 3.03\lambda_0 \times 0.79\lambda_0$	16.5	NA	2.34	2.96	10	$\sim 7.7\text{--}8.7^*$ (12.19)
[56] Triangular slot antenna loaded with metamaterial-based superstrate.	13.1–15.3 (15.5)	$2.84\lambda_0 \times 2.84\lambda_0 \times 0.7\lambda_0$	13.78	NA	1.71	2.44	8	12.8–15.2 (17.10)
[58] Slot coupled patch antenna loaded with two complementary FSS layers.	8.6–11.2 (26.26)	$2.4\lambda_0 \times 2.4\lambda_0 \times 0.5\lambda_0$	13.8	NA	2.40	4.79	$\sim 8.5^*$	8.6–11.4 (28)
[75] Patch antenna loaded with two layers dielectric superstrate.	13.8–19 (31.7)	$2.4\lambda_0 \times 2.4\lambda_0 \times 1.36\lambda_0$	15	NA	2.60	1.91	$\sim 7^*$	13.5–17.5 (25.8)
[76] Patch antenna with a shaped ground plane loaded with dielectric PRS.	4.96–6.02 (19.31)	$2.75\lambda_0 \times 2.75\lambda_0 \times 0.56\lambda_0$	16	NA	2.12	3.77	8.2	5.10–6.35 (23)
[This work] Offset fed slot antenna loaded with conducting reflector, superstrate, and side sheets.	6.03–10.12 (50.65)	$2.28\lambda_0 \times 1.34\lambda_0 \times 0.46\lambda_0$	12.04	90	3.95	8.6	9.35	6.03–9.77 (47.34)

\* Estimated from the given results as these are not directly mentioned.



In Table 4.3, the performance of the proposed antenna is compared with the existing wideband-high gain antennas working in the S-band and above. The biggest advantage of the proposed design is that it offers the highest 3 dB gain-band hence the gain flatness, the highest peak gain per unit area ( $\text{dBi}/\lambda_0^2$ ) and peak gain per unit volume ( $\text{dBi}/\lambda_0^3$ ) of all the designs in consideration. Also, it stands second in terms of the impedance band, volume, and gain improvement with respect to corresponding basic antenna as shown in Table 4.3.

### 4.3 Conclusion

This chapter discusses a directional, high gain slot antenna with superior and stable radiation performance for the 6–10 GHz band. This slot antenna achieves a measured 3 dB gain-band of 6.03–9.77 (47.34 %) with 12.04 dBi peak boresight gain by using two pairs of conducting sheets– a reflector-superstrate pair and a pair of side sheets. The 3 dB gain band covers 93% of the antenna's impedance band (6.03–10.12 GHz, or 50.65%), ensuring both gain flatness and efficient use of the impedance band. This design is attractive for its easy fabrication due to the loose tolerances provided by the simple conducting sheets-based design. This design is expected to work equally well for other types of directional antennas too. The time domain behaviour of these antennas will be addressed in the following chapter.

## Chapter 5

### Time Domain Analysis of UWB Slot Antenna

In chapters 3 and 4, wideband slot antennas were investigated with focus on their frequency domain performances such as reflection coefficient, radiation pattern, and gain to be suitable for 6–8.5 GHz UWB applications. Since UWB systems operate on pulsed mode than continuous wave carrier mode, the antenna's influence on the pulse both at the transmitter side and receiver side is critical in deciding the degree of distortion imparted to the pulse that carries the information. In other words, as stated in Chapter 1, good time domain performance is also one of the requirements of any UWB antenna.

In this chapter, the time domain characterisation of the 6-8.5 GHz ECC/Indian UWB band antenna developed in the previous chapter is presented. Firstly, the power spectral density (PSD) of the input source pulse is studied in comparison with the ECC emission mask as discussed in chapter 1. Next, a full-wave simulation model of the UWB link comprising the transmitting antenna, Friis free-space channel and receiving antenna is constructed in CST Microwave Studio [30]. The end-to-end pulse distortion is quantified by computing the pulse fidelity factor ( $FF$ ) from the overall transfer function extracted from the simulation model. Comparison is presented between the time domain performances of the basic slot antenna developed in chapter 3 and the final UWB antenna of chapter 4.

#### 5.1 Defining the UWB source pulse

The input pulse characteristics of UWB antennas is a very important factor to be considered in the time domain analysis. The pulse should optimally contain all the frequency components of required band, which means it needs to make efficient use of the spectral emission mask imposed by the regulatory authority, which is 6–8.5 GHz in the present case [2,4,110] while also resorting to a short time domain extension. A larger time-domain extension would worsen the spatial resolution in applications such as radar systems. Unfortunately, there exists this inverse relationship between spectral occupancy and time-domain extension. A very small time spike occupies an infinite frequency spectrum, whereas a frequency domain impulse that entirely fills the rectangular shape of the spectral mask has an infinite time extension. Thus, the requirements of making efficient use of the allocated mask while maintaining a good time extension are mutually contradictory.

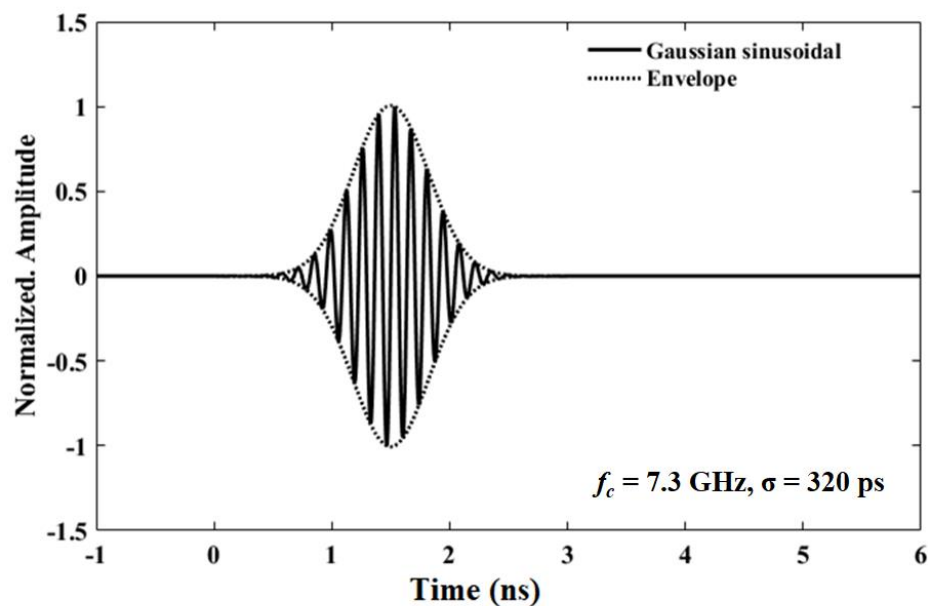
Thus, it is recommended to choose a Gaussian bell shape envelope function with sinusoidal modulation as the UWB impulse [110]. This can be represented mathematically as follows,

$$g_s(t) = \frac{1}{\sqrt{2\pi}\cdot\sigma} \exp\left(-\frac{t^2}{2\sigma^2}\right) \sin(2\pi f_c t) \quad (5.1)$$

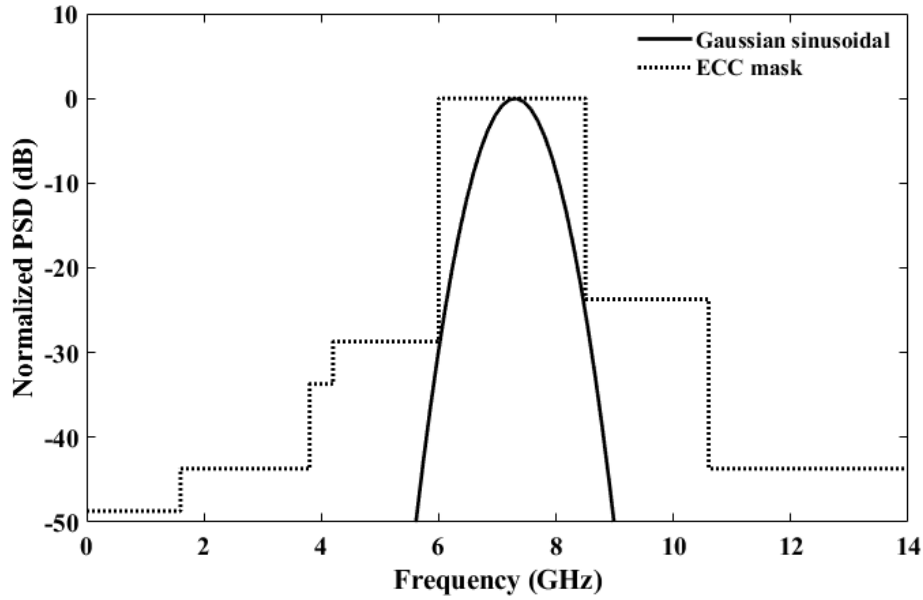
where  $\sigma$  is the standard deviation of the envelope function determining the impulse width,  $f_c$  the frequency used in the sinusoidal function determining the impulse centre frequency. With this mathematical representation, impulses fitting the FCC masks can be realized choosing  $f_c = 7$  GHz and  $\sigma = 76.5$  ps for the indoor and  $\sigma = 92$  ps for the outdoor mask [110].

Besides describing the FCC impulses, the Gaussian sinusoidal representation is well suited for describing impulses that meet the ECC standard. As discussed in chapter 1, The ECC regulation requires a much narrower spectral mask than the FCC regulation as well as steeper transitions at the spectral boundaries. Therefore, a longer impulse time extension is necessary.

Figure 5.1 shows the time domain and frequency domain shape of a Gaussian sinusoidal, which fits the ECC mask or spectrum. To obtain this impulse shape,  $f_c = 7.3$  GHz and  $\sigma = 320$  ps are used in (Eq.5.1). The impulse has a time-domain extension of 800 ps (FWHM) and makes efficient use of the ECC mask [110].



(a)



(b)

**Fig.5.1** Gaussian sinusoidal source pulse fitting the ECC mask in (a) time and (b) frequency domain.

## 5.2 Transfer function

Figure 5.2 shows the block diagram for a simple UWB communication system consists of a transmitting antenna, a receiving antenna, and the channel. Overall behaviour of the antennas and the channel is characterised at the system level by a transfer function  $H(f)$ . The impulse response can be derived from transfer function by using Inverse Fourier Transform (IFT).

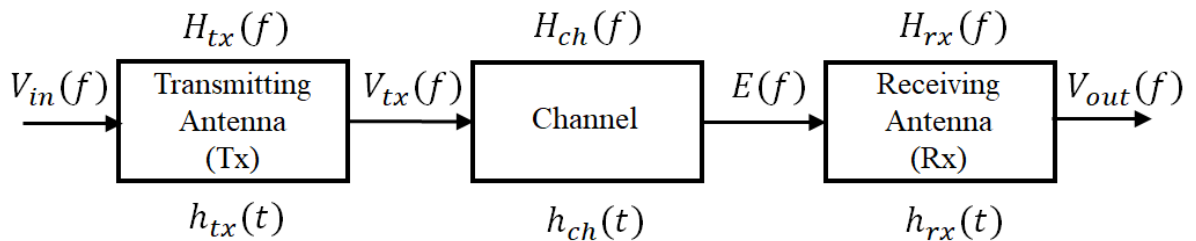


**Fig.5.2** A simple UWB communication system

The transfer function of the transmitter (Tx) antenna and the channel are defined together as the ratio of the electric field in the far-field of the antenna ( $r > 2D^2/\lambda_0$ , where  $D$

is the maximum dimension) at the desired direction  $\vec{E}(f)$  and the input voltage fed to the Tx antenna,  $V_{in}(f)$ , as stated in equation below,

$$\vec{H}_{txch}(f) = \vec{H}_{tx}(f)\vec{H}_{ch}(f) = \frac{\vec{E}(f)}{V_{in}(f)} \quad (\text{m}^{-1}) \quad (5.2)$$

Similarly, the receiver's (Rx) transfer function is defined using the following expression,

$$\vec{H}_{rx}(f) = \frac{V_{out}(f)}{\vec{E}(f)} \quad (\text{m}) \quad (5.3)$$

To establish a relationship between the excitation voltage of the Tx antenna and the received voltage at the Rx antenna,  $\vec{E}(f)$  is substituted from (5.2) into (5.3). This relationship can be thought of as the overall end-to-end transfer function of the link given as,

$$\vec{H}(f) = \vec{H}_{txch}(f)\vec{H}_{rx}(f) = \frac{V_{out}(f)}{V_{in}(f)} = \vec{S}_{21}(f) = |\vec{S}_{21}(f)|e^{-j\phi(f)} \quad (5.4)$$

This system transfer function is also identified as  $\vec{S}_{21}(f)$  where the magnitude and phase of the transfer function are represented by  $|\vec{S}_{21}(f)|$  and  $\phi(f)$  respectively.

In this UWB radio channel, the temporal impulse responses in transmission and reception are related by a time derivative for a particular antenna or related by the reciprocity theorem. In other words, the ratio of the transmitting antenna transfer function to the receiving antenna transfer function for the same UWB antenna is proportional to the operating frequency [111–114]. As a result, it is reasonable to infer that the relationship between them is described by an equation (5.5) [111-112].

$$\vec{H}_{tx}(f) = \frac{jf}{c} \vec{H}_{rx}(f) \quad (5.5)$$

Here  $c$  is the speed of light in vacuum. Also, the free-space transfer function from [111–113] is expressed as the following equation (5.6).

$$\vec{H}_{ch}(f) = \frac{\lambda}{4\pi r} e^{-jkr} \quad (5.6)$$

Where  $\lambda$  denotes the wavelength associated with the operating frequency. The distance between the transmitting and receiving antennas is denoted by the letter  $r$ . The propagation constant  $k$  is defined as  $k=2\pi/\lambda$ .

By using the above relations, the transfer function for the transmitter and receiver can be related to the system transfer function as,

$$\vec{H}_{rx}(f) = \sqrt{4\pi r |\vec{S}_{21}(f)|} \cdot e^{-j\left(\frac{\phi}{2} - \frac{\pi r f}{c} + \frac{\pi}{4}\right)} \quad (5.7)$$

$$\vec{H}_{tx}(f) = \frac{f}{c} \sqrt{4\pi r |S_{21}(f)|} \cdot e^{-j(\frac{\phi}{2} - \frac{\pi r f}{c} - \frac{\pi}{4})} \quad (5.8)$$

Now the power flow between the Tx and Rx can be written as follows using the Friis Transmission equation [31,112].

$$\frac{P_r(f)}{P_t(f)} = (1 - |\Gamma_t(f)|^2)(1 - |\Gamma_r(f)|^2) G_t(f) G_r(f) |\hat{\rho}_t(f) \hat{\rho}_r(f)|^2 \left(\frac{\lambda}{4\pi r}\right)^2 \quad (5.9)$$

Where  $P_t(f)$  and  $P_r(f)$  are the transmitting and receiving antenna powers, respectively.  $\Gamma_t(f)$ ,  $\Gamma_r(f)$  are the reflection coefficients at the transmitting and receiving antenna inputs and outputs, respectively. The gain of the transmitting and receiving antennas is represented by  $G_t(f)$  and  $G_r(f)$ , respectively. The term  $|\hat{\rho}_t(f) \hat{\rho}_r(f)|^2$  is the polarisation matching factor between the transmitting and receiving antennas.

If both antennas are both impedance and polarization matched, equation (5-9) can be simplified to,

$$\frac{P_r(f)}{P_t(f)} = G_t(f) G_r(f) \left(\frac{\lambda}{4\pi r}\right)^2 \quad (5.10)$$

Due to the relationship between the power and the voltage for the matched condition, expressed as equation (5.11 and 5.12), the transfer function of the antenna system can be given by equation (5.13).

The antenna system's transfer function can be written as equation (5.13) because of the connection between power and voltage expressed as equation (5.11 and 5.12) [115].

$$\frac{1}{2} \left[ \frac{V_{in}(f)}{2} \right]^2 = P_t(f) Z_0 \quad (5.11)$$

$$\frac{V_{out}^2}{2} = P_r(f) Z_L \quad (5.12)$$

$$S_{21}(f) = \frac{V_{out}(f)}{V_{in}(f)} = \left| \sqrt{\frac{P_r(f) \cdot Z_L}{P_t(f) \cdot 4Z_0}} \right| e^{-j\phi(f)} \quad (5.13)$$

The frequency domain characteristics of both the transmitting and receiving antennas, including impedance matching, gain, polarisation matching, and the distance between them, determine the transfer functions of the Tx-Rx antennas, and hence that of the overall system.

After obtaining the transfer function, The impulse responses of the Tx, Rx, and system may be simply determined from IFFT as follows,

$$h(t) = Re\{IFFT[\vec{S}_{21}(f)]\} \quad (5.14)$$

$$h_{tx}(t) = Re\{IFFT[\vec{H}_{tx}(f)]\} \quad (5.15)$$

$$h_{rx}(t) = Re\{IFFT[\vec{H}_{rx}(f)]\} \quad (5.16)$$

### 5.3 Pulse distortion analysis

Distortion-free information communication using a pair of identical UWB antennas can be verified by comparing the similarity between the input pulse to the Tx antenna and the output pulse to the Rx antenna. Preservation of the time domain features of the received pulse indicates distortion-free end-to-end propagation which requires the transfer function of equation (5.4) to possess both a flat amplitude response and a linear phase response over the operating frequency band. Useful parameters such as the group delay and fidelity factor ( $FF$ ) derived from the transfer function are covered in the following section.

#### 5.3.1 Group delay

Group delay refers to the negative frequency derivative of the phase response of the propagation medium including the Tx-Rx antennas ( $\vec{S}_{21}(f)$  in eq.5.4), as follow,

$$\tau_g(f) = -\frac{1}{2\pi} \frac{d\phi(f)}{df} \quad (5.17)$$

When a broadband signal propagates through a dispersive medium, it is subjected to amplitude and/or phase distortions. The level of distortion depends on the frequency dependent attenuation and phase constants of the end-to-end medium that includes both the Tx/Rx antennas and the communication channel. Equation 5.17 implies that a non-linear phase response implies a variable group delay across the bandwidth, leading to distortion of the received pulse.

#### 5.3.2 Fidelity factor

Fidelity factor ( $FF$ ) implies the fidelity or correlation between source pulse  $g_t(t)$  and received pulse  $g_r(t)$ . It is defined as the maximum correlation coefficient expressed mathematically as [111-112]:

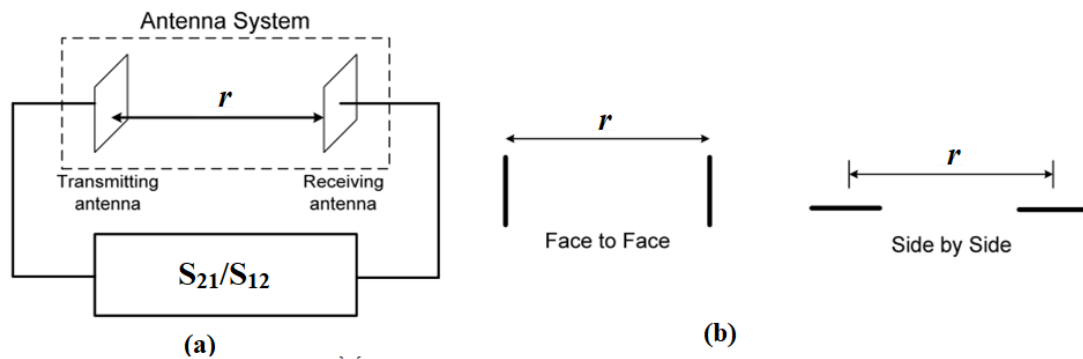
$$FF = \max \left[ \frac{\int_{-\infty}^{\infty} g_t(t) \cdot g_r(t-\tau) \cdot dt}{\sqrt{\int_{-\infty}^{\infty} |g_t(t)|^2 \cdot dt \int_{-\infty}^{\infty} |g_r(t)|^2 \cdot dt}} \right] \quad (5.18)$$

Here,  $g_t(t)$  and  $g_r(t)$  are normalized by their energy.

The fidelity factor achieves its maximum value of unity when the two signal waveforms are equal to each other, indicating that the Tx-Rx antennas do not distort the pulse at all. In the worst-case scenario, where the two pulses are completely different in shape, the fidelity becomes to zero. In UWB communications, a high  $FF$  close to unity is always required. The time domain performance study of the wideband slot antenna developed in chapters 3 and 4 is presented in the next section.

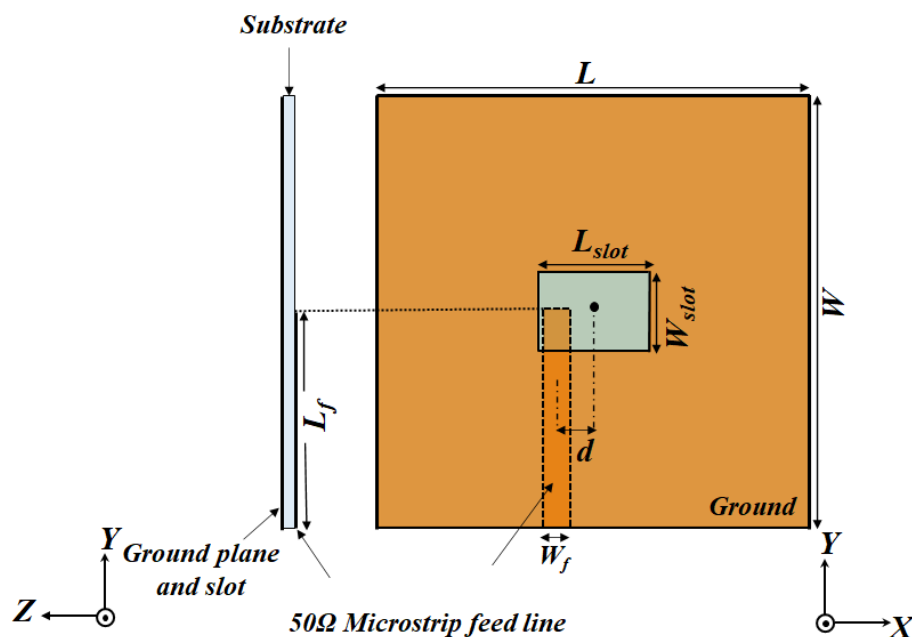
## 5.4 Time domain performance evaluation of antenna

To study the time domain performance of antennas, two identical antennas are placed in the far-field distance of each other,  $r=2D^2/\lambda_0$  as illustrated in Figure 5.3(a). One antenna is used as a transmitter while the other antenna is used as receiver. For comparison, two different alignment of the antennas namely face-to-face and side-by-side as shown in Figure 5.3(b) are considered.



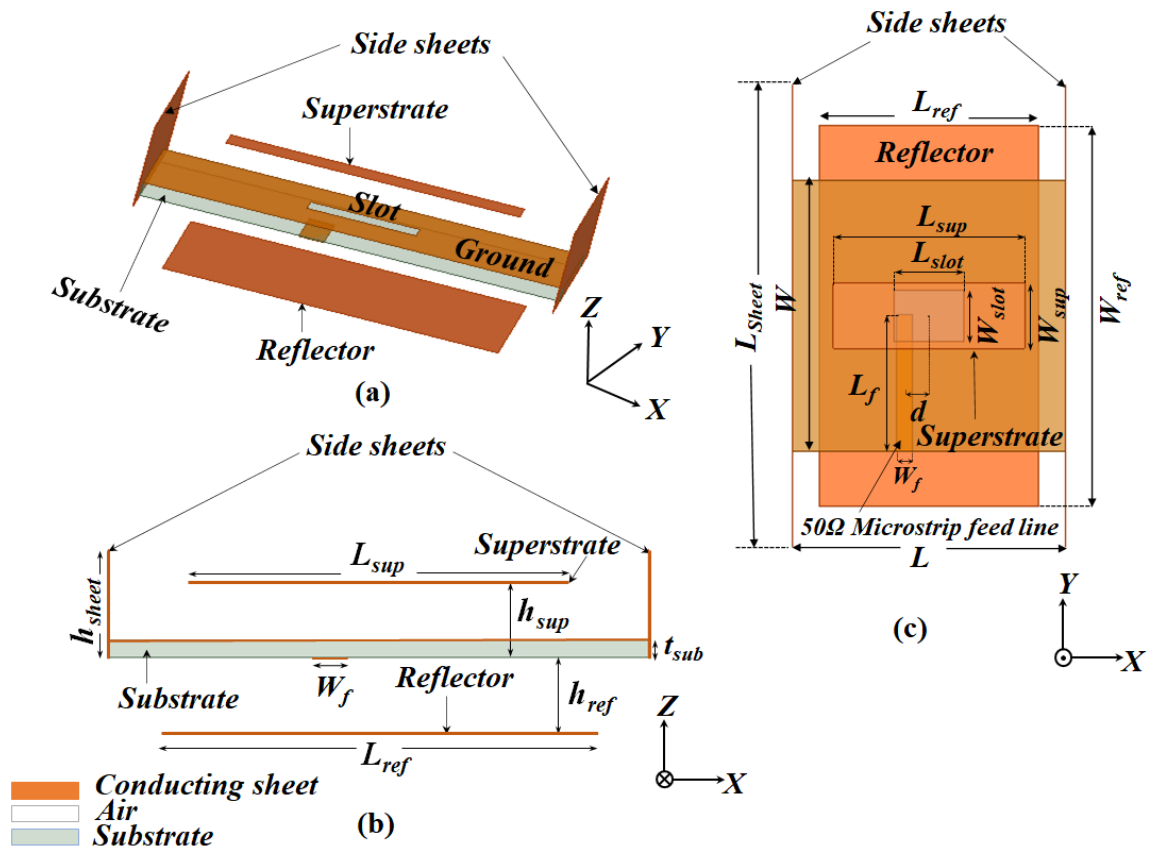
**Fig.5.3**(a)Transmitting and receiving antenna (Tx-Rx) system and (b) top view of antennas for face-to-face and side-by-side orientation [116].

Figure 5.4 and 5.5 show the wideband slot and conducting sheets loaded high gain wideband slot antenna for which the time domain performance is analysed. Though these antennas were discussed in detail in chapter 3 and 4, their important frequency domain characteristics are summarized in Table 5.1.



**Fig.5.4** Geometry of the basic slot antenna of chapter 3.





**Fig.5.5** Geometry of the final antenna of chapter 4 (a) 3-D view (b) Side view (XZ-plane) (c) Top view (XY-plane).

For the antenna system model in figure 5.3, the far field distance  $r$  for the wideband slot antenna is 284 mm and the final antenna is 551 mm at 8.50 GHz frequency which is given by equation (5.19).

$$\text{Far field distance } (r) = 2D^2/\lambda_0 \quad (5.19)$$

**Table 5.1** Performance characteristics of the slot antennas under comparison

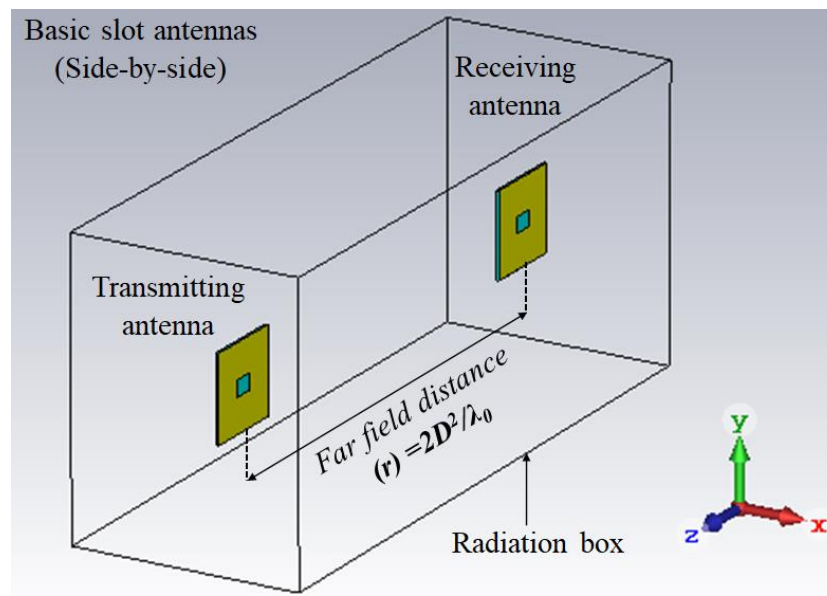
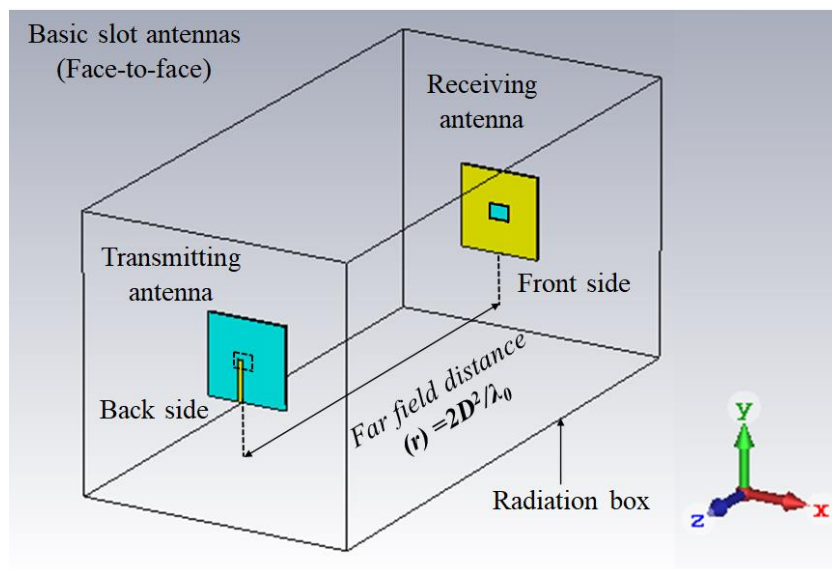
Antenna	-10 dB Impedance band (GHz, %), Band-1	Peak boresight gain (dBi)	3 dB gain band (GHz), Band-2	3 dB gain band (Intersection of band-1 and band-2) (GHz, %)
Basic slot	5.94–8.54, 35.91%	2.83	NA (as peak gain is < 3 dBi)	
Final antenna	5.94–10.53, 55.74%	12.52	4.73–10.08	5.94–10.08, 51.68%

Where,  $D$  is the maximum dimension of the antenna and  $\lambda_0$  is Free space wavelength ( $\lambda_0 = c/f$ ). Using equation (5.19), the far-field distances are given below,

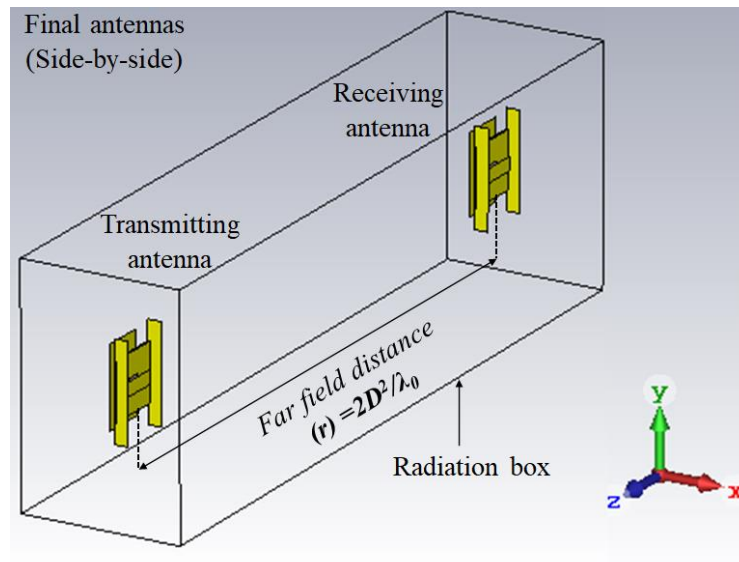
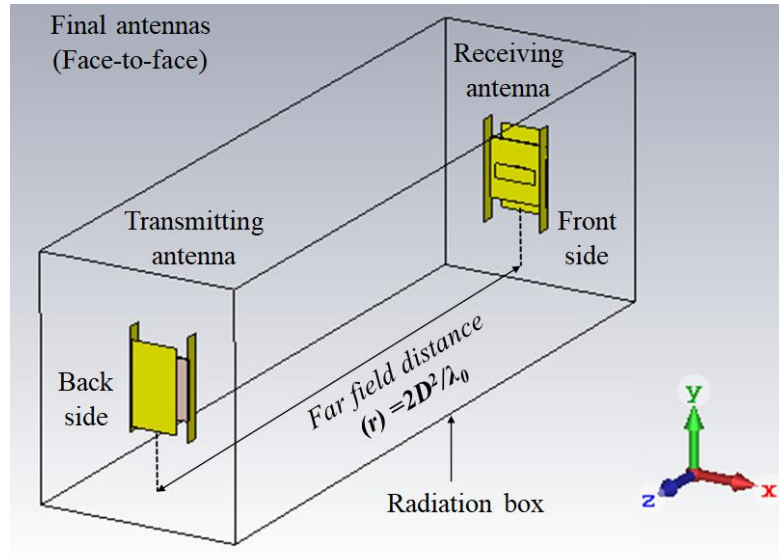
For basic slot antenna:  $D = 70.71\text{mm}$ ,  $r = 284\text{ mm}$  and

For final antenna:  $D = 88.60\text{ mm}$ ,  $r = 551\text{ mm}$

Here, the CST time domain solver is utilized to analyse the time domain characteristics of the basic slot antenna and final antenna. The simulation model is setup by placing the two identical antennas (transmitter and receiver) at the far field separation in the radiation box like illustrated in Figure 5.3. The resulting CST model of both the antennas for face-to-face and side-by-side orientations are shown in Figure 5.6.



(a)

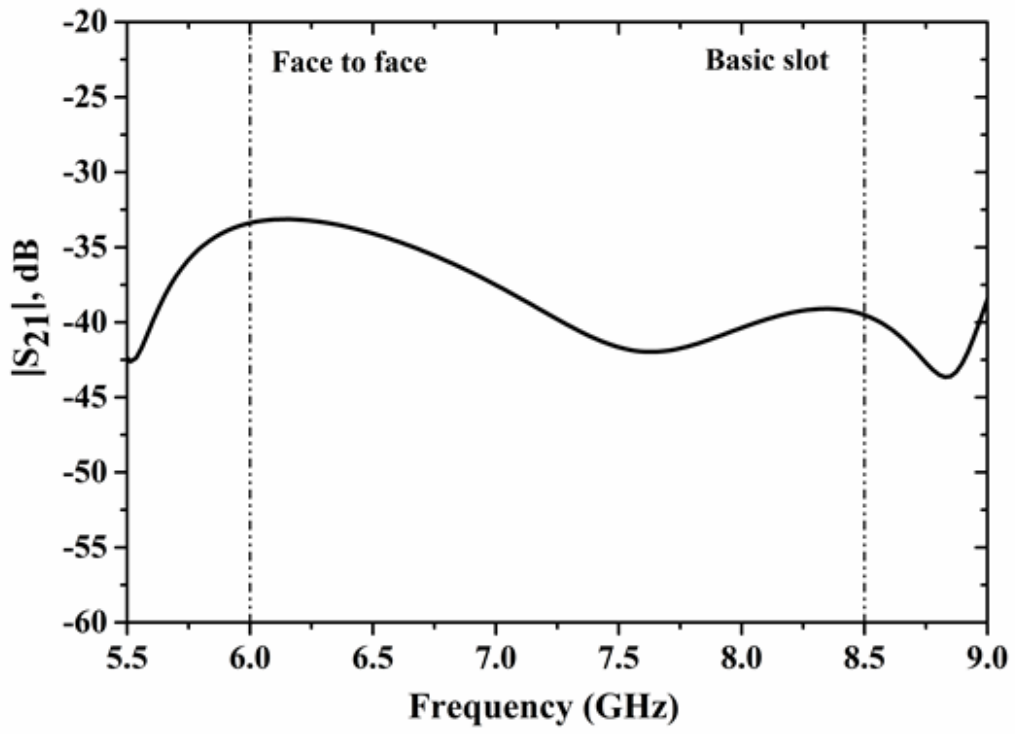


(b)

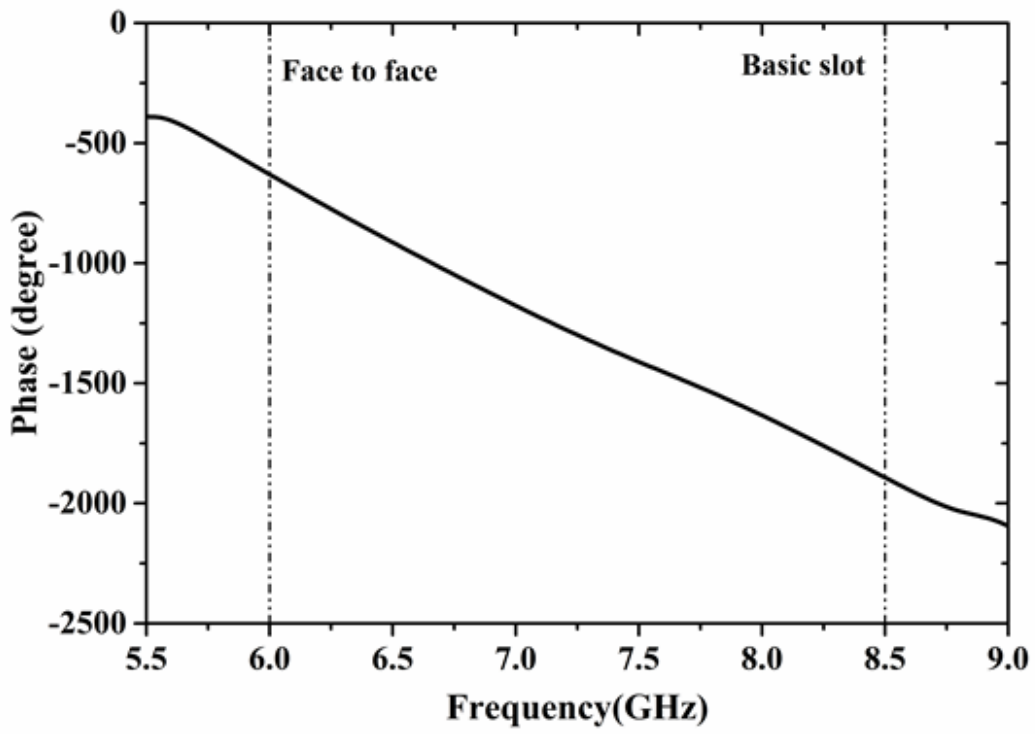
**Fig.5.6** CST model for time domain analysis of (a) basic slot antenna and (b) final antenna.

The Gaussian sinusoidal source pulse for ECC UWB band is used in the system model as mentioned in section 5.1. The simulated transfer function  $S_{21}(f)$  in magnitude and phase  $\phi(f)$  of the transmitter and receiver system (Tx-Rx system) for the above said antennas in two different orientations i.e., face to face and side by side, are shown in Figure 5.7 and 5.8. Both of them have linear phase across the ECC/Indian UWB frequency band.

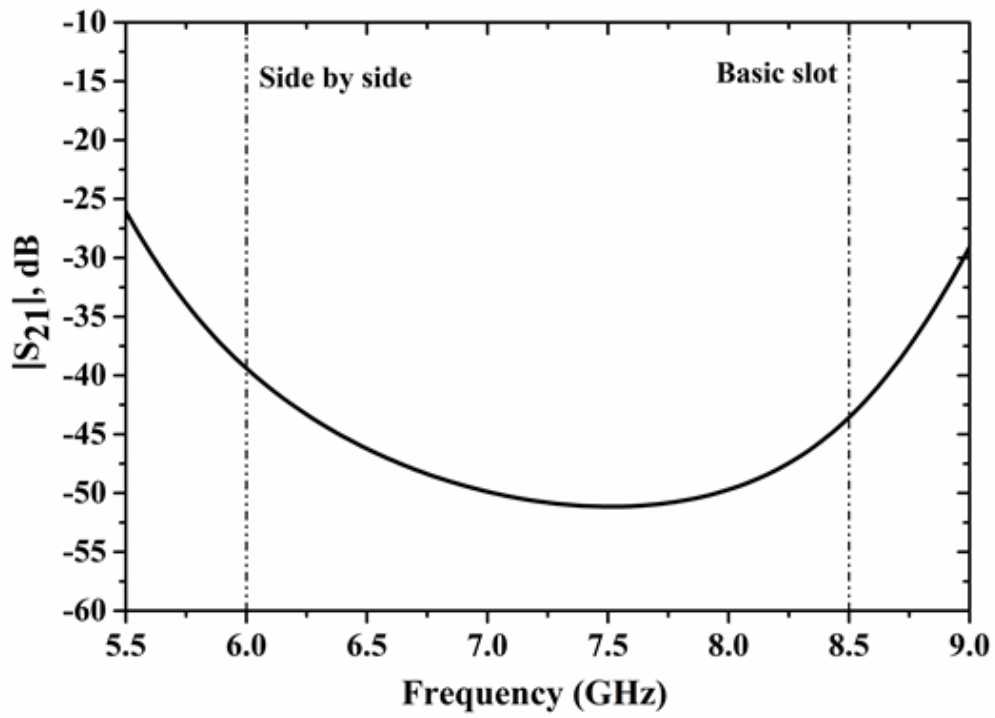
The magnitude response shows flatter response for the final antenna. The results are summarized in tables 5.2 and 5.3.



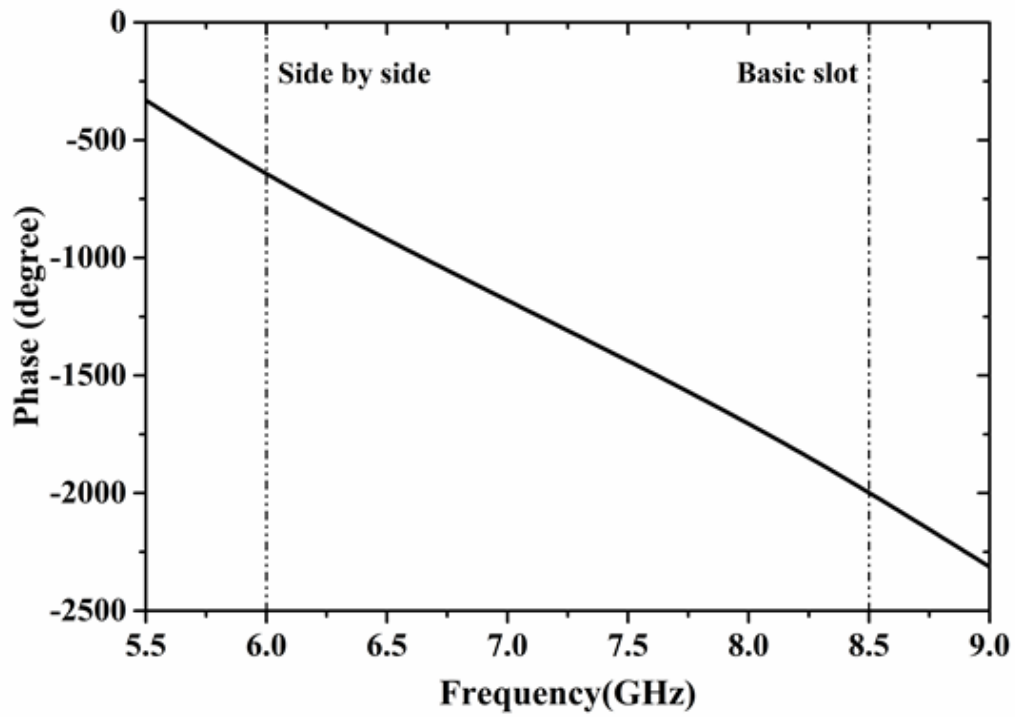
(a)



(b)

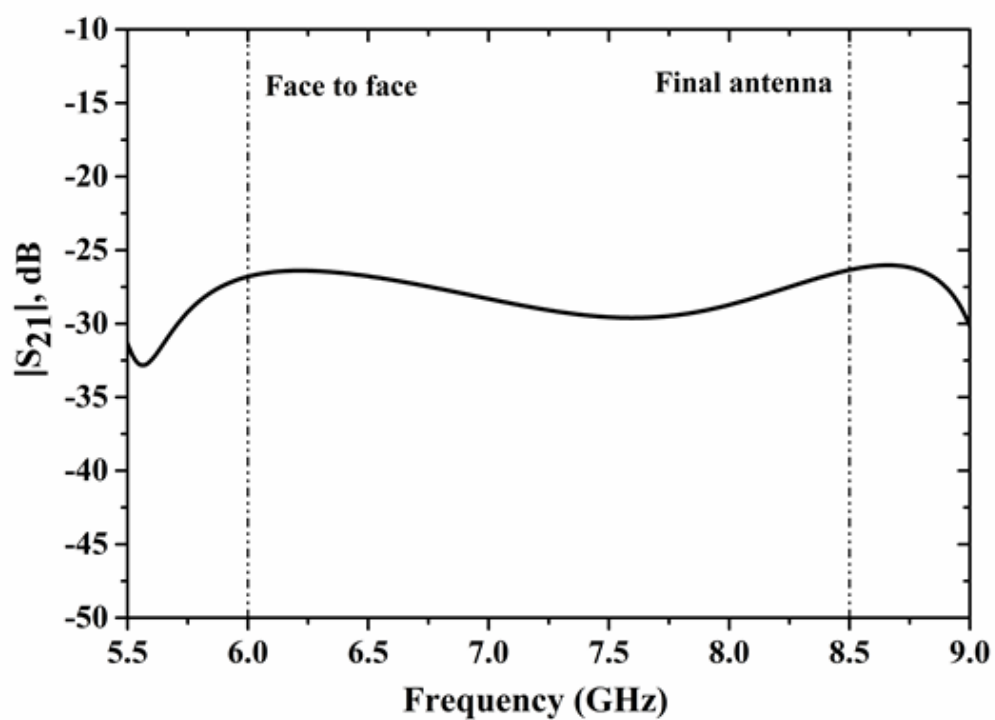


(c)

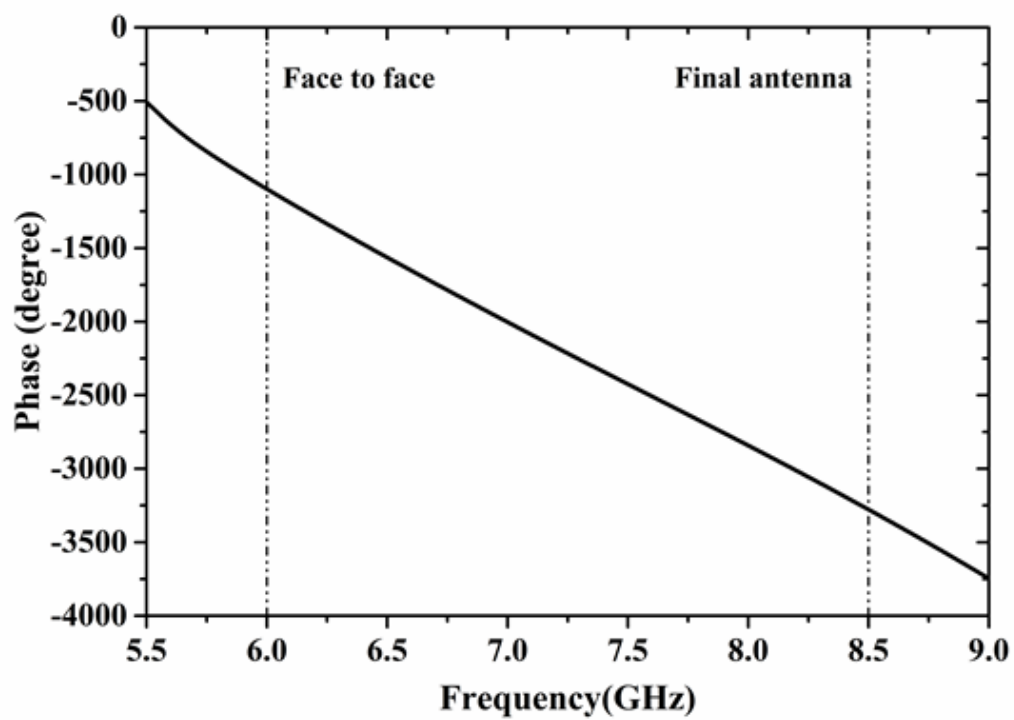


(d)

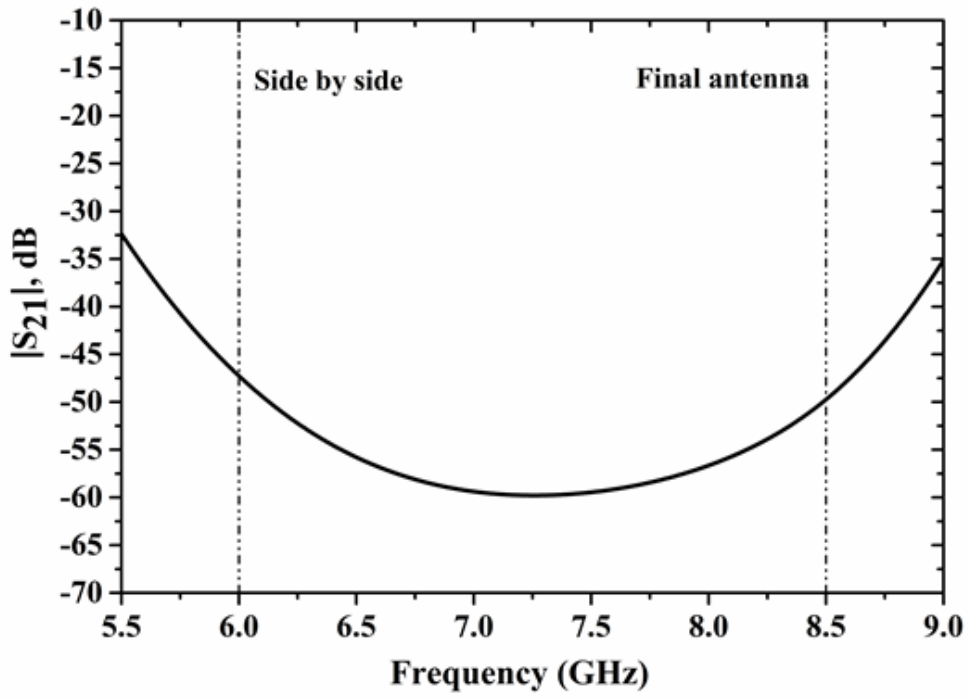
**Fig.5.7** Simulated magnitude and phase of system transfer function for basic slot antenna (a,b) face to face orientation (c,d) side by side orientations



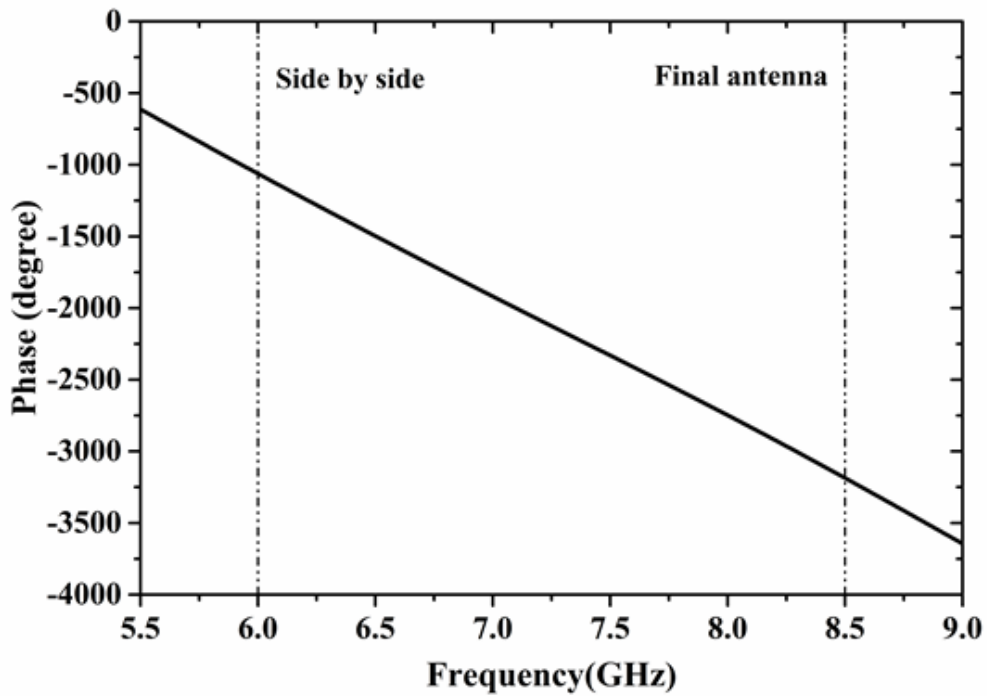
(a)



(b)



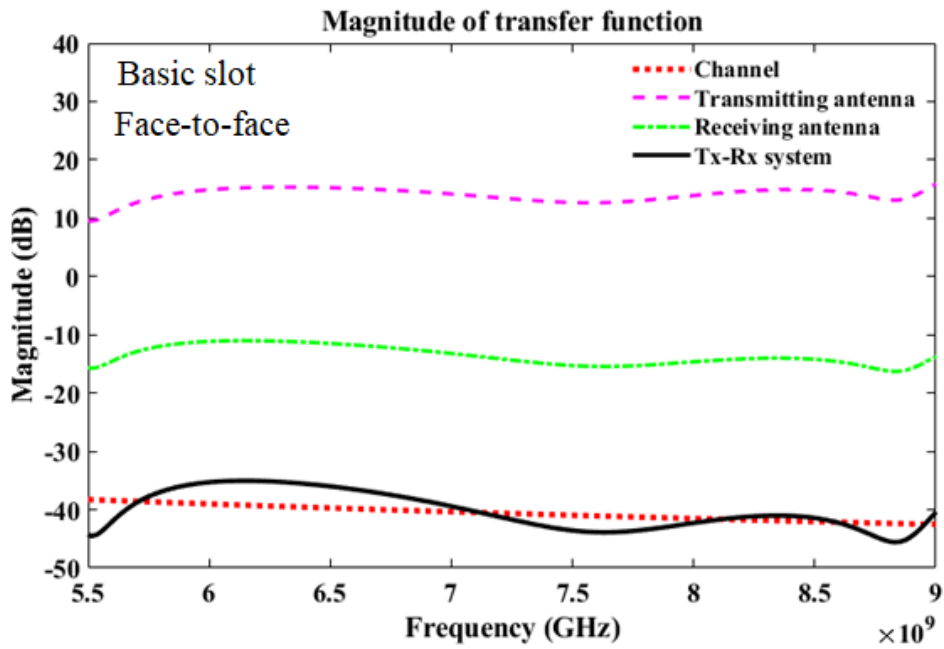
(c)



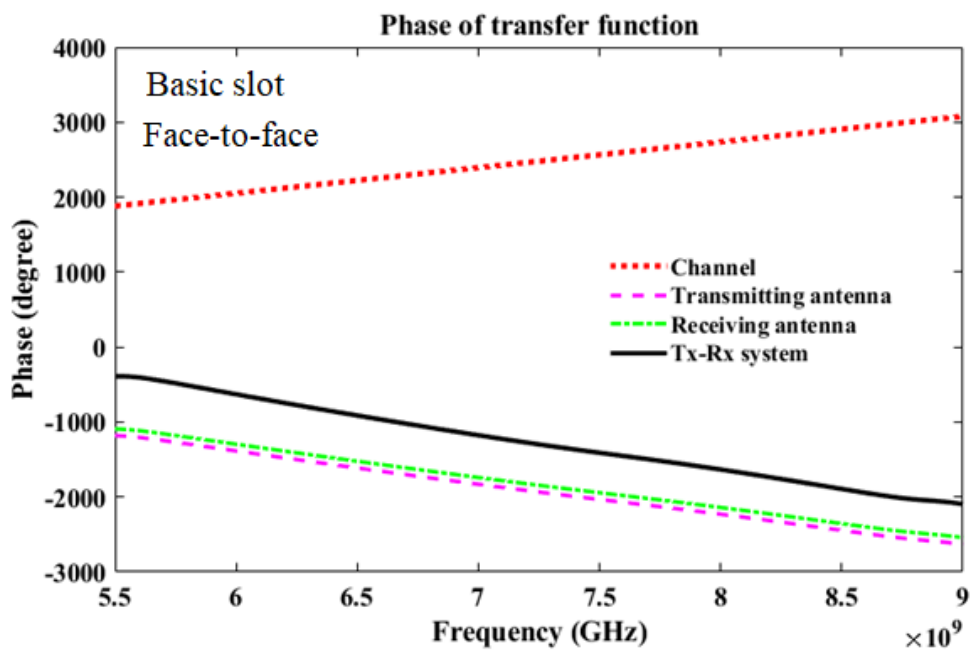
(d)

**Fig.5.8** Simulated magnitude and phase of Tx-Rx system transfer function for final antenna placed at far field distance in (a,b) face to face and (c,d) side by side orientations.

Using the equation (5.6), (5.7) and (5.8) the magnitude and phase of transfer function for the channel, Tx antenna and Rx antenna for the two antennas are calculated using MATLAB as depicted in Figure 5.9 and 5.10.



(a)



(b)



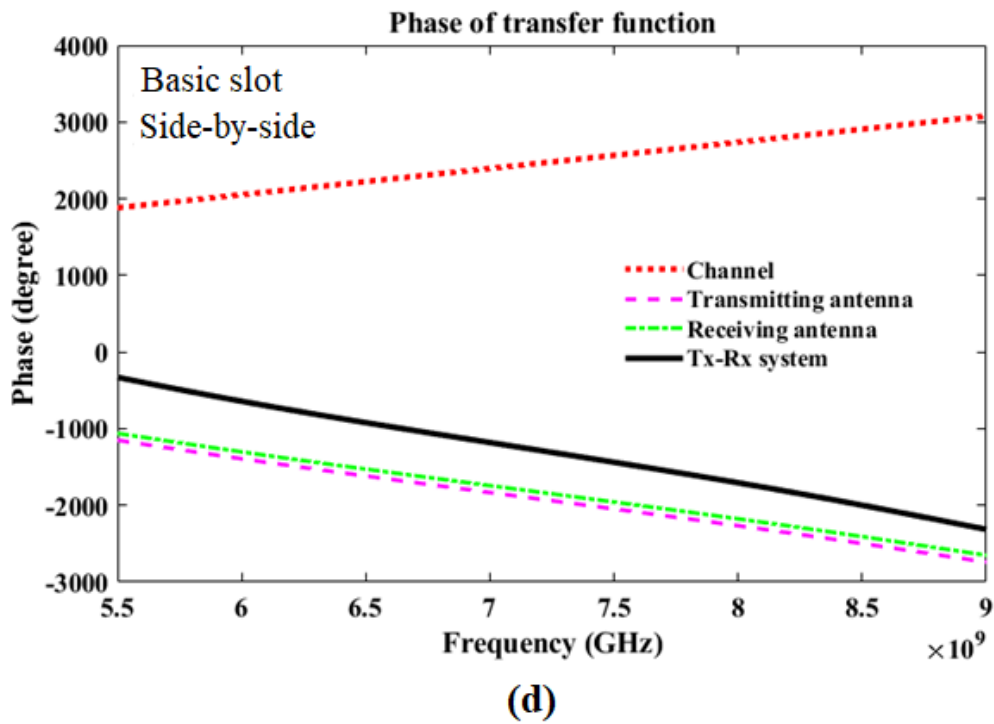
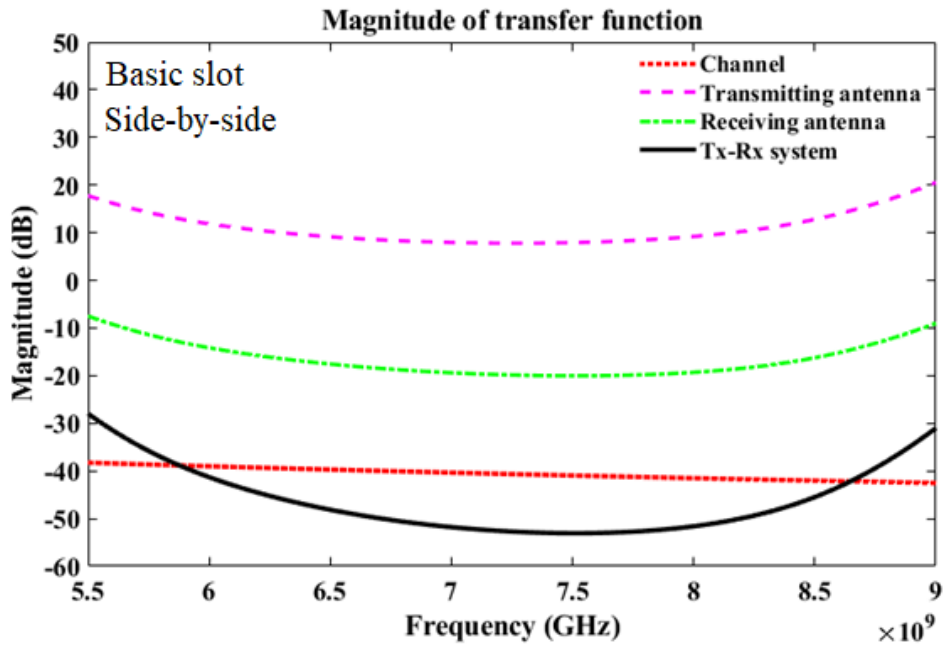
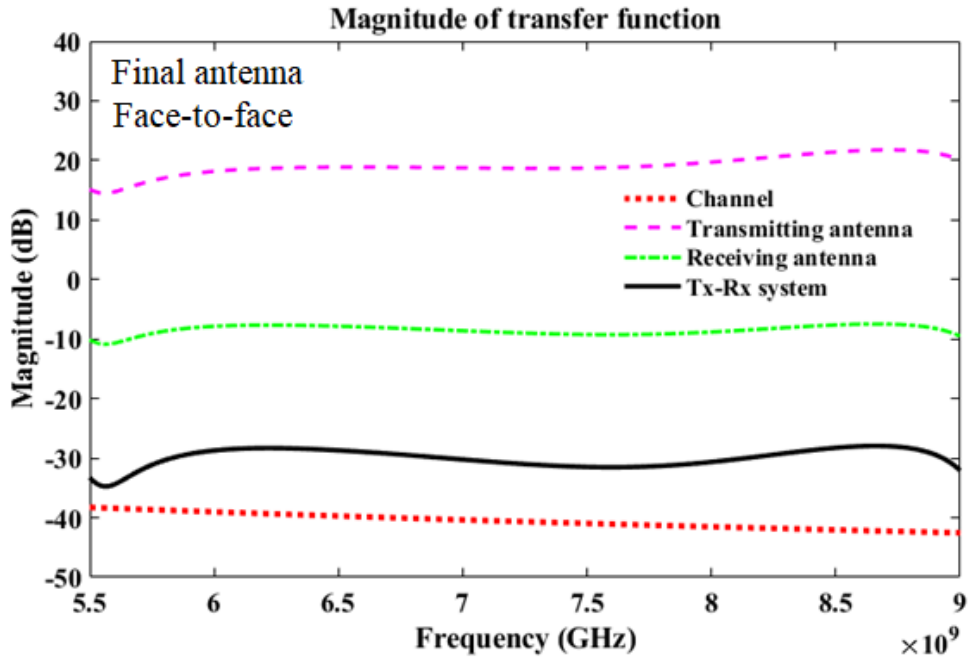
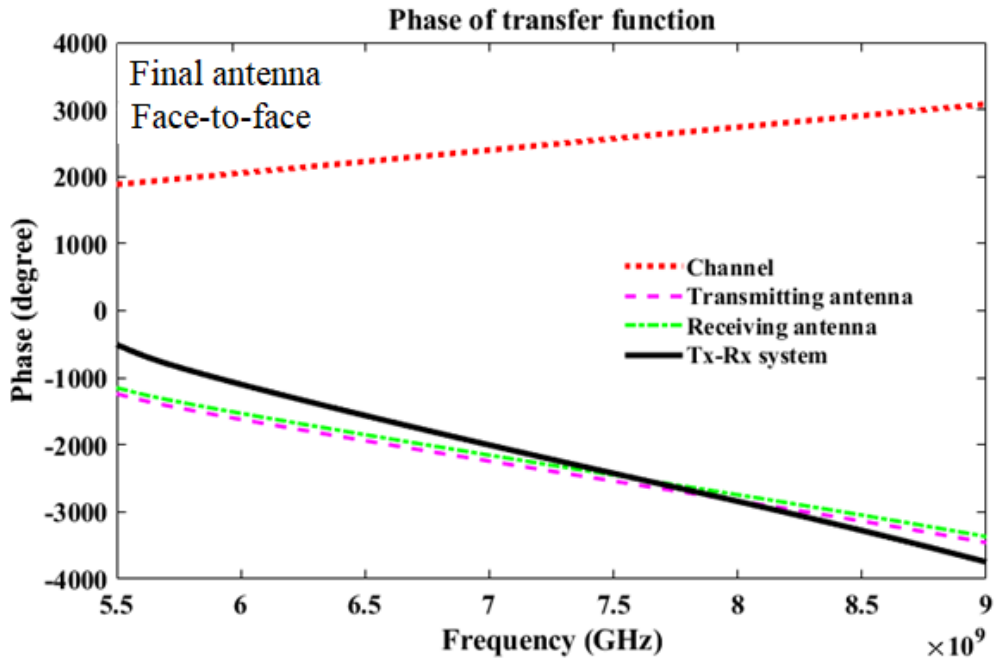


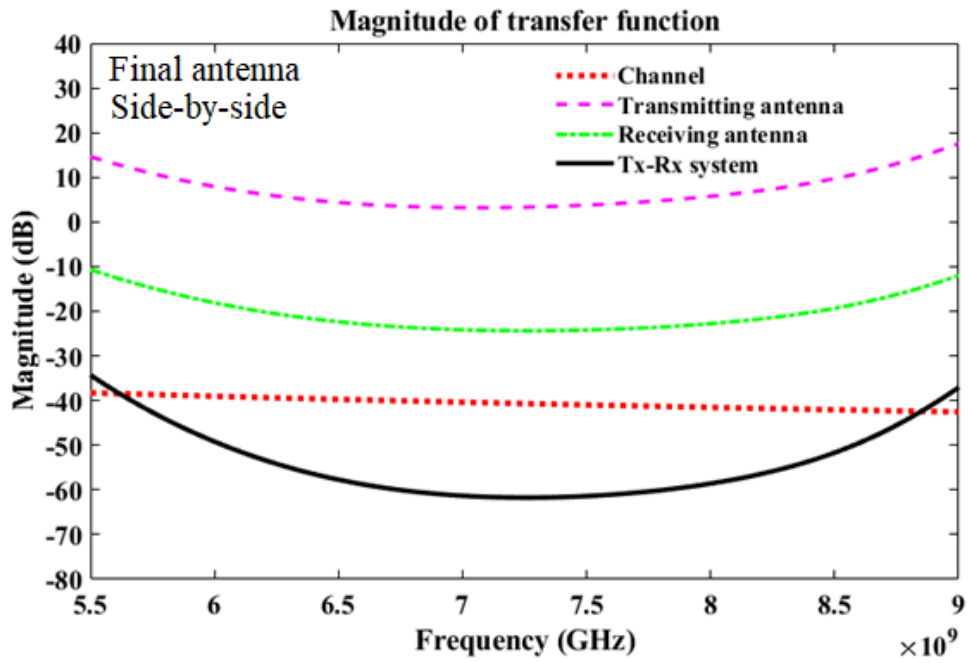
**Fig.5.9** Magnitude and phase of the transfer function of channel, transmitting antenna, receiving antenna, and Tx-Rx system for basic slot antenna placed at far field distance in (a,b) face to face (c,d) side by side orientations.



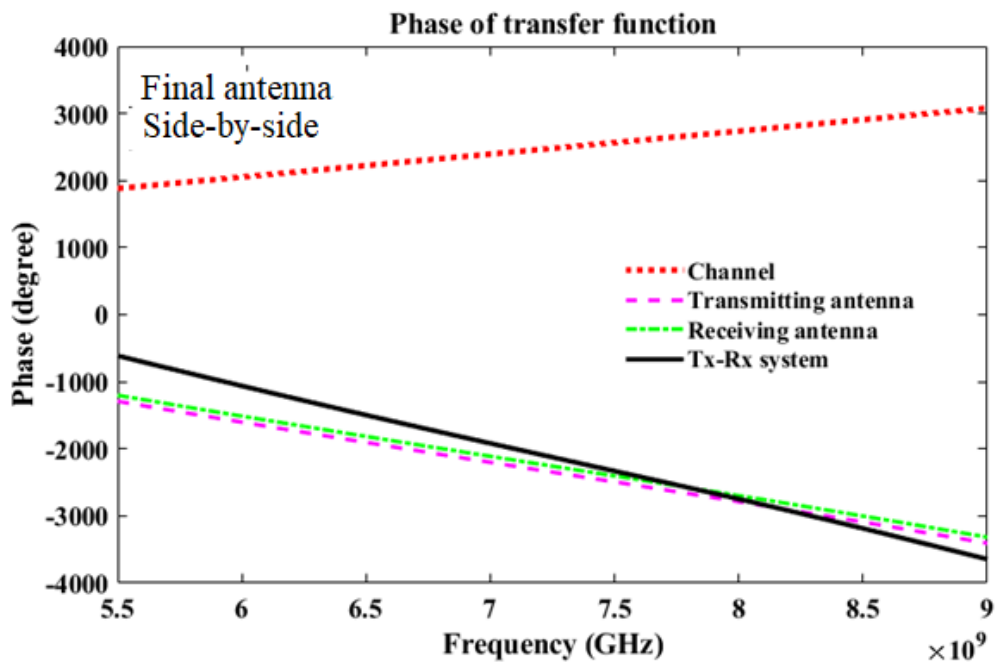
(a)



(b)



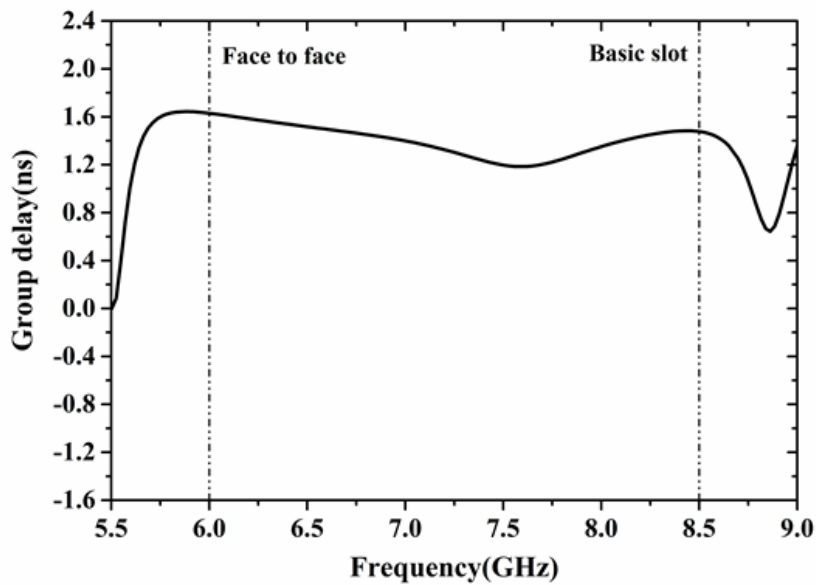
(c)



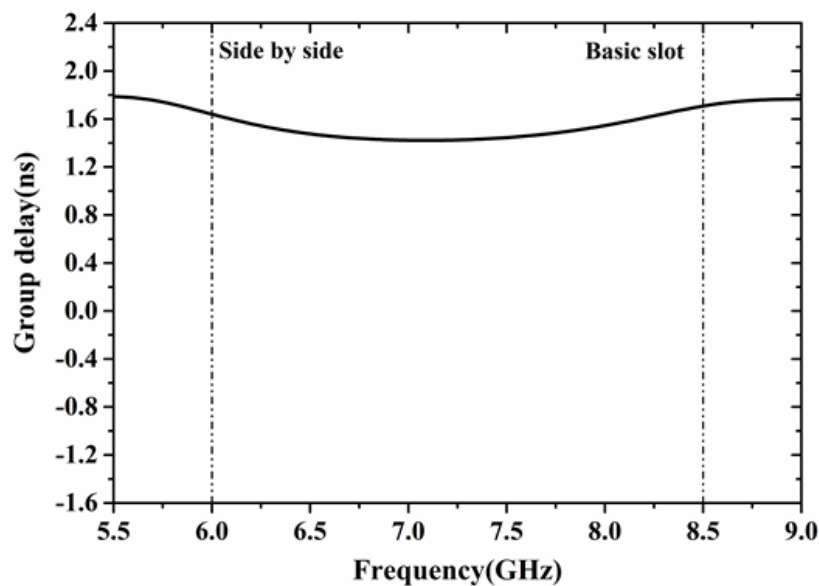
(d)

**Fig.5.10** Magnitude and phase of the transfer function of channel, transmitting antenna, receiving antenna, and Tx-Rx system for final antenna placed at far field distance in (a,b) face to face (c,d) side by side orientations.

The group delay deduced from the phase of the transfer function as in equation (5.18) is plotted in figure 5.11 and figure 5.12 for the same antennas in two face to face and side by side orientations. It can be noticed from the figure the group delay is flat within the ECC UWB band in both antennas but more flat in the conducting sheets loaded slot antenna. Tables 5.2 and 5.3 summarize the results from the plots.



(a)



(b)

**Fig.5.11** Group delay of basic slot antenna placed at far field distance in (a) face to face and (b) side by side orientation.

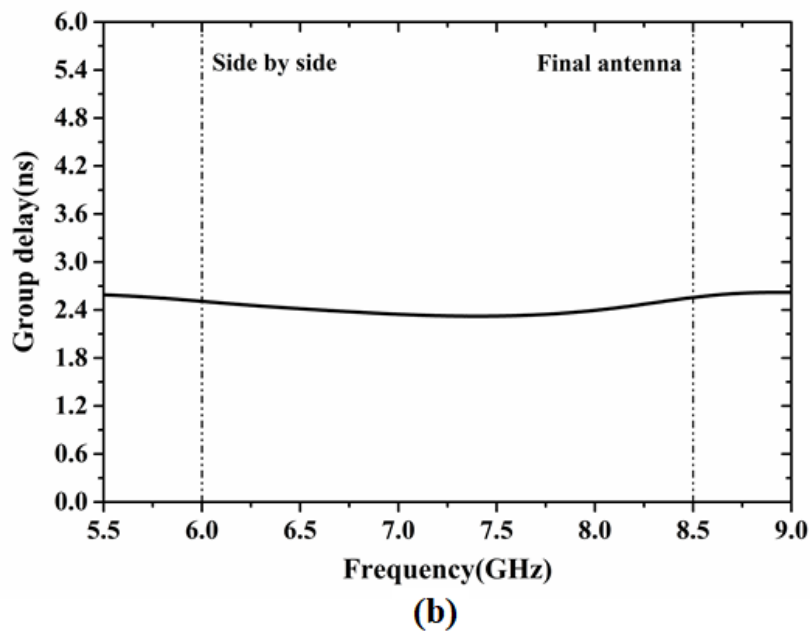
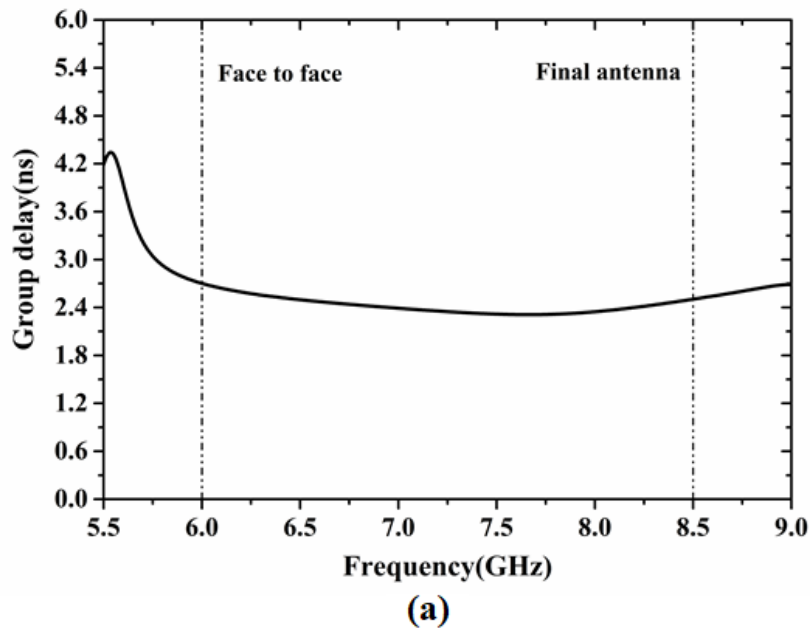


**Fig.5.12** Group delay of final antenna placed at far field distance in (a) face to face and (b) side by side orientation.

The comparison of normalised input and received pulses are shown in figure 5.13 and 5.14 for both the antennas in two different orientation face to face and side by side. As stated before (section 5.1), Gaussian sinusoidal pulse is used as the source pulse. It can be noticed that the received UWB signal pulse does not resemble the source pulse as it is

distorted in shape. Tables 5.2 shows that the conducting sheets loaded slot antenna has much higher  $FF$  of 97.67 % than the basic slot antenna (90.95%).

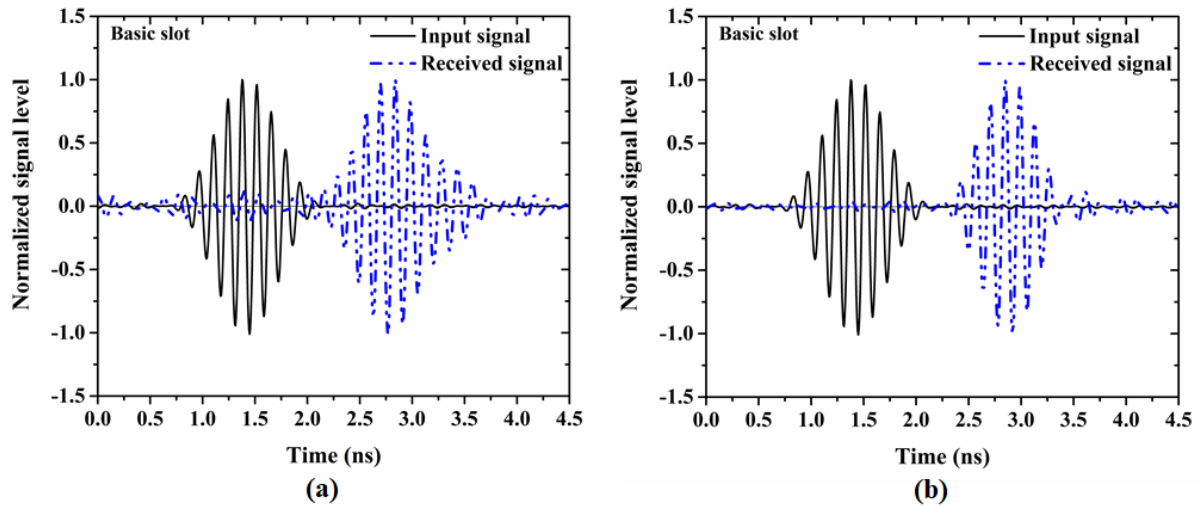


**Fig.5.13** Input and received pulses when basic slot antenna placed at far field distance in (a) face to face and (b) side by side orientations.

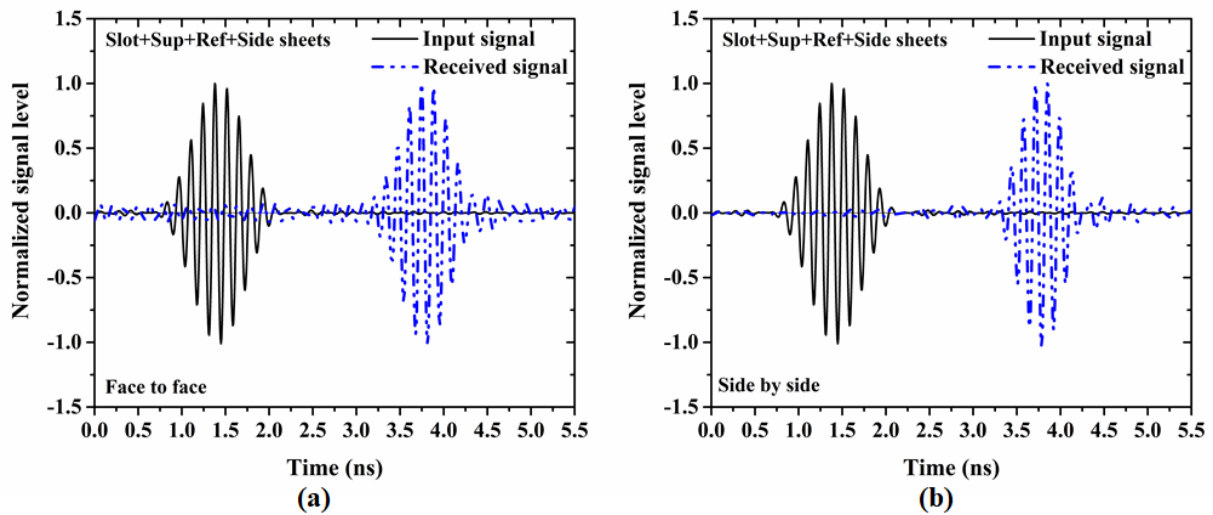


**Fig.5.14** Input and received pulses of the final antenna placed at far field distance in (a) face to face and (b) side by side orientations.

**Table 5.2** Performance characteristics of slot antenna placed at far field distance in face-to-face orientation

Antenna	Face to face							FF (Eq. (5.18)) (%)
	S <sub>21</sub>  , dB			Group delay (ns) (Eq. (5.18))				
	Max	Min	Difference	Max	Min	Difference	Standard deviation (SD)	
Basic slot	-33.13	-41.97	8.84	1.63	1.18	0.45	0.14	90.95
Final antenna	-26.29	-29.60	3.31	2.70	2.31	0.39	0.10	97.67

**Table 5.3** Performance characteristics of slot antenna placed at far field distance in side-by-side orientation

Antenna	Side by side							
	$S_{21}$  , dB			Group delay (ns) (Eq. (5.18))				FF (Eq. (5.18)) (%)
	Max	Min	Difference	Max	Min	Difference	Standard deviation (SD)	
Basic slot	-39.45	-51.15	11.70	1.71	1.42	0.29	0.08	96.45
Final antenna	-47.15	-57.79	10.64	2.56	2.32	0.24	0.07	96.70

## 5.5 Conclusion

This chapter described the time domain characteristics of the slot antennas developed in chapter 3 and 4, including the transfer function, phase, group delay and fidelity factor. The transfer function of antenna was explained in transmitting, receiving, and Tx-Rx system modes. Fundamental properties of the source pulse in time and frequency domain were introduced for ECC UWB band. The distortion in the received pulses was discussed in terms of transfer function of the system, phase linearity, group delay and fidelity factor for faces to face and side by side orientations of the antennas. It was found that the conducting sheets i.e., reflector, superstrate, and side sheets loaded slot antenna (final antenna) gives better performance parameter such as flatter group delay and higher fidelity factor than the basic slot antenna. The investigation thus concludes that the conducting sheets loaded slot antenna is a suitable candidate for the European/Indian UWB application.

## Chapter 6

### Conclusion and Future Scope

This chapter summarises and highlights the thesis work which was detailed over the previous 5 chapters. This is followed by a few points identified for future work.

#### 6.1 Concluding remarks

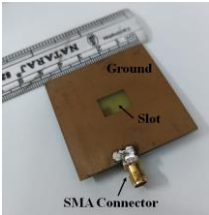
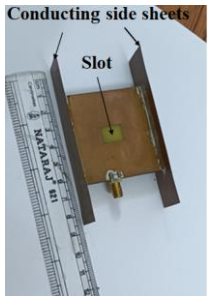
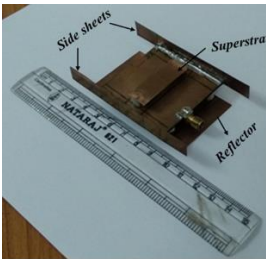
The ultra-wideband communication has emerged as a promising technology for meeting the growing demand for low-cost, low power level, high-speed wireless communication as well as specialized applications such as ground penetrating radar, level probing radar, and biomedical imaging etc. This thesis presented a comprehensive study of the design, simulation, analysis and characterisation of UWB slot antenna for European/Indian UWB range (6–8.5 GHz). Three designs of microstrip-fed wide slot UWB antenna were demonstrated. The first design was a simple offset-microstrip fed slot antenna enabling 5.92–8.56 GHz operation with bidirectional radiation pattern and low peak gain of 2.59 dBi. It has been found that the proper optimization of the offset location of the feed causes merging of the two identical polarized resonances due the fictitious short circuit placed by the offset microstrip, leading to bandwidth enhancement. In the second design, this wide offset fed slot antenna was loaded with a pair of conducting side sheets in the vertical plane to achieve bidirectional gain enhancement within the complete impedance band due to the convergence of the oblique radiation from the slot towards the boresight directions. Since this conducting side sheet loading improves the antenna gain while preserving the impedance band and bidirectional nature of radiation pattern, the technique is referred to as a non-resonant technique. This design exhibits an impedance band from 5.97-8.53 GHz with a peak boresight gain of 5.59 dBi while the average in-band gain improvement of 3.99 dB relative to the basic offset fed slot antenna. In the third design, the conducting reflector and superstrate sheets are added to the basic slot antenna to obtain directional high gain radiation. Next, a pair of conducting side sheets as done for the second antenna is also employed on the radiating side of the slot antenna to further flatten the gain throughout the band. This third or final design achieves 3 dB gain-band of 6.03-9.77 (47.34%) with 12.04 dBi peak boresight gain. This 3 dB gain-band is 93% of the impedance band of the slot antenna (6.03-10.12 GHz or 50.65%).

The evolutions of the designed antennas were explored in detail to have a better understanding of their wideband behavior. Analysis of their reflection coefficient, field



distribution, gain, and radiation pattern demonstrated their dependence on various dimensional parameters of the antenna. The antennas with the optimum dimensions were fabricated and tested, and the results were found in good match with simulated results. Next, to further validate the usefulness of the UWB antenna, time domain analysis was conducted. Time domain characteristics such as the magnitude and phase of the transfer functions, group delay, and fidelity factor for the proposed final antenna was analyzed. The final antenna was verified to have a flat magnitude and linear phase response of the transfer function over the operational band of 6–8.5 GHz that resulted in high fidelity factor of 97.67%. Characteristics of the above antennas are summarized in Table 6.1 as follows:

**Table 6.1** Measured performance characteristics of the antennas discussed in chapters

Antenna (Chapter)	Fabricated prototype	-10 dB Impedance band (GHz, %),	Peak boresight gain (dBi)	Pattern	3 dB gain band (GHz, %)
Offset microstrip fed Slot (Basic slot) (Chapter-3)		5.92–8.56, 36.46%	2.59	Bidirectional	NA (as peak gain is < 3 dBi)
Side sheets loaded slot (Chapter-3)		5.97–8.53, 35.31%	5.59	Bidirectional	5.97–8.53, 35.31%
Final antenna (Chapter-4)		6.03–10.12, 50.56%	12.04	Directional	6.03–9.77, 47.34%

## 6.2 Future scope of the study

The designs proposed in this thesis can be extended for further study some of which are addressed below.

1. Time domain analysis of the developed antenna may be validated in a practical Tx-Rx system comprising of RF subsystems, nano-second pulse generator and a high-speed digital storage oscilloscope.
2. Design for extending the impedance band down to 3.1 GHz to cover the FCC band (3.1 to 10.6 GHz) may be incorporated. With a band disable/enable feature for the 3-6 GHz, resulting antenna may be suitable for both FCC and ECC applications.
3. Influence of the geometry and alignment of various conducting sheets of the present design may be investigated for improving the performance further
4. Alternatively, frequency selective surfaces (FSS) and metamaterial-based superstrate, reflector and side sheets could be used for performance enhancement, especially for gain enhancement and size reduction.

## References

- [1] FCC 02-48, "Revision of Part 15 of the Commission's Rule Regarding Ultra-Wideband Transmission Systems", First Report and Order, ET 98-153; 2002.
- [2] H. Nikookar and R. Prasad, Introduction to Ultra Wideband for Wireless Communications, Signals and Communication Technology. *Springer Netherlands*, 2009.
- [3] G. Roberto Aiello and Gerald D. Rogerson, "Ultra-wideband Wireless Systems", *IEEE Microwave Magazine*, pp. 36-47, June 2003.
- [4] W. Wiesbeck, G. Adamiuk and C. Sturm, "Basic Properties and Design Principles of UWB Antennas," in *Proceedings of the IEEE*, vol. 97, no. 2, pp. 372-385, Feb. 2009.
- [5] Adamiuk, G., Zwick, T., & Wiesbeck, W., "UWB Antennas for Communication Systems" *Proceedings of the IEEE*, vol.100, pp. 2308-2321, 2012.
- [6] Nicholas Cravotta, "Ultrawideband: the next wireless panacea?", October 17, 2002, EDN, [www.edn.com](http://www.edn.com).
- [7] S. Colson and H. Hoff, "Ultra-Wideband Technology for Defence Applications," in *IEEE International Conference on Ultra-Wideband*, pp. 615–620, 2005.
- [8] I. Oppermann, M. Hämäläinen and J. Iinatti, UWB Theory and Applications. Chichester, UK: *John Wiley & Sons Ltd*, 2004.
- [9] Karlsson, M. "Ultra-wideband Antenna and Radio Front-end Systems" *Institutionen för teknik och naturvetenskap*, 2008. Available at: <http://liu.diva-portal.org/smash/record.jsf?pid=diva2%3A17081&dswid=-6205>
- [10] R.J. Fontana, "Recent System Applications of Short-Pulse Ultra-Wideband (UWB) Technology", *IEEE Microwave Theory and Tech.*, vol. 52, No. 9, September 2004.
- [11] R. S. Kshetrimayum, "An introduction to UWB communication systems," in *IEEE Potentials*, vol. 28, no. 2, pp. 9-13, March-April 2009.
- [12] Department of telecommunications, Government of India, "The Gazette of India: extraordinary", Retrieved October 18, 2018, from <https://dot.gov.in/spectrummanagement/license-exemption-uwband-device-gsr-1046e-dated-18102018>.
- [13] M. Li, R. Birken, N. X. Sun and M. L. Wang, "Compact Slot Antenna With Low Dispersion for Ground Penetrating Radar Application," in *IEEE Antennas and Wireless Propagation Letters*, vol. 15, pp. 638-641, 2016.

- [14] Sibille, A. "Compared Performance of UWB Antennas for Time and Frequency Domain Modulation." *28th URSI General Assembly*, NewDelhi, India, 2005.
- [15] Licul, S, Noronha, J. A. N., Davis, W. A., Sweeney, D. G., Anderson, C. R., & Bielawa, T. M. "A parametric study of time-domain characteristics of possible UWB antenna architectures." *IEEE 58th Vehicular Technology Conference*, VTC 2003-Fall, pp. 6-9, October 5, 2003.
- [16] SeGo, D. J. "Ultrawide Band Active Radar Array Antenna for Unmanned Air Vehicles." *Proc. IEEE Nat. Telesyst. Conf.*, pp. 13-17, 1994.
- [17] K. A. Abdalmalak *et al.*, "Ultrawideband Conical Log-Spiral Circularly Polarized Feed for Radio Astronomy," in *IEEE Transactions on Antennas and Propagation*, vol. 68, no. 3, pp. 1995-2007, March 2020.
- [18] Kim, S. G., & Chang, K. "Ultra Wideband Exponentially-Tapered Antipodal Vivaldi Antennas." *IEEE Antennas and Propagation Society Symposium, Monterey, CA*, pp.2273-2276, June 3, 2004.
- [19] Su, S. W., Wong, K. L., & Tang, C. L. "Ultra-wideband square planar monopole antenna for IEEE 802.16a operation in the 2-11 GHz band." *Microwave Opt. Technol. Lett.*, 42(6), pp.463-466, Sept 2004.
- [20] Chen, Z. N., Ammann, M. J., & Chia, M. Y. W. "Broadband square annular planar monopoles." *Microwave Opt. Technol. Lett.*, 36(6), pp.449-454, Mar 2003.
- [21] Ahmed, O., & Sebak, A. R. "A Printed Monopole Antenna with Two Steps and a Circular Slot for UWB Applications." *IEEE Antennas Wireless Propag. Lett.*, 7, pp. 411-413, 2008.
- [22] Chen, Z. N., Ammann, M. J., Chia, M. Y. W., & See, T. S. P. "Annular planar monopole antennas." *IEE Proc. Microw. Antennas Propag.*, 149(4), 200-203, Aug 2002.
- [23] Liang, J., Chiau, C. C., Chen, X., & Parini, C. G. "Study of a printed circular disc monopole antenna for UWB systems." *IEEE Trans. Antennas Propag.*, 53(11), 3500-3504, Nov 2005.
- [24] Haraz, O. and Sebak, A.R. "UWB antennas for wireless applications." *Advancement in microstrip antennas with recent applications*, pp.125-152, 2013.
- [25] X. D. Huang, C. H. Cheng and L. Zhu, "An Ultrawideband (UWB) Slotline Antenna Under Multiple-Mode Resonance," in *IEEE Transactions on Antennas and Propagation*, vol. 60, no. 1, pp. 385-389, Jan. 2012.

- [26] Islam, M. M., M. T. Islam, M. Samsuzzaman, and M. R. I. Faruque, "Compact metamaterial antenna for UWB applications," *Electronics Letters*, Vol. 51, No. 16, 1222-1224, August 2015.
- [27] Kshirsagar, P., S. Gupta, and B. Mukherjee, "A two segment rectangular dielectric resonator antenna for ultra-wideband application," *Electromagnetics, Taylor & Francis Electromagnetics, Taylor and Francis*, Vol. 38, No. 1, 20-33, 2018.
- [28] R. Garg P. Bhartia I. Bahl A. Ittipiboon. "Microstrip Antenna Design Handbook" *MA Norwood:Artech House*, 2001.
- [29] Ansoft, High Frequency Structure Simulator (HFSS) v15.1.
- [30] CST Microwave Studio. Computer Simulation Technology (CST), 2020.
- [31] C. A. Balanis, "Antenna Theory: Analysis and Design" *John wily & sons, Inc., New York: Wiley*,1982.
- [32] Y. Yoshimura, "A Microstripline Slot Antenna (Short Papers)," in *IEEE Transactions on Microwave Theory and Techniques*, vol. 20, no. 11, pp. 760-762, Nov. 1972.
- [33] Jia-Yi Sze and Kin-Lu Wong, "Bandwidth enhancement of a microstrip-line-fed printed wide-slot antenna," in *IEEE Transactions on Antennas and Propagation*, vol. 49, no. 7, pp. 1020-1024, July 2001.
- [34] J.Y. Jan and J.-W. Su. "Bandwidth Enhancement of a Printed Wide-Slot Antenna with a Rotated Slot." *IEEE Trans. Antennas Propag.* vol 53, no.6, pp.2111–2114, 2005.
- [35] J. Jan and J. Kao, "Novel Printed Wide-Band Rhombus-Like Slot Antenna With an Offset Microstrip-Fed Line," in *IEEE Antennas and Wireless Propagation Letters*, vol. 6, pp. 249-251, 2007.
- [36] J. Jan and L. Wang, "Printed Wideband Rhombus Slot Antenna With a Pair of Parasitic Strips for Multiband Applications," in *IEEE Transactions on Antennas and Propagation*, vol. 57, no. 4, pp. 1267-1270, April 2009.
- [37] Y Sung, "Bandwidth Enhancement of a Microstrip Line-Fed Printed Wide-Slot Antenna with a Parasitic Centre Patch", *IEEE Trans. Antenna and Propagation*, Vol. 60, no. 4, pp. 1712-6, Apr. 2012.
- [38] S. T. Fan, Y. Z. Yin, B. Lee, W. Hu and X. Yang, "Bandwidth Enhancement of a Printed Slot Antenna With a Pair of Parasitic Patches," in *IEEE Antennas and Wireless Propagation Letters*, vol. 11, pp. 1230-1233, 2012.
- [39] Krishnendu Chattopadhyay, Tannistha Mitra, Dhruva Das, Santanu Das & Sekhar Ranjan Bhadra Chaudhuri, "Bandwidth Enhancement of Hexagonal Wide Slot Antenna Using a Tuning Stub", *IETE Journal of Research*, vol.59, no.6, pp.732-738, 2013.

- [40] X. Qing, M. Y. W. Chia, and X. Wu, "Wide-slot antenna for UWB applications," in *Proc. IEEE Antennas and Propagation Soc. Int. Symp.*, vol.1, pp. 834–837, Jun. 22–27, 2003.
- [41] N. Behdad and K. Sarabandi, "A wide-band slot antenna design employing a fictitious short circuit concept," in *IEEE Transactions on Antennas and Propagation*, vol. 53, no. 1, pp. 475-482, Jan. 2005.
- [42] Lei Zhu, Rong Fu and Ke-Li Wu, "A novel broadband microstrip-fed wide slot antenna with double rejection zeros," in *IEEE Antennas and Wireless Propagation Letters*, vol. 2, pp. 194-196, 2003.
- [43] W. J. Lui, C. H. Cheng, and Y. Cheng, "A novel broadband multislot antenna fed by microstrip line," *Microw. Opt. Technol. Lett.*, vol. 45, no. 4, pp. 55–57, Apr. 2005.
- [44] W. Lu and L. Zhu, "Wideband Stub-Loaded Slotline Antennas Under Multi-Mode Resonance Operation," in *IEEE Transactions on Antennas and Propagation*, vol. 63, no. 2, pp. 818-823, Feb. 2015.
- [45] W. Lu and L. Zhu, "A Novel Wideband Slotline Antenna with Dual Resonances: Principle and Design Approach," in *IEEE Antennas and Wireless Propagation Letters*, vol. 14, pp. 795-798, 2015.
- [46] Liu, G., Gu, J., Gao, Z. and Xu, M., "Wideband printed slot antenna using Koch fractal metasurface structure," *International Journal of RF and Microwave Computer-Aided Engineering*, 30(3), 2020, p.e22058.
- [47] F. Viani, L. Lizzi, R. Azaro, and A. Massa, "Spline-shaped ultra wideband antenna operating in the ECC released frequency spectrum," *Electronic Letters*, vol. 44, no. 1, pp. 7-8, January 2008.
- [48] M. Klemm, I. Z. Kovcs, G. F. Pedersen and G. Troster, "Novel small-size directional antenna for UWB WBAN/WPAN applications," in *IEEE Transactions on Antennas and Propagation*, vol. 53, no. 12, pp. 3884-3896, Dec. 2005.
- [49] D. Mitra, A. Sarkhel, O. Kundu and S. R. B. Chaudhuri, "Design of Compact and High Directive Slot Antennas Using Grounded Metamaterial Slab," in *IEEE Antennas and Wireless Propagation Letters*, vol. 14, pp. 811-814, Dec. 2015.
- [50] S. Chaimool, C. Rakluea and P. Akkaraekthalin, "Mu-near-zero metasurface for microstrip-fed slot antennas", *Appl. Phys. A Solids Surf.*, vol. 112, no. 3, pp. 669-675, 2013.
- [51] Shaw, T., D. Bhattacharjee, and D. Mitra, "Gain enhancement of slot antenna using zeroindex metamaterial superstrate," *International Journal of RF and Microwave Computer-Aided Engineering*, Vol. 27, e21078, 2016.

- [52] A. Chatterjee and S. K. Parui, "Gain enhancement of a wide slot antenna using a second-order bandpass frequency selective surface", *Radioengineering*, vol. 24, no. 2, pp. 455-461, Jun. 2015.
- [53] A. Chatterjee and S. K. Parui, "Gain enhancement of a wide-slot antenna using dual-layer bandstop frequency selective surface as a substrate", *Microw. Opt. Technol. Lett.*, vol. 57, no. 9, pp. 2016-2020, Sep. 2015.
- [54] Y. Cheng, X. Ding, X. Xu, X. Zhong and C. Liao, "Design and Analysis of a Bow-Tie Slot-Coupled Wideband Metasurface Antenna," in *IEEE Antennas and Wireless Propagation Letters*, vol. 18, no. 7, pp. 1342-1346, July 2019.
- [55] Z.-Z. Yang, F. Liang, Y. Yi, D. Zhao and B.-Z. Wang, "Metasurface-based wideband low-profile and high-gain antenna", *IET Microw. Antennas Propag.*, vol. 13, no. 4, pp. 436-441, Mar. 2019.
- [56] M. A. Meryche, H. Attia, A. Messai, S. S. I. Mitu and T. A. Denidni, "Directive Wideband Cavity Antenna With Single-Layer Meta-Superstrate," in *IEEE Antennas and Wireless Propagation Letters*, vol. 18, no. 9, pp. 1771-1774, Sept. 2019.
- [57] Wu, J. Chen and P.-F. Wu, "Broadband and multi-mode Fabry-Pérot cavity antenna with gain enhancement", *AEU-Int. J. Electron. Commun.*, vol. 127, Dec. 2020.
- [58] N. Wang, Q. Liu, C. Wu, L. Talbi, Q. Zeng and J. Xu, "Wideband Fabry-Perot Resonator Antenna With Two Complementary FSS Layers," in *IEEE Transactions on Antennas and Propagation*, vol. 62, no. 5, pp. 2463-2471, May 2014.
- [59] B. Majumder, K. Kandasamy, J. Mukherjee and K. P. Ray, "Wideband compact directive metasurface enabled pair of slot antennas", *Electron. Lett.*, vol. 51, no. 17, pp. 1310-1312, Aug. 2015.
- [60] B. Majumder, K. Krishnamoorthy, J. Mukherjee and K. P. Ray, "Compact Broadband Directive Slot Antenna Loaded With Cavities and Single and Double Layers of Metasurfaces," in *IEEE Transactions on Antennas and Propagation*, vol. 64, no. 11, pp. 4595-4606, Nov. 2016.
- [61] H. L. Zhu, X. H. Liu, S. W. Cheung and T. I. Yuk, "Frequency-Reconfigurable Antenna Using Metasurface," in *IEEE Transactions on Antennas and Propagation*, vol. 62, no. 1, pp. 80-85, Jan. 2014.
- [62] B. Majumder, K. Krishnamoorthy, J. Mukherjee and K. P. Ray, "Frequency-Reconfigurable Slot Antenna Enabled by Thin Anisotropic Double Layer Metasurfaces," in *IEEE Transactions on Antennas and Propagation*, vol. 64, no. 4, pp. 1218-1225, April 2016.

- [63] H. L. Zhu, S. W. Cheung, X. H. Liu and T. I. Yuk, "Design of Polarization Reconfigurable Antenna Using Metasurface," in *IEEE Transactions on Antennas and Propagation*, vol. 62, no. 6, pp. 2891-2898, June 2014.
- [64] X. Chen and Y. Zhao, "Dual-band polarization and frequency reconfigurable antenna using double layer metasurface", *AEU-Int. J. Electron. Commun.*, vol. 95, pp. 82-87, Oct. 2018.
- [65] K. Dutta, D. Guha, C. Kumar and Y. M. M. Antar, "New Approach in Designing Resonance Cavity High-Gain Antenna Using Nontransparent Conducting Sheet as the Superstrate," in *IEEE Transactions on Antennas and Propagation*, vol. 63, no. 6, pp. 2807-2813, June 2015.
- [66] Z.-H. Tu, Q.-X. Chu and Q.-Y. Zhang. High-gain slot antenna with parasitic patch and windowed metallic superstrate. *Prog. Electromagn. Res. Lett.* vol15, pp.27-36, 2010.
- [67] R. Fakhte and H. Ghorbaninejad. High gain and improved waveguide slot antenna using a metallic superstrate as main radiator. *Microw. Antennas Propagation.*, vol.11, no. 4, pp.557-563, 2016.
- [68] L. Leger, T. Monediere, and B. Jecko, "Enhancement of gain and radiation bandwidth for a planar 1-D EBG antenna," *IEEE Microw. Wireless Compon. Lett.*, vol. 15, no. 9, pp. 573–575, Sep. 2005.
- [69] L. Moustafa and B. Jecko, "Design of a wideband highly directive EBG antenna using double-layer frequency selective surfaces and multifeed technique for application in the Ku-band," *IEEE Antennas. Wireless Propag. Lett.*, vol. 9, pp. 342–346, 2010.
- [70] Z. G. Liu, W. X. Zhang, and D. L. Fu, "Broadband Fabry-Perot resonator printed antennas using FSS superstrate with dissimilar size," *Microw. Opt. Technol. Lett.*, vol. 50, no. 6, pp. 1623–1627, Jun. 2008.
- [71] Y. Ge, K. P. Esselle, and T. S. Bird, "The use of simple thin partially reflective surfaces with positive reflection phase gradients to design wideband, low-profile EBG resonator antennas," *IEEE Trans. Antennas Propag.*, vol. 60, no. 2, pp. 743–750, Feb. 2012.
- [72] B. A. Zeb, R. M. Hashmi, and K. P. Esselle, "Wideband gain enhancement of slot antenna using one unprinted dielectric superstrate," *Electron. Lett.*, vol. 51, no. 15, pp. 1146–1148, Jul. 2015.
- [73] R. M. Hashmi and K. P. Esselle, "A class of extremely wideband resonant cavity antennas with large directivity-bandwidth products," *IEEE Trans. Antennas Propag.*, vol. 64, no. 2, pp. 830–835, Feb. 2016.



- [74] K. Konstantinidis, A. P. Feresidis, and P. S. Hall, "Multilayer partially reflective surfaces for broadband Fabry-Perot cavity antennas," *IEEE Trans. Antennas Propag.*, vol. 62, no. 7, pp. 3474–3481, Jul. 2014.
- [75] N. Wang et al., "Wideband Fabry-Perot resonator antenna with two layers of dielectric superstrates," *IEEE Antennas Wireless Propag. Lett.*, vol. 14, pp. 229–232, 2015.
- [76] L. Ji, P. Qin and Y. J. Guo, "Wideband Fabry-Perot Cavity Antenna with a Shaped Ground Plane," in *IEEE Access*, vol. 6, pp. 2291-2297, 2018.
- [77] Boukern D, Bouacha A, Aissaoui D, Belazzoug M, Denidni TA. "High-gain cavity antenna combining AMC-reflector and FSS superstrate technique," *Int J RF Microw Comput Aided Eng*. Vol. 31: 22674, 2021.
- [78] Belmessaoud, D., Rouabah, K., Messaoudene, I. and Denidni, T.A. "Broadband planar slot antenna using a simple single-layer FSS stopband," *IET Microw. Antennas Propag.*, vol.14, pp. 203-210, 2020. <https://doi.org/10.1049/iet-map.2019.0365>
- [79] T. Wu, J. Chen and P.-F. Wu, "Broadband and multi-mode Fabry–Pérot cavity antenna with gain enhancement", *AEU-Int. J. Electron. Commun.*, vol. 127, Dec. 2020.
- [80] A. K. Iyer, A. Alù and A. Epstein, "Metamaterials and Metasurfaces—Historical Context, Recent Advances, and Future Directions," in *IEEE Transactions on Antennas and Propagation*, vol. 68, no. 3, pp. 1223-1231, March 2020, doi: 10.1109/TAP.2020.2969732.
- [81] P. Kumar, T. Ali and M. M. M. Pai, "Electromagnetic Metamaterials: A New Paradigm of Antenna Design," in *IEEE Access*, vol. 9, pp. 18722-18751, 2021, doi: 10.1109/ACCESS.2021.3053100.
- [82] C. Miliás *et al.*, "Metamaterial-Inspired Antennas: A Review of the State of the Art and Future Design Challenges," in *IEEE Access*, vol. 9, pp. 89846-89865, 2021, doi: 10.1109/ACCESS.2021.3091479.
- [83] Hao Bai, Guang-ming Wang, Xiao-jun Zou. "A wideband and multi-mode metasurface antenna with gain enhancement" *AEU - International Journal of Electronics and Communications*, vol 126, 2020,153402. <https://doi.org/10.1016/j.aeue.2020.153402>.
- [84] D. Samantaray and S. Bhattacharyya, "A Gain-Enhanced Slotted Patch Antenna Using Metasurface as Superstrate Configuration," in *IEEE Transactions on Antennas and Propagation*, vol. 68, no. 9, pp. 6548-6556, Sept. 2020, doi: 10.1109/TAP.2020.2990280.
- [85] D. Chen, W. Yang, W. Che and Q. Xue, "Broadband Stable-Gain Multiresonance Antenna Using Nonperiodic Square-Ring Metasurface," in *IEEE Antennas and Wireless Propagation Letters*, vol. 18, no. 8, pp. 1537-1541, Aug. 2019, doi: 10.1109/LAWP.2019.2919692.

- [86] A. K. Singh, M. P. Abegaonkar and S. K. Koul, "A compact near zero index metasurface lens with high aperture efficiency for antenna radiation characteristic enhancement", *IET Microw. Antennas Propag.*, vol. 13, no. 8, pp. 1248-1254, Mar. 2019.
- [87] Z. Wani, M. P. Abegaonkar and S. K. Koul, "High-Low-Epsilon Biaxial Anisotropic Lens for Enhanced Gain and Aperture Efficiency of a Linearly Polarized Antenna," in *IEEE Transactions on Antennas and Propagation*, vol. 68, no. 12, pp. 8133-8138, Dec. 2020, doi: 10.1109/TAP.2020.2983787.
- [88] A. K. Singh, M. P. Abegaonkar, and S. K. Koul, "Compact ultrathin linear graded index metasurface lens for beam steering and gain enhancement," *Int. J. RF Microw. Comput.-Aided Eng.*, vol. 30, no. 6, Jun. 2020, Art. no. e22186.
- [89] Wang Z, Yang Z, Zhao X, Guo L, Guo M. "Ultra-wideband and high gain antipodal tapered slot antenna with planar metamaterial lens." *International Journal of Microwave and Wireless Technologies*, pp.1-11, 2021.
- [90] Mohammad Isaac Mirzapour, Ayaz Ghorbani, Farhad Azadi Namin, "A wideband low RCS and high gain phase gradient metalens antenna." *AEU - International Journal of Electronics and Communications*. vol 138, 153887, 2021. <https://doi.org/10.1016/j.aeue.2021.153887>.
- [91] Dash, UA, Sahu, S. "Gain enhancement of truncated conical dielectric ring resonator antenna based on metasurface walls." *Int J RF Microw Comput Aided Eng*. Vol 28, no. 7, 2018.
- [92] A. K. Skrivervik, "System Fidelity Factor: A New Method for Comparing UWB Antennas," in *IEEE Transactions on Antennas and Propagation*, vol. 59, no. 7, pp. 2502-2512, July 2011.
- [93] Akhoondzadeh-Asl, L., M. Fardis, A. Abolghasemi, and G. Dadashzadeh, "Frequency and time domain characteristic of a novel notched frequency UWB antenna," *Progress In Electromagnetics Research*, Vol. 80, 237-348, 2008.
- [94] V. A. Shameena, S. Mridula, A. Pradeep, S. Jacob, A. O. Lindo and P. Mohanan, "A compact CPW fed slot antenna for ultra wide band applications", *Int. J. Electron. Commun.*, vol. 66, pp. 189-194, 2012.
- [95] Mighani, M. and Akbari, M., "New UWB monopole planer antenna with dual band notched", *Progress In Electromagnetics Research C*, 52, pp.153-162, 2014.
- [96] M. Manohar, R. S. Kshetrimayum and A. K. Gogoi, "Printed monopole antenna with tapered feed line feed region and patch for super wideband applications", *IET Microw. Antennas Propag.*, vol. 8, no. 1, pp. 39-45, Jan. 2014.

- [97] J. Malik, P. C. Kalaria and M. V. Kartikeyan, "Transient response of dual-band-notched ultra-wideband antenna", *International Journal of Microwave & Wireless Technologies*, vol. 7, no. 01, pp. 61-67, 2015.
- [98] Sanyal, R., Patra, A., Sarkar, P. and Chowdhury, S.K. "Frequency and time domain analysis of a novel UWB antenna with dual band-notched characteristics," *International Journal of Microwave and Wireless Technologies*, vol. 9, no.2, pp.427-436, 2017.
- [99] C. A. Balanis, *Advanced Engineering Electromagnetics*, John Wiley & Sons, New York, 1989.
- [100] J. D. Kraus, R. J. Marhefka and A. S. Khan, *Antennas and Wave Propagation*, New York, NY, USA:McGraw-Hill, 2006.
- [101] C. Meagher and S. K. Sharma, "A Wideband Aperture-Coupled Microstrip Patch Antenna Employing Spaced Dielectric Cover for Enhanced Gain Performance," *IEEE Transactions on Antennas and Propagation*, Vol.58, no. 9, pp.2802-2810, 2010.
- [102] N. Behdad and K. Sarabandi, "A wideband multi resonant single-element slot antenna," *IEEE Antennas and Propagation Society Symposium Monterey, CA, USA.2*: pp.1891-1894, 2004.
- [103] C. Meagher and S. K. Sharma, "A Wideband Aperture-Coupled Microstrip Patch Antenna Employing Spaced Dielectric Cover for Enhanced Gain Performance," *IEEE Transactions on Antennas and Propagation*, Vol.58, no. 9, pp.2802-2810, 2010.
- [104] I. Bahl, P. Bhartia, and S. Stuchly, "Design of microstrip antennas covered with a dielectric layer," *IEEE Trans. Antennas Propag.*, Vol.30, no. 2, pp. 314–318, 1982.
- [105] R. Fakhte and H. Ghorbaninejad., "High-gain waveguide slot antenna using simple parasitic patch's cover," *Int. J. RF Microw. Comput. Aided Eng.*, Vol.28, no. 2, 2018.
- [106] A. Sharma, D. Gangwar, B.K. Kanaujia , & S. Dwari, "RCS reduction and gain enhancement of SRR inspired circularly polarized slot antenna using metasurface," *Aeu-international Journal of Electronics and Communications.*, Vol.91, pp.132-142, 2018.
- [107] N. Guerin, S. Enoch, G. Tayeb, P. Sabouroux, P. Vincent and H. Legay. A metallic Fabry Perot directive antenna. *IEEE Trans. Antennas Propag.*, vol 54, no.1; pp. 220-224, 2006.
- [108] S. Fakhte, H. Oraizi and R. Karimian. A Novel Low-Cost Circularly Polarized Rotated Stacked Dielectric Resonator Antenna. *IEEE Antennas and Wireless Propagation Letters*. vol 13; pp.722-725, 2014.

- [109] P. K. Jain and B. N. Basu. The inhomogeneous loading effects of practical dielectric supports for the helical slow wave structure of a TWT. *IEEE Trans. Electron Devices.*, vol 34; pp. 2643-2648; 1987.
- [110] B. Schleicher, *Impulse-Radio Ultra-Wideband Systems for Vital-Sign Monitoring and Short-Range Communications*, München, Germany:Verlag Dr. Hut, 2012.
- [111] Yvan Duroc, "On the System Modeling of Antennas," *Progress In Electromagnetics Research B*, Vol. 21, 69-85, 2010.
- [112] A. K. Skrivervik, "System Fidelity Factor: A New Method for Comparing UWB Antennas," in *IEEE Transactions on Antennas and Propagation*, vol. 59, no. 7, pp. 2502-2512, July 2011.
- [113] Z. Min, *Design and Time-domain Analysis of Antenna Array for UWB Imaging Application* (Queen Mary University of London, June 2014).
- [114] J. Liang, *Antenna study and design for ultra wideband communication applications*, Dec. 2006.
- [115] Zhi Ning Chen, Xuan Hui Wu, Hui Feng Li, Ning Yang and M. Y. W. Chia, "Considerations for source pulses and antennas in UWB radio systems," in *IEEE Transactions on Antennas and Propagation*, vol. 52, no. 7, pp. 1739-1748, July 2004.
- [116] Sharma, Manmohan. "Ultra Wideband Wearable Sensors for Motion Tracking Applications." *Queen Mary University of London*, 2015.

## List of Publications

### Peer Reviewed Journal

1. **Ritish Kumar** and A.V.Praveen Kumar, Conducting Sheets-Loaded Slot Antenna for High Gain and Wide 3 dB Gain-Band Operation, In *International Journal of RF and Microwave Computer-aided Engineering, John and Wiley*, pp.1-13, March 2022. (DOI:10.1002/mmce.23138) (SCI-E).
2. **Ritish Kumar** and A. V. Praveen Kumar, Conducting Side Sheet Loading to Enhance the Bidirectional Gain of a Wide Rectangular Slot Antenna in the 6–8.5 GHz Band, *IETE Journal of Research, Taylor & Francis*, 2021. DOI: 10.1080/03772063.2021.1999865. (SCI-E).
3. **Ritish Kumar**, and A.V. Praveen Kumar, A rectangular slot antenna with perfectly conducting superstrate and reflector sheets for superior radiation in the 6–9 GHz band, *International Journal of Microwave and Wireless Technologies, Cambridge University Press*, vol. 12, no. 10, pp. 1039-1046, 2020 (SCI-E).
4. **Ritish Kumar and A.V.Praveen Kumar**, Investigation on the Aspect Ratio of Conducting Superstrates in Deciding its Function as a Gain Enhancer / Suppressor for Wideband Slot Antenna, *Microsystem Technologies, Springer*. (SCI). (Major revision under review)

### Conference Proceedings

1. **Ritish Kumar**, S. Piyush, and A.V. Praveen Kumar, Offset fed slot antenna for broadband operation, In *IOP Conference Series: Materials Science and Engineering*, vol. 331, no. 1, p. 012022. **IOP Publishing**, 2018 (SCOPUS)
2. Girish, Bangaru, M. Nikhil, **Ritish Kumar**, and A.V. Praveen Kumar. "FDTD Analysis of Offset-fed Wideband Slot Antennas" In *IEEE Indian Conference on Antennas and Propagation (InCAP)*, pp. 1-4, 2019 (SCOPUS)

## **Brief Biography of the Candidate**

Ritish Kumar received his B.Tech. degree in electronics and communication engineering from UPTU, Lucknow, India and M.E. degree in electronics engineering from Devi Ahilya Vishwavidyalaya (DAVV), Indore, India in 2013. He is currently working towards the Ph.D. degree at Department of Electrical and Electronics Engineering, Birla Institute of Technology and Science, Pilani, (BITS Pilani), Rajasthan, India. His research interests are microstrip antennas, ultra-wideband antennas, time-domain analysis, and material characterization.

## **Brief Biography of the Supervisor**

**A.V. Praveen Kumar** received his Ph.D. degree in microwave electronics from the Department of Electronics, Cochin University of Science and Technology (CUSAT), Kerala in 2009. His thesis was on the fabrication, characterization and development of dielectric resonators and its application in wideband dielectric resonator antennas. He joined the Engineering department, Lancaster University, UK as a post-doctoral fellow where he worked on the development of radiofrequency cavities for particle accelerators. His major research interest is in RF and microwave engineering which includes antennas, cavity resonators, sensors, particle accelerators and material characterization techniques. He has published several international journal / conference papers on various aspects of RF engineering. Since 2013 he has been working as an Associate Professor in the Department of Electrical and Electronics Engineering, Birla Institute of Technology and Science, BITS Pilani, (Pilani campus), Rajasthan, India.